POLITECNICO DI TORINO
Repository ISTITUZIONALE

Optical Transponders

Original
Optical Transponders / Bosco, G.; Elbers, J. -P. (SPRINGER HANDBOOKS). - In: Springer Handbooks of Optical NetworksSTAMPA. - [s.l] : Springer Science and Business Media Deutschland GmbH, 2020. - ISBN 978-3-030-16249-8. - pp. 83-136 [10.1007/978-3-030-16250-4_4]

Availability:
This version is available at: 11583/2870892 since: 2021-02-15T12:29:36Z

Publisher:
Springer Science and Business Media Deutschland GmbH

Published
DOI:10.1007/978-3-030-16250-4_4

Terms of use:

This article is made available under terms and conditions as specified in the corresponding bibliographic description in the repository

Publisher copyright
Springer postprint/Author's Accepted Manuscript

This version of the article has been accepted for publication, after peer review (when applicable) and is subject to Springer Nature's AM terms of use, but is not the Version of Record and does not reflect post-acceptance improvements, or any corrections. The Version of Record is available online at: http://dx.doi.org/10.1007/978-3-030-16250-4_4

(Article begins on next page)

19 December 2025

Chapter 4. Optical transponders

Gabriella Bosco, Politecnico di Torino, Italy;

Jörg-Peter Elbers, ADVA Optical Networking, Germany

Short summary

The first commercial 10 Gb/s transponders, deployed in the mid 90's, were based on a very simple modulation technique, i.e., a binary light on/off approach with detection of the signal by means of a single photo-diode. To extend the fiber capacity, bandwidth-efficient modulation techniques such as duobinary line coding and multi-level intensity-modulation formats gained popularity in optical communications in the late 90's and the deployment in the following years of transponders based on differential phase modulation with interferometric detection allowed to increase the data rate up to 40 Gb/s. However, despite all improvements, the system performance of these 40 Gb/s solutions was still not on par with state-of-the art 10 Gb/s systems at that time. With the advent of coherent detection, things suddenly changed and transmission rates of 100 Gb/s and beyond could soon be achieved, thanks to the use of high-order modulation formats and advanced digital signal processing techniques.

In this chapter, the configuration and performance of the most common transmitter and receiver pairs that are currently used in optical transmission systems will be described, including an overview of transponder types and their hardware architectures. Finally, relevant standards will be discussed and pluggable optical transceiver modules used in modern transponder implementations will be explained.

Acronyms

4WDM	4 wavelengths WDM
ADPSK	Adaptive DPSK
AMP	Bit-asynchronous mapping
AMZI	Asymmetric Mach-Zehnder interferometer
ASE	Amplified spontaneous emission
ASK	Amplitude-shift keying
AUI	Attachment unit interface
BER	Bit error rate
BMP	Bit-synchronous mapping
BPD	Balanced photodetector
BPSK	Binary PSK
CAUI	100G AUI
CFP	Small form factor pluggable
CBR	Constant bit rate
CD	Chromatic dispersion
CEI IA	Common electrical I/O implementation agreement
CLR4	100G with 4 wavelength WDM
CMIS	Common MIS
COBO	Consortium on on-board optics
CPLD	Complex programmable logic device
CPRI	Common public radio interface
CRZ	Chirped return-to-zero
CSRZ	Carrier-suppressed return-to-zero
CWDM	Coarse wavelength division multiplexing
DB	Duobinary
DCI	Data-center interconnect
DD	Direct-detection
DGD	Differential group delay
DEMUX	De-multiplexer
DML	Directly modulated laser
DMT	Discrete multitoned transmission
DPSK	Differential PSK
DQPSK	Differential QPSK
DR	Datacenter of 500m scrambled signal (in IEEE 802.3 standard)
DWDM	Dense wavelength division multiplexing
EAM	Electro-absorption modulator
EDFA	Erbium-doped fiber amplifier
EEPROM	Electronically erasable programmable read-only memory
EFEC	Enhanced forward error correction
ER	Extinction ratio
ER	Extended reach; extra long wavelength or 40km reach scrambed signal (in IEEE 802.3 standard)
FDM	Frequency-domain multiplexing
FEC	Forward error correction
FIC	Fabric interface chip
FOIC	FlexO Interface
FPGA	Field-programmable gate array
FR	Fiber or 2km reach scrambled signal (in IEEE 802.3 standard)

FWHM	Full-width half-maximum
FWM	Four-wave mixing
FX	Fiber or 2 km reach signal with external coding (in IEEE 802.3 standard)
GBIC	Gigabit interface converter
GFP	Generic framing procedure
GMP	Generic mapping
GVD	Group-velocity dispersion
HPC	High-performance computing
HU	Height unit
IBTA	Infiniband Trade Association
IEEE	Institute of Electrical and Electronics Engineers
IFWM	Intra-channel four-wave mixing
IM	Intensity-modulation
IMDD	Intensity-modulation direct-detection
IMP	Idle mapping
Incits	International committee for information technology standards
IQ	In-phase/quadrature
ISI	Inter-symbol interference
ITU	International Telecommunications Union
IXPM	Intra-channel cross-phase modulation
LAN	Local area network
LAUI	50G AUI
LO	Local oscillator
LPF	Low-pass filter
LPN	Laser phase noise
LR	Long reach or 10km reach scrabled signal (in IEEE 802.3 standard)
LX	Long wavelength or 10km signal with external coding (in IEEE 802.3 standard)
MDIO	Management data input/output
MI	Modulation instability
MIS	Management interface specification
MLD	Multi-lane distribution
MMF	Multi-mode fiber
MPO	Multi-fiber push on (connector)
MSA	Multi-source agreement
MZ	Mach-Zehnder
MZM	Mach-Zehnder modulator
MUX	Multiplexer
NLPM	Non-linear phase noise
NRZ	Non-return-to-zero
OAM	Operations, administration and maintenance
OBO	On-board optics
ODB	Optical duobinary
ODU	Optical data unit
OFDM	Orthogonal frequency-domain multiplexing
OIF	Optical Internetworking Forum
OOK	On-Off Keying
OPU	Optical payload unit
OTU	Optical transport unit
OSFP	Octal SFP

OSNR	Optical signal-to-noise ratio
OTLC	Optical transport lane group
OTN	Optical transport network
PAM	Pulse-amplitude modulation
PBC	Polarization beam combiner
PBS	Polarization beam splitter
PCB	Printed circuit boards
PD	Photo-detector
PDG	Polarization-dependent gain
PDL	Polarization-dependent loss
PM	Polarization multiplexing
PMD	Polarization mode dispersion
POTP	Packet-optical transport platform
PS	Probabilistic shaping
PSBT	Phase-shaped binary transmission
PSM	Parallel single mode (interface)
PSP	Principal state of polarization
PSK	Phase-shift keying
QAM	Quadrature-amplitude modulation
QPSK	Quadrature phase-shift keying
QSFP	Quad small form factor pluggable
QSFP+	10 Gb/s 4x pluggable
QSFP-DD	QSFP double density
RC	Raised-cosine
RF	Radio frequency
ROADM	Reconfigurable optical add-drop multiplexer
RX	Receiver
RZ	Return-to-zero
SAN	Storage area network
SAR	Segmentation and reassembly
SBS	Stimulated Brillouin scattering
SCM	Sub-carrier multiplexing
SDH	Synchronous digital hierarchy
SE	Spectral efficiency
SER	Symbol error rate
SFF	Small form factor
SFI	SFP interface
SFP	Small form factor pluggable
SFP+	1 x 10 Gb/s small form factor
SFP-DD	SFP double density
SMF	Single mode fiber
SMPTE	Society of motion picture and television engineers
SMSR	Side-mode suppression ratio
SNIA	Storage networking industry association
SNR	Signal-to-noise ratio
SONET	Synchronous optical network
SOP	State of polarization
SPM	Self-phase modulation
SpS	Samples per symbol

SSMF	Standard single-mode fiber
SR	Short reach; short wavelength or 100m scrambled signal (in IEEE 802.3 standard)
SRRC	Square-root raised-cosine
SRS	Stimulated Raman scattering
SX	Short wavelength or 100m signal with external coding (in IEEE 802.3 standard)
TDHF	Time-domain hybrid formats
THN	Thermal noise
TTT	Timing-transparent transcoding
TRCV	Transceiver
TWS	Two-wire serial
TX	Transmitter
XC	Cross-connected
XENPACK	10 Gigabit Ethernet transceiver package
XFP	10 Gigabit small form factor pluggable
XFI	XFP interface
XLAUI	40G AUI
XPM	Cross-phase modulation
XSBI	10 Gigabit Sixteen-Bit Interface
XTK	Crosstalk
WDM	Wavelength-division multiplexing

Main symbols

β_2	Chromatic dispersion coefficient [ps^2/km]
c	Speed of light in vacuum
D	Chromatic dispersion parameter [ps/nm/km]
Δ_{AMZI}	AMZI delay error in the interferometric receiver
Δ_{BPD}	BPS delay error in the interferometric receiver
δ_{PMD}	PMD parameter [ps/$\sqrt{\text{km}}$]
$\Delta\tau_{CD}$	Pulse broadening due to GVD
$\Delta\tau_{DGD}$	DGD between the two PSPs
E_b	Energy per bit
E_s	Energy per symbol
F	Amplifier noise figure
f_{ADC}	Sampling frequency of the ADC
f_{DAC}	Sampling frequency of the DAC
G	Amplifier gain
h	Planck's constant
L	Fiber length
λ	Propagation wavelength
N_0	Noise power spectral density
N_b	Number of bits per symbol
n_{sp}	Spontaneous emission factor
N_{ADC}	Number of resolution bits of the ADC
N_{DAC}	Number of resolution bits of the DAC

N_{sps}	Number of samples per symbol
P	Optical power
R	Photodiode responsivity
R_b	Bit rate
R_s	Symbol rate
T_s	Symbol interval
T_b	Bit interval

4.1 Introduction

Transponders are essential building blocks in any optical communication system. The term “transponder” stems from an amalgamation of two words “trans(mitter)” and “(res)ponder”, first coined in about 1940 to describe radio and radar systems [kingsley95]. In optical communications, a transponder is a receiver-transmitter combination, which translates an optical signal from one wavelength into another optical signal at a different wavelength by means of optical-electrical-optical (O/E/O) conversion [G.691]. During the conversion process, the received signal is re-amplified and normally also re-shaped and re-timed, i.e. 3R regenerated. Optical transponders commonly operate in full-duplex mode and comprise transmitter and receiver functions on each of their ports. The ports can support different optical interface classes, which are characterized by properties such as the fiber medium, link distance, wavelength range, signaling rate, modulation format, forward error correction, line coding, and/or signal type.
Network (or line) ports are connected to a multi-channel wavelength division multiplexing (WDM) networks. They are also called “colored interfaces”, as they are available in or can be tuned to multiple WDM colors. Client ports typically connect to subtended equipment such as routers or switches which act as clients of the optical transport network. These ports are termed “grey interfaces” if they only support a single channel per fiber (as opposed to colored interfaces, which can be wavelength multiplexed onto the same fiber). Wavelength grids for dense (DWDM) and coarse wavelength division multiplexing (CWDM) are defined in the ITU-T G.694.1 and G.694.2 recommendations [G.694.1, G.694.2]. In this chapter, the focus will be on colored DWDM interfaces.

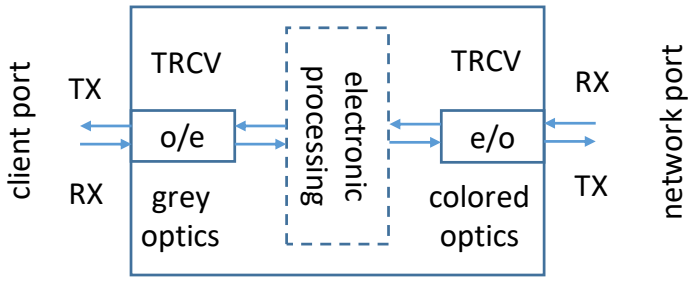

Fig. 4.1.1: Basic block diagram of an optical transponder. TX: transmitter, RX: receiver, o/e: opto-electric conversion, e/o: electro-optic conversion, TRCV: transceiver.

Another very similar device to the transponder, and might be confused with it, is the “transceiver” (TRCV) which is a device that can simultaneously transmit and receive signals. As a portmanteau of “trans(mitter)” (TX) and “(re)ceiver” (RX), the term “transceiver” first appeared in the early 1920s and was used in descriptions of military communication equipment [sterling07]. An optical transceiver comprises an optical transmit and receive interface on the so called line side and a bidirectional electrical interface on the so called host side. Transceivers can be realized as pluggable optical modules or as fixed host board implementations. An optical transponder can then be split into a client and line side optical transceiver function with an electronic processing block in between (Fig. 4.1.1).
In most cases, optical transponders are delivered as part of a complete DWDM network solution by one vendor. In other cases, transponders and the corresponding DWDM systems as supplied independently by different vendors. Colored interfaces may also be integrated into third party switches or routers on the client side, thereby eliminating the need for separate transponders. When colored interfaces are separated from a WDM system and externally provided, such scenario is referred to as a alien wavelength or black link approach [G.698.2] and has been used in commercial networks for many years. More recently, WDM systems supporting alien wavelengths have also been termed “open line systems” [filer16]. A line system is not restricted to just a point-to-point link in this context, but also includes optical networks in ring or mesh topologies.
A typical WDM system is depicted in Fig. 4.1.2. For simplicity, only one direction is shown. Colored interfaces are connected to a WDM multiplexer, which combines all of the WDM transmit channels onto one fiber before they are

optically amplified by a booster amplifier and sent over a fiber link. The fiber link comprises one or more fiber spans of between 50 and 120 km in length (80 km is a typical span length in terrestrial systems). Erbium-doped fiber amplifiers (EDFAs) and/or distributed Raman amplifiers periodically compensate the span loss. At the receiving end, the WDM channels are optically pre-amplified, de-multiplexed and terminated by colored receiver interfaces. If access to the WDM channels is required at intermediate sites then reconfigurable optical add-drop multiplexers (ROADMs) are used on the transmission link. Multi-Degree ROADMs (MD-ROADMs) can offer additional wavelength-selective cross-connect functionality for dynamic routing of channels across a meshed network.

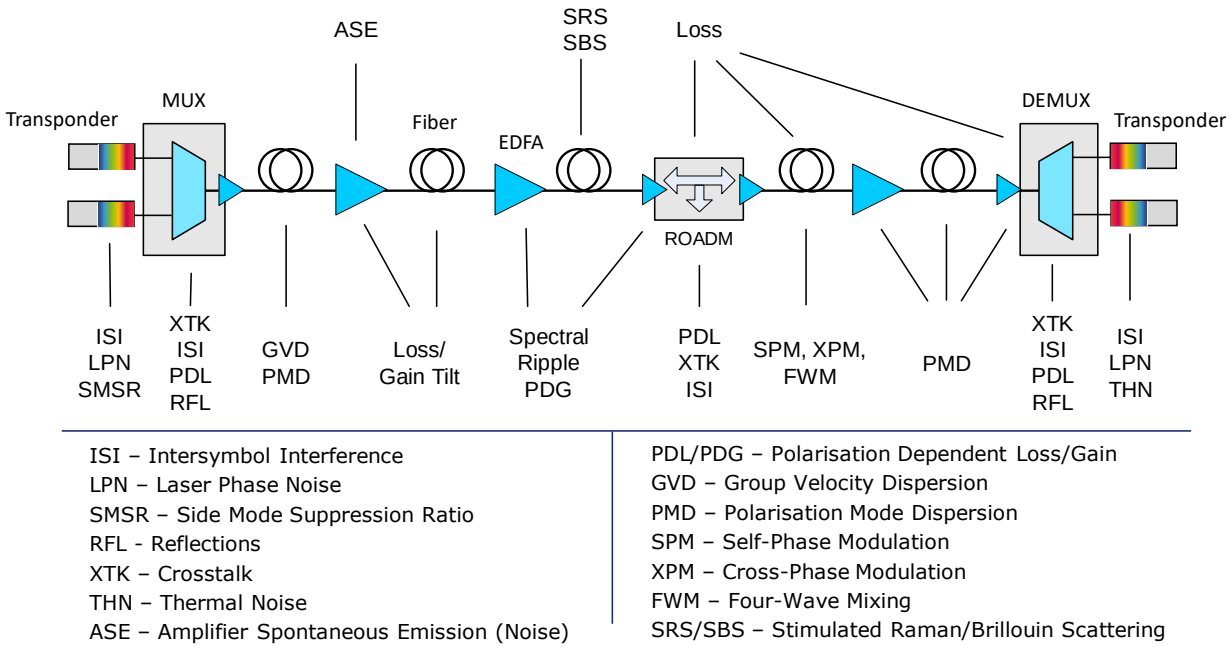

Fig. 4.1.2: A typical WDM line system and related transmission impairments. MUX: WDM multiplexer, DEMUX: WDM demultiplexer.

The colored interface performance is limited by inter-symbol interference (ISI), thermal noise (THN), crosstalk (XTK), laser phase noise (LPN), laser side-mode suppression ratio (SMSR) and optical reflections (RFL). Transmission impairments such as amplified spontaneous emission noise (ASE), spectral loss/gain tilt and ripples, polarization dependent loss/gain (PDL/PDG), group velocity dispersion (GVD) and polarization mode dispersion (PMD) limit the optical performance of the channels. With higher optical power levels then fiber nonlinearities will be triggered which will limit the transmission performance further. Nonlinearities include stimulated Raman scattering (SRS) leading to Raman tilt and crosstalk, stimulated Brillouin scattering (SBS) which imposes an upper limit on optical channel carrier powers, and the Kerr effect which introduces intra-channel and inter-channel nonlinearities. The Kerr nonlinearities are caused by signal-signal or signal-noise interactions and can be separated into a number of manifestations as shown below in Tab. 4.1.1. More specifically the intra-channel nonlinearities are self-phase modulation (SPM) induced non-linear phase noise (NLPN), modulation instability (MI), isolated pulse SPM, intra-channel cross-phase modulation (IXPM), and intra-channel four-wave mixing (IFWM). The inter-channel nonlinearities can be split into XPM-induced NLPN and inter-channel XPM and FWM.

Intra-channel nonlinearities					Inter-channel nonlinearities		
Signal-noise interaction		Signal-signal interaction			Signal-noise interaction	Signal-signal interaction	
NLPN	Parametric amplification	SPM			NLPN	WDM nonlinearities	
SPM-induced NLPN	MI	Isolated pulse SPM	IXPM	IFWM	XPM-induced NLPN	XPM	FWM

Table 4.1.1: Transmission impairments due to fiber Kerr nonlinearity [essiambre10]. SPM: self-phase modulation, XPM: cross-phase modulation, FWM: four-wave mixing, NLPN: non-linear phase noise, MI: modulation instability, IXPM: intra-channel cross-phase modulation, IFWM: intra-channel four-wave mixing

The choice of colored interface technology depends on the network application and is typically determined by such considerations as cost, performance, spectral efficiency, power consumption and equipment footprint. Point-to-point enterprise and data-center interconnect (DCI) links can be distinguished from ring-based metro access and metro core networks as well as meshed regional and long-haul networks on the typical reaches involved, the number of ROADMs and the fiber cost, as shown below in (Fig. 4.1.3). Submarine systems can be separated into unrepeated point-to-point systems with passive wet plant over link distances of less than 600 km and repeated ultra-long haul systems over link distances of several thousand kilometers. The larger the network reach, the higher is the fiber infrastructure cost and the more important is the spectral efficiency, but the most challenging are the transmission impairments. It is important to note that cascading of ROADMs also causes impairments such as insertions losses, inter-symbol interference and cross-talk, so that a metro network with many ROADMs can show a similar performance to a long-haul network with few or no ROADMs despite the difference in network size.

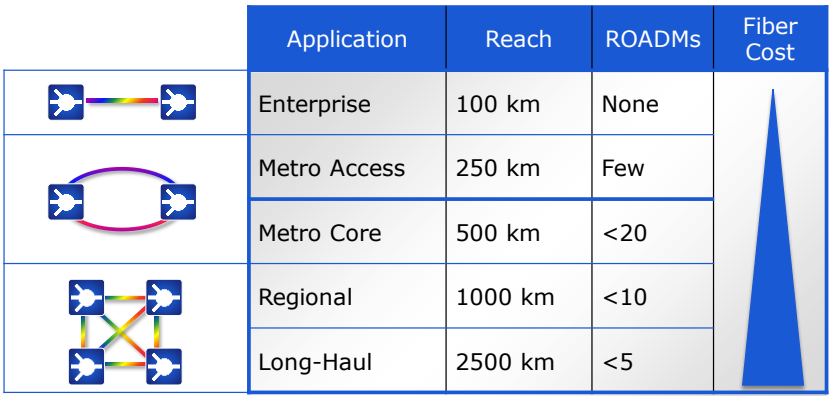

Fig. 4.1.3: Terrestrial WDM applications and main characteristics

4.1.1 Evolution of modulation formats and symbol rates

Due to its simplicity and cost efficiency, non-return to zero (NRZ) modulation with direct detection has long been the solution of choice for terrestrial DWDM systems. Based on a binary light on/off approach, this modulation technique is also known as On-Off Keying (OOK) [proakis07]. OOK signals can be generated using an intensity-modulation (IM) transmitter, in which the intensity of an optical source is modulated by an RF signal, and demodulated using a direct-detection (DD) receiver, which converts the optical power into an electrical signal current using a photodetector. For this reason, optical systems based on OOK modulation are also classified as IMDD systems. Commercial 10 Gb/s

NRZ transponders have been available since 1995 and were designed to guarantee a bit error ratio of 10^{-15} without forward error correction. They were deployed in 32-channel DWDM systems with 100 GHz channel spacing, yielding a total system capacity of 320 Gb/s over distances beyond 500 km of standard single-mode fiber (SSMF) in the C-band (1530-1565 nm) [sun97]. Motivated by the higher tolerance to fiber-nonlinearities, return-to-zero (RZ) modulation was introduced as an alternative to NRZ modulation. RZ modulation was first used in submarine systems [bergano98] but found also commercial adoption in ultra-long-haul terrestrial networks [pratt03]. Aided by forward error correction (FEC) and Raman amplification, terrestrial DWDM systems with 10 Gb/ RZ modulation could achieve C-band capacities of 800 Gb/s (80 channels at 50 GHz channel spacing) over distances of more than 3000 km SSMF [haxell00b]. By adding another 80 channels in the L-band (1565-1625nm), this capacity could be doubled, albeit with some impact on reach [bigo01]. Many terrestrial 10 Gb/s DWDM systems continued to use NRZ modulation, though. As enhanced forward error correction (EFEC) helped to increase the transmission distance up to 1500 km with EDFA-only amplification and more than 2500 km with Raman amplification, this was deemed to be sufficient for most practical applications.

To extend the fiber capacity, more bandwidth efficient modulation techniques such as duobinary line coding and multi-level IMDD formats gained popularity in optical communications in the late 1990's [walklin99]. Duobinary line coding (DB) is a partial-response format [proakis07] and was first proposed in the 1960's for radio communications [lender63]. Comprehensive review papers on the advantages and disadvantages of optical duobinary (ODB) modulation have been published (see for example [ono98]). It has been pointed out that ODB, besides achieving higher bandwidth efficiency, also features a high resilience to GVD [gu96, yonenaga97, yonenaga98, penninckx97]. Further research has been published showing that improvements in the sensitivity of duobinary receivers is possible through careful optimization of both the electric and optical filter bandwidths in the system[zheng01, kim02, lyubomirsky04, bosco04, pavlovic05]. At 10 Gb/s line rate, ODB found only little commercial adoption apart from single span transmission over extended link distances (for example 150 km) without optical dispersion compensation. At 40 Gb/s, though, ODB was found to be much more applicable, as it allows transmission of 40 Gb/s channels using 50 GHz filters and therefore a quadrupling of the system capacity compared to 10 Gb/s channels. It then substituted earlier realizations based upon NRZ or RZ modulation. In 2001, ODB modulation was successfully employed to transmit 80 channels at 40 Gb/s over 300 km SSMF [bissesur01]. Commercial deployments over several hundred kilometers followed in around 2005 [birk05]. Though ODB was by far not the only option for 40 Gb/s transmission.

The use of differential phase shift keying (DPSK) with interferometric demodulation and direct detection was investigated in the late 1990's. DPSK demonstrated a sensitivity advantage over OOK [humblet91, chinn96] and ODB as well as a high resilience to linear and non-linear fiber propagation effects [gnauck02, griffin02, wang04, bosco04, gnauck05, winzer06]. Both binary (DPSK) and quaternary formats (DQPSK) were extensively studied in the following years, leading to their commercial deployment in around 2006 [fishman06, ohta08]. While 40 Gb/s DQPSK could fit into a 50 GHz channel grid, this proved challenging initially for DPSK. Partial DPSK was able to overcome this limitation by reducing the differential delay of the Mach-Zehnder demodulator [mikkelsen06] and was commercially deployed from 2007 onwards under the name adaptive DPSK (ADPSK). Despite all improvements, the system performance of these 40 Gb/s solutions was still not on a par with state of the art 10 Gb/s systems at that time. Stringent requirements on GVD and PMD tolerance required careful network planning and lead to operational challenges.

With the advent of coherent detection, the transponder landscape changed dramatically. Earlier work on coherent optical communication systems in the 1980's had been hampered by a lack of digital signal processing (DSP) and large laser linewidths (compared to the Mb/s data rates used at that time). With much higher data rates and advances in CMOS technology now, coherent optical communications suddenly became a very practical option. Polarization-multiplexed quarternary phase shift keying (PM-QPSK) reduces symbol rates by a factor of four compared to the information bit rate, while at the same time offering a 6dB sensitivity gain over OOK. Furthermore, powerful DSP performs all the required GVD and polarization mode dispersion compensation, frequency and phase locking, and polarization demultiplexing in the electronic domain [derr92, taylor04, noe05, savory06, laperle08, fludger08, savory08]. As a result, coherent transmission can deliver comparable system performance and reach as 10 Gb/s OOK and 40 Gb/s PM-QPSK signals. Furthermore, optical dispersion compensation is not required any more, a major operational advantage. Commercial 40 Gb/s PM-QPSK systems were first introduced in 2007 [laperle07].

With the development of the 100 Gigabit Ethernet, a modulation format for its onward transmission across an optical DWDM network was urgently required. This triggered the development of 100 Gb/s PM-QPSK, which rapidly superseded 40 Gb/s technology. The higher capacity of a 100 Gb/s optical carrier allowed much better cost per bit performance compared to what was achievable at 40 Gb/s. The first commercial single carrier 100 Gb/s PM-QPSK solutions were introduced in 2010 [winzer10]. Competing solutions which achieved 100 Gb/s capacity by bonding two 50 Gb/s PM-QPSK carriers together (2C-PM-QPSK) [roberts09, nagarajan11] had only limited market success.
Coherent transponder technology was first introduced in long-haul transmission and subsequently penetrated other areas such as metro and submarine networks as well. For shorter metro links and inter-data center interconnects, the performance and spectral efficiency of coherent solutions is not always required, where the cost and power consumption of this technology can be prohibitive. As a consequence, alternative solutions based on direct detect technology have emerged to address this market segment. A 4 x 25 Gb/s multi-carrier ODB metro DWDM solution was introduced in 2011 to fulfill these needs for lower cost and lower power consumption and can operate on a 50 GHz or smaller channel grid to maximize spectral efficiency [tibuleac15]. Using multi-level modulation formats in which each constellation symbol carries more than one bit, the spectral efficiency can be further increased. The transmission bandwidth of an M-ary signal (i.e. a modulation format whose constellation is composed of M points) scales at a factor of $1/\log_2(M)$ compared to a binary signal operating at the same bit-rate. Multi-level IMDD systems are based on the use of the pulse-amplitude modulation (PAM), where only the amplitude of the optical field is modulated. Since the constellation points for this modulation format are "unipolar" (i.e. only zero or positive values can be encoded), a non-negligible loss in sensitivity is experienced. For this reason, multi-level IMDD formats have mainly been used in shorter reach applications. Utilizing the PAM4 modulation format to support the IEEE802.3bs and the OIF CEI56 standards, a dual-carrier 25GBaud PAM4 solution (two carriers occupying 100GHz of bandwidth) was demonstrated in 2016 for DWDM data center interconnects over 80km distance [filer16], offering twice the fiber capacity compared to earlier 25GBaud NRZ or ODB OOK implementations.

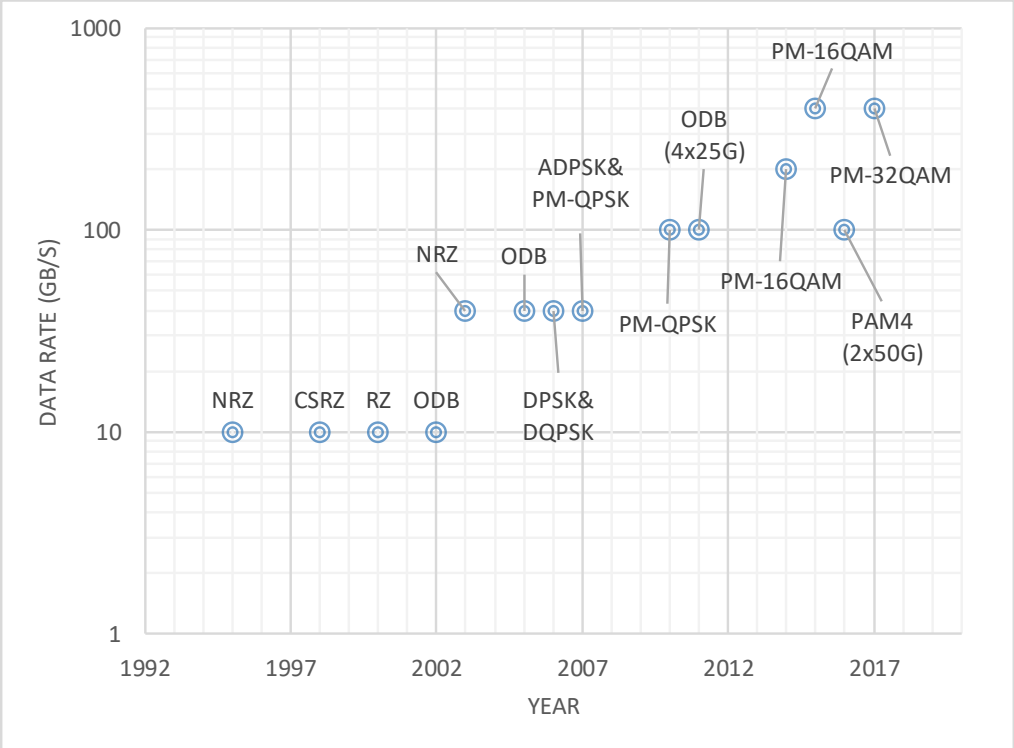

Fig. 4.1.4: Historical development of WDM transponder symbol rates and modulation formats

Higher order modulation has also improved the fiber capacity and cost per bit in coherent communications employing quadrature-amplitude modulation (QAM). Maintaining a symbol rate of about 30 GBd, 200 Gb/s PM-16QAM [gnauck10] (and 150 Gb/s PM-8QAM [ghazisaeidi13]) was first commercially introduced in 2014 providing 100% (or 50%) more channel and fiber capacity at the cost of roughly 25% (or 50%) of the 100 Gb/s PM-QPSK reach. 200 Gb/s 8QAM [lavigne16] and 400 Gb/s 32QAM [roberts17] have since then been presented as intermediate evolution steps. The next step change, though, is expected to be to 60 GBd technology, which has already been chosen as the basis for the 400G-ZR standard currently under development by the OIF. 60 GBd technology doubles the symbol rate per optical carrier and can be used with a variety of modulation formats, for example 200 Gb/s PM-QPSK, 300 Gb/s PM-8QAM, 400 Gb/s 16-QAM, 500 Gb/s 32-QAM and 600 Gb/s 64 QAM. Real time 400 Gb/s PM-16QAM was first demonstrated in 2015 [li16]. While doubling the symbol rate when maintaining the modulation format does not yield spectral efficiency gains for a given link distance, the use of fewer optical carriers results in cost, footprint and power savings. Moving forwards, future developments will concentrate on a) increasing the symbol rate even further and b) providing more flexibility by adapting the modulation format to the requirements and available margins on a given optical path. Fig. 4.1.45 graphically summarizes the historical development of WDM transponder symbol rated and modulation formats in commercial systems.

In the following sections, the architecture and performance of DWDM transponder line interfaces employing different modulation formats and detection schemes will be discussed. Section 4.2 starts with IMDD, to be followed by ODB in section 4.3, then differential phase modulation in section 4.4 and coherent interfaces in section 4.5. Different transponder types and hardware architectures will then be explained in section 4.6.

4.2 Intensity Modulation with Direct Detection

This section reviews the transmitter and receiver architectures required to generate and detect different types of IMDD optical signals. The intensity-modulation (IM) formats are introduced in Section 4.2.1, together with the most common line coding techniques used in IMDD transponders. The structures of several types of binary intensity-modulation (IM) transmitters are detailed in Section 4.2.2, while Section 4.2.3 describes the architecture of a receiver based on direct-detection (DD). Section 4.2.4 shows the back-to-back performance of binary IMDD systems, including the optimization of the TX and RX filters and the impact of sub-system components implementation. Tolerance to GVD and PMD is also analyzed. Finally, Section 4.2.5 discusses multi-level IMDD formats.

4.2.1 Intensity-Modulation

The complex envelope of an IM signal at the output of the modulator can be written as [proakis07]:

$$s_T(t) = \sum_k a_k \, q_T(t - kT_s) \tag{4.2.1}$$

where a_k are the symbols carrying the information, T_s is the symbol time interval (one symbol is sent every T_s seconds) and $q_T(t)$ is the optical pulse shape in the time domain. The symbols a_k may assume $M = 2^{n_b}$ values, where n_b is the number of information bits carried by each symbol. The symbol rate R_s is defined as the number of symbols that are transmitted in each time unit. It is equal to the inverse of the symbol time (R_s=1/ T_s) and is measured in baud or symbols per second. The bit rate R_b is defined as the number of bits that are conveyed per unit of time. It is measure in bit per second and is related to the symbol rate by $R_b = n_b R_s$. In case of binary IM, also known as On-Off Keying (OOK), $n_b = 1$ and $a_k \in \{0,1\}$. In each bit slot, one of two alternative waveforms can be transmitted, depending on the value of the information bit: $s_0(t) = 0$, $s_1(t) = q_T(t)$. These two analog waveforms are represented in the signal space [proakis07] by the two points shown in Fig. 4.2.1 (left). The constellation of quaternary IM, also known as PAM-4 (pulse amplitude modulation), is shown, as well. In practice, a "constellation diagram" shows all the possible symbols that can be transmitted by the system as a *constellation* of points, each characterized by and amplitude (distance from the origin) and a phase. The energy of each symbol is proportional to the square distance of the corresponding constellation point from the origin. For IM signals, only the intensity (amplitude) varies among different symbols, while the phase is constant, thus the constellation points lie on a single straight line.

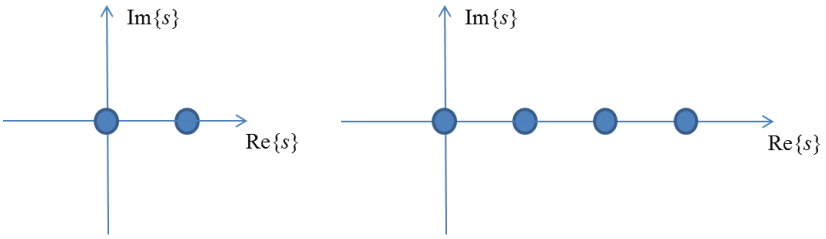

Fig. 4.2.1 OOK (left) and PAM-4 (right) constellations.

Depending on the shape of $q_T(t)$ in equation (4.2.1), the modulation format is defined as either non-return to zero (NRZ), when the time duration of $q_T(t)$ is close to the symbol interval T_s, or return-to-zero (RZ), when the duration of the pulse is lower than T_s and the power returns to zero between two successive "1" bits.

The power spectral density of the signal $s_T(t)$ is given by [proakis07]:

$$G_s(f) = \frac{|Q_T(f)|^2}{T_s}\sigma_a^2 + m_a^2 \sum_n \frac{|Q_T(nR_s)|^2}{T_s^2}\delta(f - nR_s) \tag{4.2.2}$$

where $Q_T(f)$ is the Fourier transform of the pulse $q_T(t)$ and m_a and σ_a^2 are the mean and variance of the random variable a_k, respectively. For instance, in case of OOK with equi-probable bits, m_a= σ_a^2=1/2. The power spectrum of IM signals

is composed of two terms: a continuous spectrum, which contains the information to be transmitted, and a discrete spectrum, which does not carry any information and whose lines are placed at the harmonics of the bit rate.

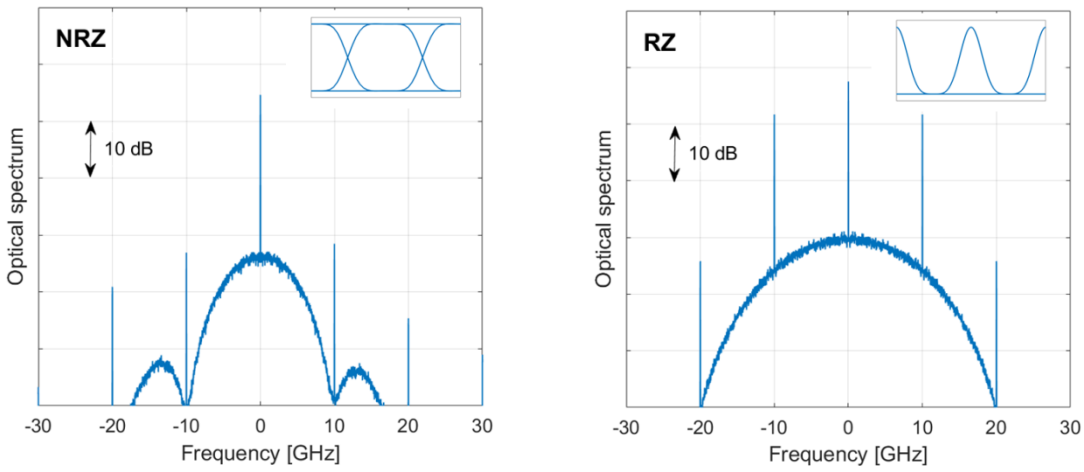

Fig. 4.2.2 Examples of NRZ and RZ optical spectra at 10 Gbaud. The corresponding eye diagrams are shown in the insets.

Figure 4.2.2 show two examples of noiseless spectra of NRZ and RZ signals. The time duration of RZ pulses is shorter, therefore their bandwidth occupation can be significantly larger. The "eye diagram", i.e. the synchronized superposition of all possible realizations of a signal viewed within a particular signaling interval (equal to $2T_s$ in Fig. 4.2.2), is also shown in the right upper part of the figures. The eye diagram can be easily displayed on an oscilloscope, is a useful tool for a the evaluation of the combined effects of channel noise and intersymbol interference on the transmitted or received signals [proakis07].

4.2.2 On-Off Keying Optical Transmitter

At the transmitter, there are two alternative ways to convert electrical data into optical form, known as *direct modulation* and *external modulation* [kazovsky96]. In case of direct modulation, the output power of the light source depends directly on the input drive current (or voltage), e.g. light is emitted from the device when a binary one is being transmitted and no light is emitted when a binary zero is being transmitted. The schematic of an OOK transmitter employing direct modulation is shown in Fig. 4.2.3(a). In case of external modulation, the light source is always on and an external modulator, driven by the electrical data signal, acts as a switch in order to control the intensity/phase of the generated optical signal. The schematic of an OOK transmitter employing external modulation is shown in Fig. 4.2.3(b).

Since transmitters employing directly modulated lasers (DMLs) do not require the use of external modulators, they are simpler and cheaper, but their transmission performance is strongly limited by the *chirp* phenomenon [tucker85, czotscher99] (a residual phase modulation superimposed to the desired intensity modulation). Interacting with chromatic dispersion, chirp may introduce a relevant performance penalty, limiting the application of direct modulation to short-reach transponders [sato05, eiselt16, lyubomirsky16]. In this chapter, we focus on external modulation by chirp-free Mach-Zehnder modulators (MZMs).

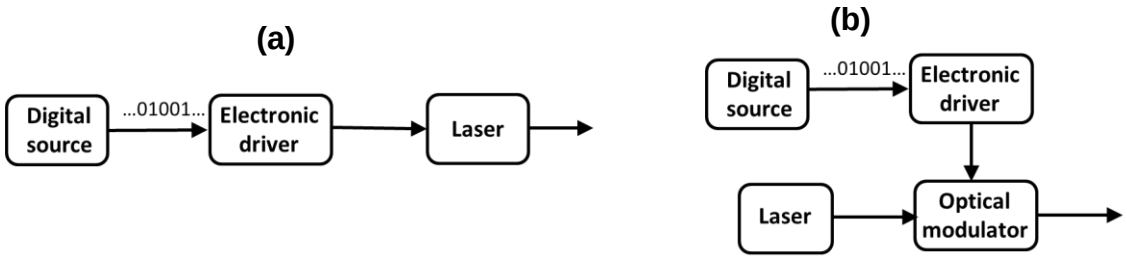

Fig. 4.2.3 Scheme of an OOK transmitter using (a) direct modulation and (b) external modulation.

NRZ-OOK transmitter

An NRZ-OOK signal can be generated using the transmitter scheme shown in Fig. 4.2.4, by properly driving a MZM with an RF signal carrying the information bits.

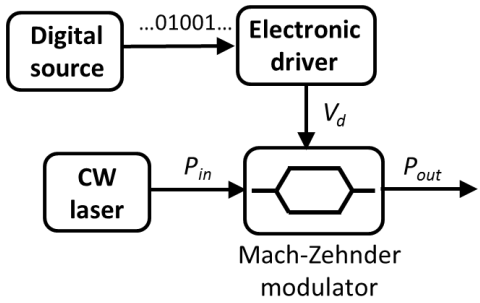

Fig. 4.2.4 Scheme of an NRZ-OOK transmitter.

The electrical field and power transmission of a MZM as a function of the applied voltage V_d are, respectively:

$$\frac{E_{out}}{E_{in}} = \sin\left(\frac{\pi}{2}\frac{V_d - V_0}{V_\pi}\right) - j\frac{1}{ER}\cos\left(\frac{\pi}{2}\frac{V_d - V_0}{V_\pi}\right) \quad (4.2.3a)$$

$$\frac{P_{out}}{P_{in}} = \sin^2\left(\frac{\pi}{2}\frac{V_d - V_0}{V_\pi}\right) + \frac{1}{ER}\cos^2\left(\frac{\pi}{2}\frac{V_d - V_0}{V_\pi}\right) \quad (4.2.3b)$$

where V_0 is the input voltage corresponding to minimum transmission, V_π is the input voltage difference between maximum and minimum transmission and ER is the extinction ratio of the MZM, defined as the ratio between the maximum and the minimum output power. A non-infinite value of ER means that the minimum transmission is not zero and a performance penalty can be experienced, as shown in Section 4.2.4.

The ideal power transmission of a MZM is shown in Fig. 4.2.5, where V_0=0 and ER=∞. The black circles indicate the 50% transmission points, also referred to as *quadrature points*. In order to generate OOK pulses, the MZM needs to be biased at a *quadrature point* and driven with an input voltage ranging from minimum to maximum transmission, as schematically shown in Fig. 4.2.6.

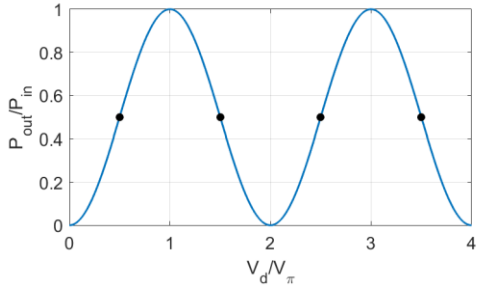

Fig. 4.2.5 Ideal MZM power transmission. The black dots indicate the quadrature points.

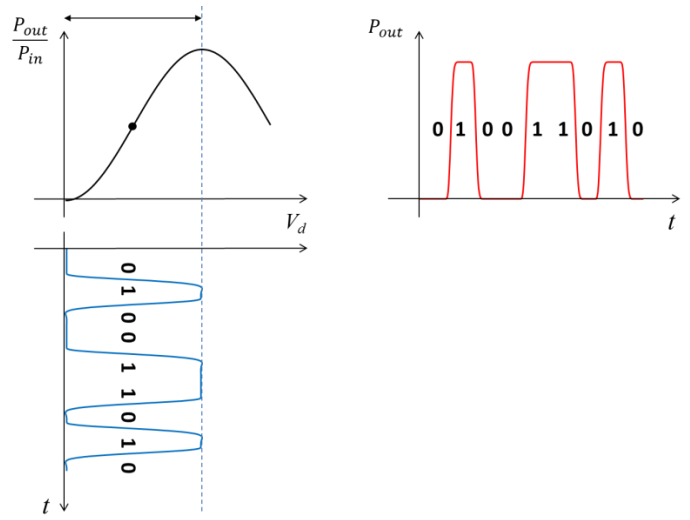

Fig. 4.2.6 MZM driven by an NRZ drive signal.

RZ transmitter

RZ transmitters can be implemented either by electronically generating an RZ drive waveform (using the architecture shown in Fig. 4.2.4) or by carving out pulses from an NRZ signal using an additional modulator, called a *pulse carve*r, as shown in Fig. 4.2.7. A pulse carver is usually implemented by driving a MZM with a sinusoidal signal. The width of the RZ pulses can be varied by tuning the sinusoidal signal amplitude and frequency. If the sinusoidal signal has a frequency equal to the bit rate and drives the modulator between minimum and maximum transmission, optical pulses with full-width half-maximum of 50% of the bit duration (i.e. with a duty cycle of 50%) are obtained. The pulse width can be reduced by driving the modulator between its transmission minima with a sinusoidal signal whose frequency is equal to half the bit rate. In this case, a duty cycle of 33% can be obtained, as shown in Fig. 4.2.8.

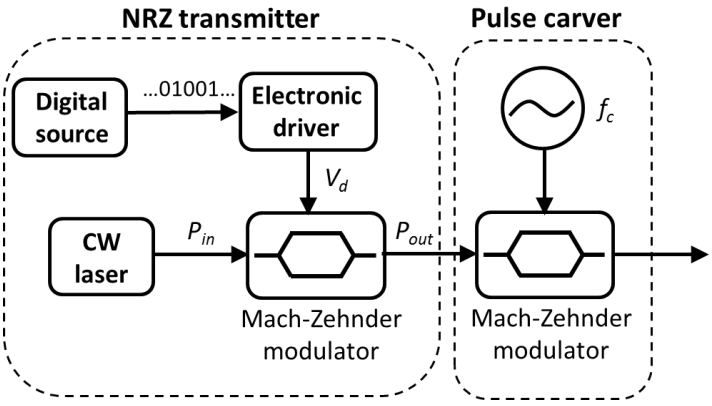

Fig. 4.2.7 Scheme of an RZ-OOK transmitter

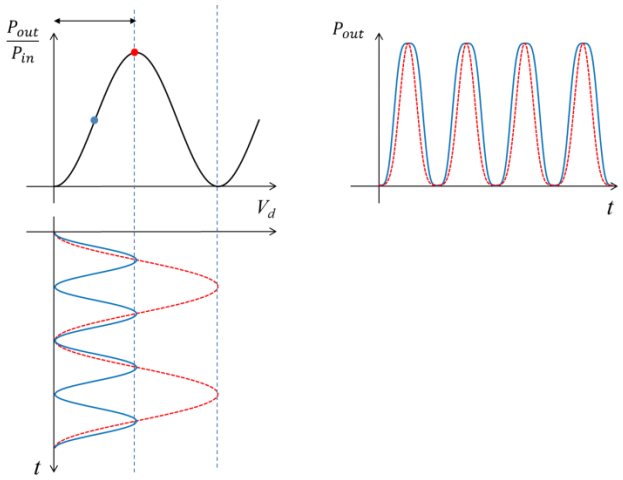

Fig. 4.2.8 MZM operation as a pulse carver to generate RZ pulses with 33%-duty-cycle (dashed lines) and 50%-duty-cycle (solid lines).

CSRZ transmitter

A modification of the RZ line coding, with an increased tolerance to nonlinear propagation effects, was proposed in [miyamoto99]. As for standard OOK formats, the information is encoded on the intensity levels {0,1}, but the phase is changed by π every bit, regardless of the data information. Thus, on average, the optical field of half the 1-bits has positive sign, while the other half has negative sign, resulting in a zero-mean optical field envelope. As a consequence, the carrier at the optical center frequency vanishes. For this reason, the format is called carrier-suppressed RZ (CSRZ). CSRZ signals can be generated using the same transmitter used for RZ (please see Fig. 4.2.8), sinusoidally driving the MZM in the pulse carver at half the data rate between its transmission maxima, as shown in Fig. 4.2.9. The result is the generation of pulses with 67% duty cycle and alternating phase. Note that the larger duty cycle leads to a lower optical filter penalty (due to either ISI or XTK) with respect to standard RZ pulses.

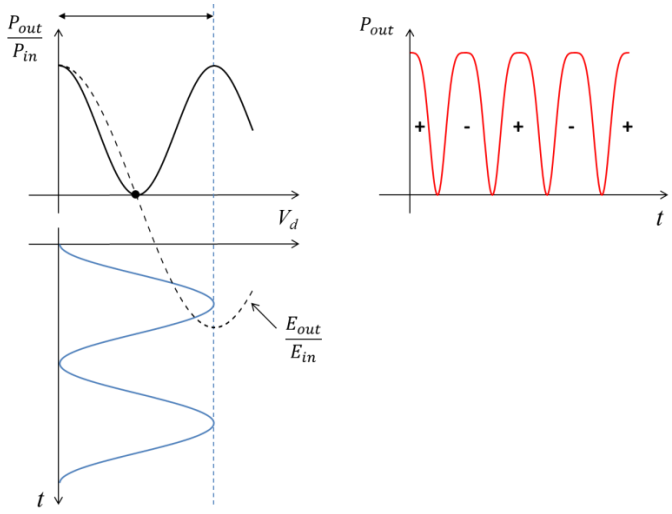

Fig. 4.2.9 MZM operation as a pulse carver to generate CSRZ pulses with 67% duty-cycle.

Chirped return-to-zero (CRZ) transmitter

The chirped-RZ modulation format is obtained by adding a controlled amount of phase modulation to RZ pulses. This can be achieved by inserting a bit-synchronous phase modulator, with an adjustable peak-to-peak level and phase relative to the center of the bit [bergano02], after a standard RZ transmitter (just like the one shown in Fig. 4.2.8). The generated optical phase term is equal to $e^{-jm\cos(2\pi f_0 t)}$, where m is the *phase modulation index* and f_0 is the sinusoidal modulation frequency, which is equal to the data rate. The applied phase modulation reduces the non-linear propagation distortions [saito91], but it also increases the signal spectrum bandwidth, and consequently the cross-talk between adjacent channels in a WDM system. The optimum amount of phase modulation for CRZ is thus a compromise between tolerance to linear and non-linear cross-talk. CRZ is typically used in ultra-long-haul point-to-point fiber communications, such as submarine systems, with a phase modulation index of approximately 1 rad [bakhshi01].
Alternatively to the three-stage modulation scheme (NRZ modulator, pulse carver, phase modulator), a dual-drive MZM can be used as a chirped pulse carver at various duty cycles by controlling the imbalance of the drive signal amplitudes or their relative phase, as shown in [winzer04].

4.2.3 Direct-Detection Optical Receiver

The general scheme of an optically-pre-amplified direct-detection receiver is shown in Fig. 4.2.10. It is composed of an optical amplifier, followed by an optical filter with impulse response $h_o(t)$, a photodetector, an electrical amplifier, an electrical filter with impulse response $h_e(t)$ and a threshold decision device.

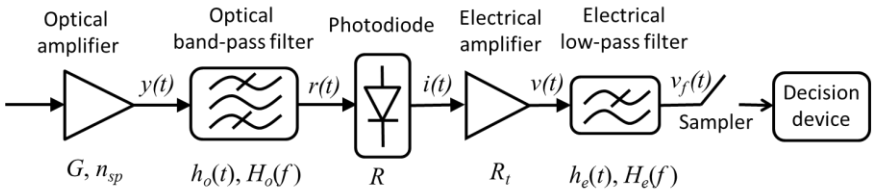

Fig. 4.2.10 Schematic of an optically pre-amplified direct-detection receiver.

The received optical field at the output of the optical amplifier can be written as:

$$y(t) = s_R(t) + n(t) \tag{4.2.4}$$

where $n(t)$ is the ASE noise introduced by the optical amplifier and $s_R(t)$ is the useful signal component, which is given by:

$$s_R(t) = \sum_k a_k\, q_R(t - kT_s) \tag{4.2.5}$$

where a_k are the information symbols and $q_R(t)$ is the received optical pulse after propagation in the optical fiber.
ASE noise is modeled as a white Gaussian noise with spectral density $N_0/2$ [kazovsky96], where:

$$N_0 = n_{sp} h\nu (G - 1). \tag{4.2.6}$$

n_{sp} is the spontaneous emission factor, h is the Plank's constant, ν is the transmission frequency and G is the amplifier gain. The noise figure F of the optical amplifier, defined as the ratio between the input and output signal-to-noise ratio, is approximately equal to $2n_{sp.}$

The signal at the output of the optical filter can be written as:

$$r(t) = s(t) + m(t) \tag{4.2.7}$$

with:

$$s(t) = s_R(t) * h_o(t),\ \ m(t) = n(t) * h_o(t) \tag{4.2.8}$$

where the star denotes a convolution and $m(t)$ is a colored Gaussian noise with power spectral density given by:

$$G_m(f) = \frac{N_0}{2} |H_o(f)|^2 \tag{4.2.9}$$

and variance given by:

$$\sigma_m^2 = \frac{N_0}{2}\int_{-\infty}^{+\infty}|H_o(f)|^2\,df = \frac{N_0}{2}\int_{-\infty}^{+\infty}|h_o(t)|^2\,dt \tag{4.2.10}$$

The detected current is proportional to the incident optical power $P_R(t)$, which is in turn proportional to the squared magnitude of the optical field as shown in equation (4.2.7):

$$i_R(t) \propto P_R(t) = |r(t)|^2 = |s(t) + m(t)|^2 = |s(t)|^2 + |m(t)|^2 + 2Re\{s(t)m^*(t)\} \tag{4.2.11}$$

The first term is the useful signal, the second term is the (noise x noise) beat term and the third term is the (signal x noise) beat term. The complete photo-detection current, including the noise signals generated by the electrical amplifier and the photodetector, can be written as:

$$i(t) = i_s(t) + i_{s,ASE}(t) + i_{ASE,ASE}(t) + i_{th}(t) + i_{sh}(t) \tag{4.2.12}$$

The terms on the right hand side represent the useful signal, the (signal x noise) and (noise x noise) beat terms, the thermal noise and the shot noise respectively [kazovsky96].

The signal after the electrical filter can be written as:

$$v(t) = R_t i(t) * h_e(t) = v_s(t) + v_{s,ASE}(t) + v_{ASE,ASE}(t) + v_{th}(t) + v_{sh}(t) \tag{4.2.13}$$

where R_t accounts for the photodiode and amplifier resistances and $h_e(t)$ is the impulse response of the electrical filter. The signal $v(t)$ is then sampled at the sampling instants $t_k = t_0 + kT$ and compared to a threshold v_{th}. The decision algorithm is then:

$$a_k = \begin{cases} 0 \text{ if } v(t_k) < v_{th} \\ 1 \text{ if } v(t_k) > v_{th} \end{cases} \tag{4.2.14}$$

In general, the system performance is limited by ASE noise, shot noise, and thermal noise. However, in pre-amplified multi-span DWDM systems as addressed in this chapter, shot noise and thermal noise are typically negligible compared to ASE noise. These systems are said to be "ASE limited" and their performance can be characterized by the optical signal-to-noise ratio (OSNR), which is defined as:

$$\text{OSNR} = \frac{P_S}{P_N} = \frac{P_S}{2N_0B_N} \tag{4.2.15}$$

where P_s is the average power of the optical signal at the input of the receiver optical filter, P_N is the ASE noise power on both polarizations measured over an optical reference bandwidth equal to B_N and N_0 is the corresponding single-sided ASE noise power spectral density, as shown in equation (4.2.6). Often a fixed reference bandwidth B_N of 12.5 GHz is used (corresponding to 0.1nm wavelength range), which is a standard setting in many optical spectrum analyzers. Alternatively, the symbol rate of the signal R_S can serve as reference bandwidth. In this chapter, we follow the latter approach.

In the 1.55 μm window and with sufficiently high optical amplifier gain, the OSNR (referenced to the symbol rate) can then be rewritten in logarithmic form as:

$$OSNR_{dB} = 58dBm + 10\log(P_s/1mW) - 10\log(F) - 10\log(B_N/R_S). \tag{4.2.16}$$

where the signal power P_s is given in mW and F is a known amplifier noise figure.

Figure 4.2.11 shows an example of an eye diagram after direct detection in an NRZ-OOK system limited by ASE noise (where the other noise terms are negligible). Due to the (signal x noise) beat term, the variance of noise is higher on the "1" level and, consequently, the optimum decision threshold v_{th} is closer to the "0" level.

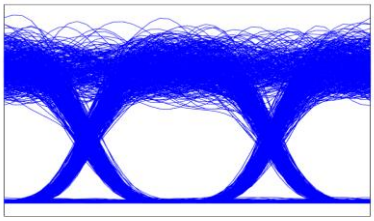

Fig. 4.2.11 Noisy NRZ-OOK eye-diagram after direct-detection.

4.2.4 Back-to-back Performance and Dispersion Tolerance

Ideal performance of a binary IMDD system

In ASE-limited systems, for all formats based on intensity-modulation and direct-detection the optimum receiver is based on the use of an optical filter whose impulse response is matched to the received pulses $q_R(t)$ [proakis07]. The optimum achievable performance is independent of the pulse shape, provided that the receiver optical filter is perfectly matched to the electrical field of the input signal. This optimum performance (also known as the *quantum limit* [atia99, winzer01]) is shown in Fig. 4.2.12 in terms of BER versus optical signal-to-noise ratio (OSNR), as defined by equation (4.2.16). In Fig. 4.2.12, the reference noise bandwidth is equal to the symbol rate. This means that the performance curve is valid for any value of the symbol rate (which for binary formats is equal to the bit rate).

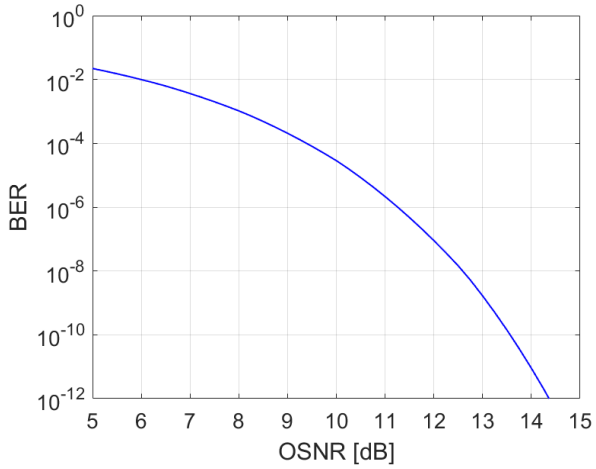

Fig. 4.2.12 Ideal performance of an IMDD optical system.

An analytical derivation of the BER of ASE-noise limited systems can be found in [humblet91]. In case of a matched optical filter (where M=2 in [humblet91]):

$$BER = \frac{1}{2}\left[e^{-\phi}(1+\phi) + 1 - Q_2\left(\sqrt{8\,OSNR}, \sqrt{2\phi}\right)\right] \quad \text{with} \quad \phi = \frac{v_{th}}{N_0 R_s} \tag{4.2.17}$$

where Q_2 is the generalized Marcum Q function of order 2 and ϕ is the normalized decision threshold that needs to be optimized in order to minimize the BER. A good approximation of the curve shown in Fig. 4.2.12 is:

$$BER \cong \frac{1}{2} e^{-0.98\,OSNR} \tag{4.2.18}$$

Optimization of filter bandwidths

The ideal performance of IMDD systems is independent of the pulse shape, but only if a perfectly matched optical filter is available, a condition which is difficult to achieve with analog optical filters. This is the reason why a different performance is typically achieved using NRZ and RZ/CSRZ pulses, with the latter showing a better sensitivity in most cases [atia99, winzer99, pauer01]. Several research papers have been published on the optimization of the optical and

electrical filters in order to achieve system performances as close as is possible to quantum limit [winzer01, pfennigbauer02, bosco01, bosco02, rebola02, lyubomirsky02]. The final results depend on the filter shapes, but the same general behavior is shown in all papers.

As an example of receiver filter optimization, we report in the following a set of simulation results obtained for NRZ, RZ and CSRZ transceivers. The transmitter architectures are the ones shown in figures 4.2.5 and 4.2.8. For NRZ, the bandwidth limitation of the TX is emulated using a 5-pole Bessel low-pass filter with 3 dB bandwidth equal to 0.7· R_s. The FWHM of RZ and CSRZ pulses obtained after the pulse carving operation is 50% and 66%, respectively. At the RX side, the passband optical filter has a 2nd-order Super-Gaussian shape with 3 dB bandwidth B_o. An ideal photodetector and a 5-pole Bessel electrical low-pass filter with 3 dB bandwidth B_e follow. Since we are considering ASE-noise limited systems, thermal and shot noise have not been included in the simulations. Noise loading was performed at the receiver input in order to set the OSNR value. The target BER was set to 10^{-3}, which corresponds to the pre-FEC BER value of standard hard-decision EFECs with 7% overhead [G975.1]. BER values were evaluated through direct error counting over 2^{18} bits.

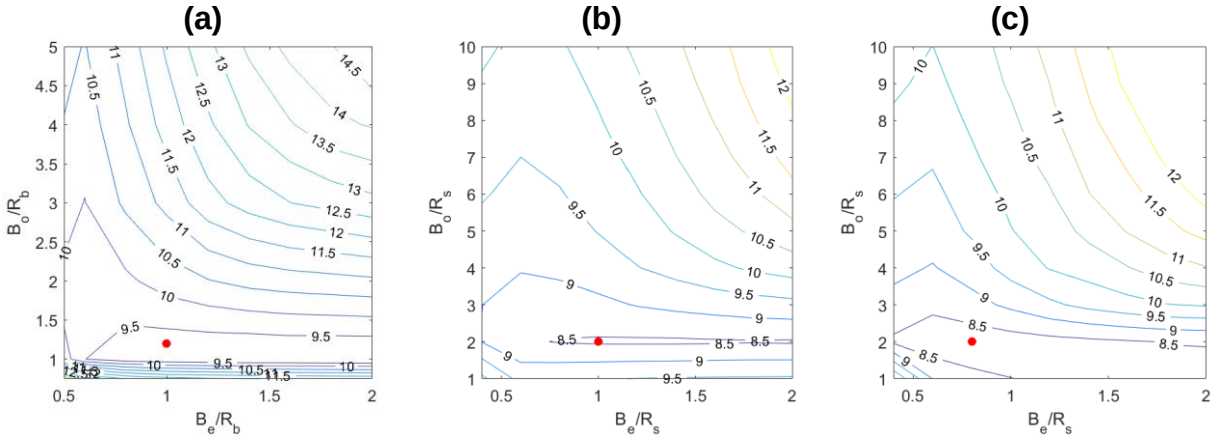

Fig. 4.2.13 Contour plots of the required OSNR to achieve BER=10^{-3} as a function of the receiver optical and electrical 3 dB bandwidths (B_o and B_e) for (a) NRZ, (b) and (c) CSRZ pulses. The red dots indicate the optimum points (i.e. the points with minimum required OSNR).

The results are shown in Fig. 4.2.13. The matched filter performance, identical for all systems, is obtained with an OSNR of 8 dB (over a bandwidth equal to R_s). For the NRZ case, the minimum OSNR (with a ~1 dB penalty with respect to the optimum matched filter performance) is achieved for B_o=1.2· R_s and B_e=R_s. For both the RZ and CSRZ format the penalty with respect to the matched filter performance is lower (~0.5 dB) and the optimum performance is achieved with a larger optical filter bandwidth equal to B_o=2· R_s. The reason why the performance of RZ formats is closer to the matched filter limit than NRZ is that there is a greater matching between the RZ pulses and the Super-Gaussian optical filter. The reason why the best performance for NRZ is obtained for a lower B_o value is that NRZ has an intrinsically better bandwidth-efficiency than RZ formats. It's also worth mentioning that RZ/CSRZ contours are less pronounced and therefore low penalty operation can be achieved over a wider (B_o,B_e) range than for NRZ.

Impact of finite MZM extinction ratio

The extinction ratio ER of a modulator corresponds to the ratio of the power P_1 used to transmit a logic level '1' to the power P_0 used to transmit a logic level '0'. Ideally, P_0=0 and ER=∞, but in practice P_0>0 and ER<∞, due to the presence of spontaneous emission noise and bias errors, as well as to electronic bandwidth limitations in modulator and driver.

A finite value of ER induces a performance penalty, which can be defined as the increase in average power needed to obtain the same bit error rate as an ideal pulse with infinite extinction ratio. In case of systems limited by additive white Gaussian noise (e.g. IMDD systems limited by thermal noise), the power penalty is given by [agrawal11]:

$$\delta_{ER} = 10\log_{10}\left(\frac{ER+1}{ER-1}\right) \tag{4.2.19}$$

In IMDD systems limited by ASE noise there is an additional penalty due to the increase of ASE noise on the zero-level, as shown in [fyath89]:

$$\delta_{ER} = 10\log_{10}\left(\frac{ER+1}{ER-1}\right) + 10\log_{10}\left(\frac{\sqrt{ER}+1}{\sqrt{ER}-1}\right) \tag{4.2.20}$$

Both equations (4.2.19) and (4.2.20) assume that the eye diagram is perfectly open, i.e. no inter-symbol interference (ISI) is present at the sampling instant. Figure 4.2.14 shows the power penalty as a function of the ER value, for both thermal-noise-limited and ASE-noise-limited receivers. In ASE-noise limited systems, the power penalty shown in Fig. 4.2.14 is equivalent to an OSNR penalty. Note that the penalty due to a finite ER might be lower in the presence of ISI and non-perfectly matched receivers, as shown in [rebola02, winzer01]. An approximate estimation of the required OSNR for a certain bit error rate can then be obtained if an effective extinction ratio is calculated from the electrical eye diagram at the receiver and the resulting penalty is added to the reference OSNR at the quantum limit.

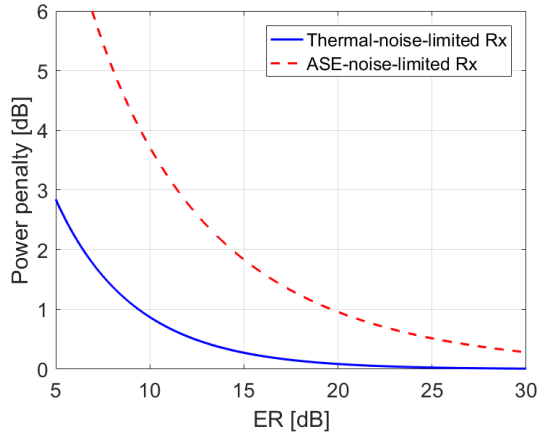

Fig. 4.2.14 Power penalty due to a finite ER in the absence of ISI.

Dispersion tolerance

Group velocity dispersion (GVD) is the result of the different wavelengths in a light beam arriving at their destination at slightly different times, due to the frequency dependence of the refractive index of the fiber. In the literature, the GVD phenomenon is also referred to as chromatic dispersion (CD). Polarization mode dispersion (PMD) is a form of modal dispersion where two different polarizations of light in a waveguide travel at different speeds, due to random imperfections and asymmetries [agrawal11]. Both phenomena cause a time spreading of the optical pulses, which in turn induces a performance penalty.

PMD is related to the *differential group delay* (DGD) caused by birefringence in optical fibers. However, birefringence varies along the length of the fiber, with different sections exhibiting a difference birefringence both in terms of levels of refractive index asymmetry and of relative orientation of the slow and fast polarization axis, also known as *principal states of polarization* (PSPs). As a result, the instantaneous value of DGD measured at the output of a fiber is a random variable, that is well approximated by a Maxwellian distribution [foschini99]. The PMD of a fiber is typically described through the parameter δ_{PMD}, which is an estimate of the average value of the statistical distribution of DGD.

The tolerance to GVD and PMD is strongly dependent on the symbol rate of the modulated signal. In particular, the pulse broadening $\Delta\tau_{CD}$ due to GVD and the average value of DGD between the two principal states of polarizations (normalized to the symbol time T_s=1/R_s) are given by [kahn07]:

$$\frac{\Delta\tau_{CD}}{T_s} = 2\pi|\beta_2|kR_s^2L\cdot 10^{-6} \qquad \frac{\langle\Delta\tau_{DGD}\rangle}{T_s} = \delta_{PMD}\sqrt{L}\,R_s\cdot 10^{-3} \tag{4.2.21}$$

where β_2 is the CD coefficient in ps^2/km, δ_{PMD} is the PMD parameter that can be found in fiber data sheets and is expressed in ps/$\sqrt{\text{km}}$, R_s is the symbol rate in Gbaud (which for binary formats is identical to the bit rate R_b), L is the fiber length in km and k is a coefficient which depends on the modulation formats, defined as the ratio between the spectral width of the modulated signal and the symbol rate. The coefficient β_2 is related to the dispersion parameter D [ps/nm/km] through the relationship: $D = -2\pi c\,\beta_2/\lambda^2$, where c is the speed of light in vacuum and λ is the propagation wavelength.

Equation (4.2.21) shows that the effect of DGD scales linearly with R_s, while the impact of GVD scales quadratically with R_s, for example a doubling in the symbol rate reduces the GVD tolerance by approximately a factor of 4. Also, the normalized pulse broadening due to GVD scales linearly with the normalized spectral width of the modulation format, resulting in a higher GVD tolerance (in linear propagation regime) for NRZ modulation formats. The tolerance to DGD is instead in general higher for RZ modulation formats [jopson99].

As an example, Fig. 4.2.15 shows the performance of NRZ, RZ and CSRZ modulation formats in the presence of either GVD or a first-order PMD. The simulation setup is the same as described in the first part of this section, with optimized RX filters bandwidth (corresponding to the red dots in Fig. 4.2.13). Linear fiber propagation was assumed, while first-order PMD was emulated by inserting a deterministic DGD value $\Delta\tau_{DGD}$ between the two principal sates of polarization (PSPs) [foschini99]. The worst-case of equal power splitting ratio between the two PSPs was considered [gene10].

In order to make the results symbol rate independent, the x-axes have been normalized with respect to either or R_s^2 (in the GVD plot) or R_s (in the PMD plot). The value of accumulated dispersion at a given symbol rate ($D\cdot L$) in ps/nm can be obtained by multiplying the value read on the x-axis of Fig. 4.2.15(a) by the coefficient $\left(\frac{2\pi c}{R_s^2\lambda^2}\cdot 10^6\right)$, with c expressed in m/s, R_s in Gbaud and λ in nm. In the 1.55 μm window, this corresponds to a multiplication by a factor ~$0.784\cdot 10^6/R_s^2$, with R_s measured in Gbaud. As an example, at 10.7 Gb/s the GVD tolerance for 2 dB penalty is equal to ~550 ps/nm for RZ and to ~750 ps/nm for NRZ and CSRZ. The DGD tolerance for 2 dB penalty at 10.7 Gb/s is instead equal to 44, 46.5 and 50 ps/nm for NRZ, RZ and CSRZ respectively. Note that, considering the statistical nature of DGD and allowing a limited outage time, the tolerated PMD (based on the δ_{PMD} parameter) is typically smaller than the tolerable DGD by a factor of ~3 [winzer04b].

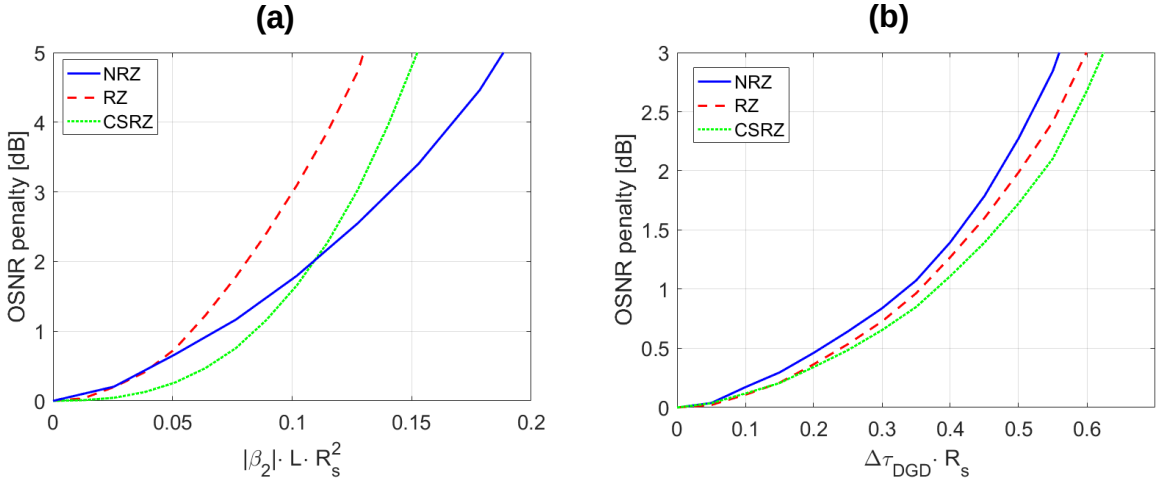

Fig. 4.2.15 GVD and first-order PMD tolerance of NRZ, RZ and CSRZ in terms of OSNR penalty with respect to back-to-back performance as a function of either (a) the normalized accumulated dispersion or (b) the normalized

DGD in the worst-case power splitting ratio between the two PSPs. The target BER is 10^{-3} and the value of the reference back-to-back OSNR (over a bandwidth equal to R_s) is 9.0, 8.5 and 8.4 dB for NRZ, RZ and CSRZ, respectively.

GVD and DGD tolerance, like back-to-back OSNR requirements, can depend in a non-negligible way on pulse and filters shapes used in the system, as well as on other residual distortions [G.Sup9, winzer03c, xie03, winzer06, poggiolini07]. In general, the impact on a modulation format of various impairments cannot be taken in isolation, but has to be evaluated in the context of the system it is operating in, which might include dispersion maps for non-linearity mitigation [tanaka99, gnauck08] and/or advanced digital signal processing techniques [savory08] that can for instance significantly increase the dispersion tolerance.

4.2.5 Multi-Level Intensity Modulation

An M-ary PAM optical signal can be obtained by applying an M-ary electrical signal to a MZM biased at the quadrature point, i.e., half point of its transfer characteristic (please see figures 4.2.5 and 4.2.7). The signal bandwidth of an M-ary signal is scaled by a factor $1/\log_2(M)$ compared to a binary signal operating at the same bit rate R_b, where $R_b=R_s \log_2(M)$ and R_s is the symbol rate.

For any optical extinction ratio, it is easy to show that the M levels should be equally-spaced (for example {0, 1/3, 2/3, 1} for PAM-4) when the noise is stationary, i.e., not signal dependent. This is the case, for example, when receiver thermal noise dominates. Given that the noise in an optically pre-amplified receiver is strongly signal dependent, it is clear that the lowest probability of error will be achieved when unequal level spacing is used [walklin99]. In particular, the photocurrent of each level is approximately Gaussian distributed, with a variance proportional to the intensity. In order to equalize the error probabilities at the M-1 different thresholds, the intensity levels should form a quadratic series, i.e., 0, 1, 4, 9, etc. [rebola00]. Under these assumptions, and assuming Gray coding, it can be shown that the BER in the optimum matched filter configuration is approximately given by [kahn04]:

$$BER \cong \frac{1}{\log_2(M)} \frac{1}{2} \operatorname{erfc}\left(\sqrt{\frac{3}{(2M-1)(M-1)} \mathrm{OSNR}}\right) \qquad (4.2.22)$$

where OSNR is the optical signal-to-noise ratio at the input of the DD receiver, as defined as in Eq. (4.2.15), with $B_N=R_s$. Equation (4.2.22) assumes single polarization filtering at the RX side, i.e. a polarization tracking receiver with a polarization analyzer that blocks the ASE polarized orthogonal to the signal [kahn04]. If no polarization filtering is used, the performance is slightly degraded (a fraction of dB of OSNR penalty is typically experienced). Figure 4.2.16 shows the ideal performance for PAM-2, PAM-4 and PAM-8 constellations, obtained using equation (4.2.22). Note that these results hold only at the zero dispersion point. If there is substantial residual dispersion, then a more equidistant level spacing is required. In general, best performance is obtained if the level spacing is optimized. Figure 4.2.17 shows an example of the back-to-back noisy eye diagrams after the post detection electrical filter with either quadratic or linear level spacing.

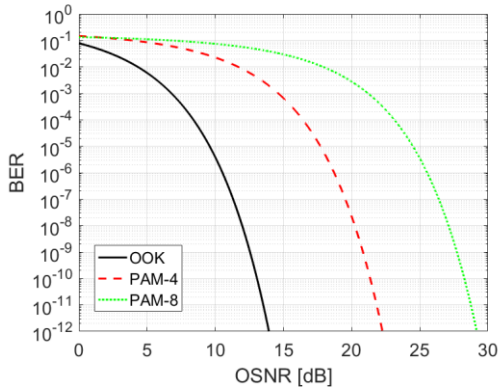

Fig. 4.2.16 Ideal performance of PAM signals with direct-detection in ASE-noise limited systems (with single-polarization filtering at the RX).

(a) **(b)**

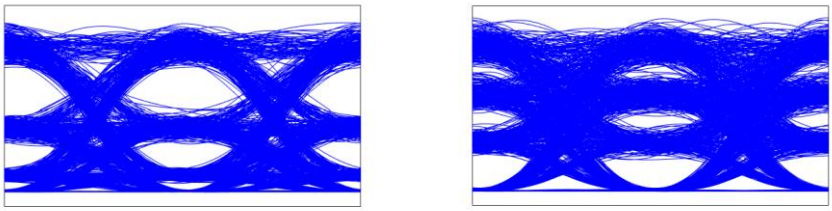

Fig. 4.2.17 Noisy eye diagrams after direct-detection of PAM-4 signals with (a) quadratic and (b) linear level spacing.

Fig. 4.2.18 shows the dispersion tolerance of PAM-4 with either equally spaced or quadratically spaced levels. 5-pole electrical Bessel low-pass filters with 3 dB bandwidth equal to R_s are used both at the TX and at the RX side, and a 2nd order Super-Gaussian passband optical filter with 3 dB bandwidth $2.5 \cdot R_s$ is present at the RX input. As expected, while the OSNR sensitivity in back-to-back is significantly better for the quadratic-spacing, the linear-spacing configuration has a higher tolerance to GVD.

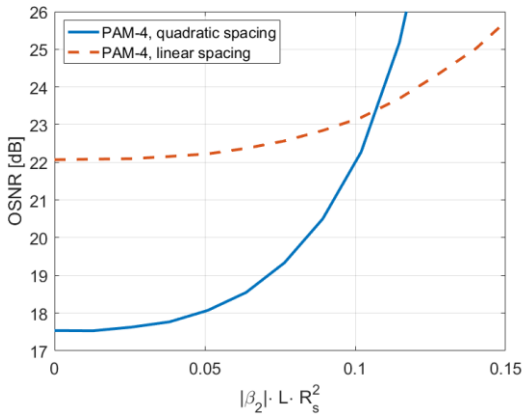

Fig. 4.2.18 GVD tolerance of PAM-4 in terms of OSNR required to obtain BER=10^{-3} as a function of the normalized accumulated dispersion.

4.3 Optical Duobinary with Direct Detection

This section reviews the transmitter and receiver architectures required to generate and detect different types of optical duobinary (ODB) signals. In Section 4.3.1, the duobinary modulation concept is introduced. Section 4.3.2 describes the practical implementation of a DB transceiver in an optical system, while Section 4.3.3. discusses its back-to-back performance and dispersion tolerance.

4.3.1 Duobinary Line Coding

Figure 4.3.1 shows the canonical duobinary transmitter structure that can be found in early papers and textbooks [proakis07]. It is composed of a precoder, followed by pulse shaping and a duobinary encoder.

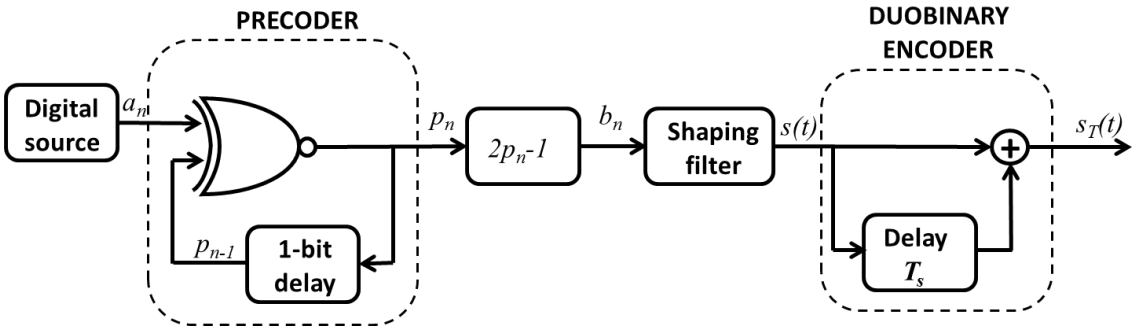

Fig. 4.3.1 Schematics of a duobinary transmitter.

The precoder transforms the information bit sequence $a_n \in \{0,1\}$ an into a new bit sequence $p_n \in \{0,1\}$ by performing a logical negative exclusive or (xor) operation between the sequences a_n and p_{n-1}. Then the normalization $b_n = 2p_n - 1$ is applied in order to obtain a bipolar sequence $b_n \in \{-1, +1\}$ [ono98]. Note that the presence of the precoder at the transmitter side allows for easier recovery of the data stream on a bit-by-bit basis and avoids error propagation at the receiver.

The modulated signal after pulse shaping is a standard bi-polar ASK signal which can be written as:

$$s(t) = \sum_n b_n \, q_T(t - nT_s) \tag{4.3.1}$$

where $b_k \in \{-1, +1\}$ are the binary symbols carrying the information, T_s is the symbol time and $q_T(t)$ is the pulse shape in the time domain. The duobinary coded signal is obtained by adding the data delayed by one symbol period to the present data [proakis, ono98], therefore:

$$s_T(t) = s(t) + s(t - T_s) = \sum_n b_n \, q_T(t - nT_s) + \sum_n b_n \, q_T(t - nT_s - T_s) = \sum_n b_n \, q_{T,DB}(t - nT_s) \tag{4.3.2}$$

with $q_{T,DB}(t) = q_T(t) + q_T(t - T_s)$. Note that the signal $s_T(t)$ can be also expressed as:

$$s_T(t) = \sum_n 2 \, c_n \, q_T(t - nT_s) \tag{4.3.3}$$

with $c_n = b_n + b_{n-1}$. The obtained symbols can thus assume three possible levels ($c_n \in \{-1,0,+1\}$), corresponding to the constellation diagram shown in Fig. 4.3.2.

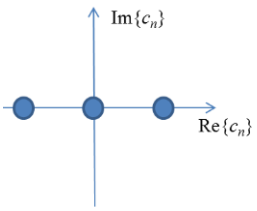

Fig. 4.3.2 The DB constellation diagram.

At the receiver side, the received signal is filtered by a filter with impulse response $h_R(t)$, generating the signal:

$$s_R(t) = \sum_n b_n\, q_{R,DB}(t - nT_s) = \sum_n 2\, c_n\, q_R(t - nT_s) \tag{4.3.4}$$

with $q_{R,DB}(t) = q_{T,DB}(t) * h_R(t) = q_R(t) + q_R(t - T_s)$ and $q_R(t) = q(t) * h_R(t)$. The correlated three level signal is finally demodulated into a binary signal by performing a "modulus" operation which converts "-1" and "+1" to a "1 bit" and "0" to a "0 bit". If the precoder shown in Fig. 4.3.1 is used, $|c_n| = a_n$ and the transmitted sequence is recovered without the need of any further processing. Note that the "modulus" operation is automatically performed by a DD receiver, where the input signal is squared by the photo-detector. Figure 4.3.3 shows an example of the noisy three level eye diagram before detection and the two level eye diagram after quadratic detection.

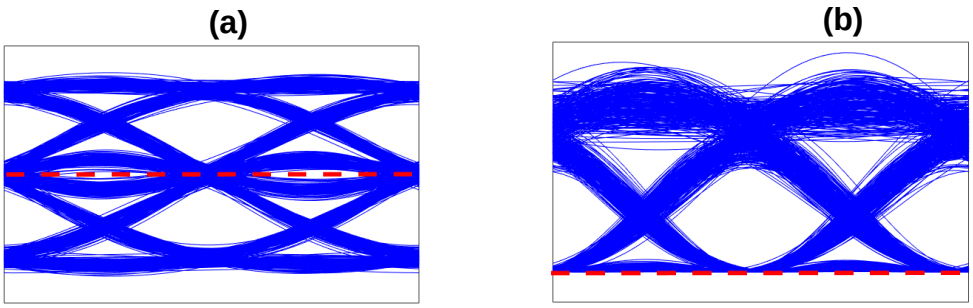

Fig. 4.3.3 The eye diagram of the noisy DB signal (a) before and (b) after DD. The red dashed lines indicate the zero power level.

If the pulse $q_R(t)$ satisfies the Nyquist criterion for the absence of ISI, i.e. $q_R(0) \neq 0,\ q_R(nT_b) = 0, \forall n \neq 0$, then the duobinary pulse $q_{R,DB}(t)$ has *two* identical non-zero samples T seconds apart [proakis07], where:

$$q_{R,DB}(0) = q_{R,DB}(T_s) \neq 0, \quad q_{R,DB}(nT_s) = 0, \quad \forall n \neq 0,1 \tag{4.3.4}$$

In practice, DB pulses are defined as pulses that spread over two bit intervals, i.e., pulses that correlate adjacent bits through the introduction of a controlled amount of ISI [proakis07].

The DB encoder is equivalent to a filter with transfer function:

$$H_{DB}(f) = 1 + e^{-j2\pi f T_s} = 2e^{-j\pi f T_s} \cos(\pi f T_s) \tag{4.3.5}$$

If an ideal low-pass filter is used for pulse shaping, the minimum bandwidth duobinary signal is obtained [proakis07], whose Fourier transform is equal to:

$$Q_{R,DB}(f) = \begin{cases} 2e^{-j\pi f T_b} \cos(\pi f T_s) & \text{if } |f| < 1/2T_s \\ 0 & \text{if } |f| > 1/2T_s \end{cases} \tag{4.3.6}$$

The time domain and frequency domain characteristics of the minimum bandwidth DB pulse are shown in Fig. 4.3.4. Note that the spectrum decays to zero smoothly, which means that physically realizable filters can be designed that approximate this spectrum very closely.

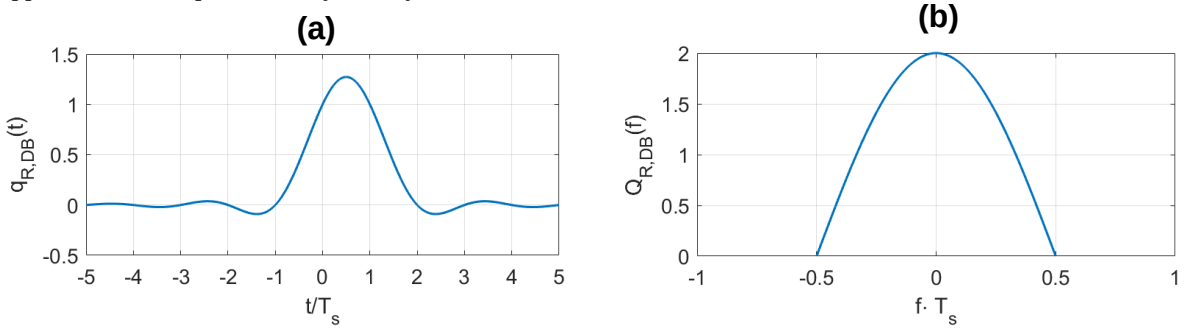

Fig. 4.3.4 The (a) time domain and (b) frequency domain characteristics of the minimum bandwidth DB pulse

In [bosco03] a rigorous analysis of the ASE noise limited back-to-back sensitivity performance of DB modulation was presented, showing that the quantum limit of DB modulation with DD is 0.91 dB better than that of IMDD (please see Fig. 4.3.5). However, as for IMDD, the quantum limit can be reached only using a perfectly matched filter at the receiver (before quadratic detection) [joindot08], a condition which is hard to achieve with analog optical filters. In fact, the actual performance of optical systems employing the DB modualtion depends on the particular method that is used to perform DB encoding and on the degree of optimization of the system components (for example optical and electrical filters), as shown in the following section.

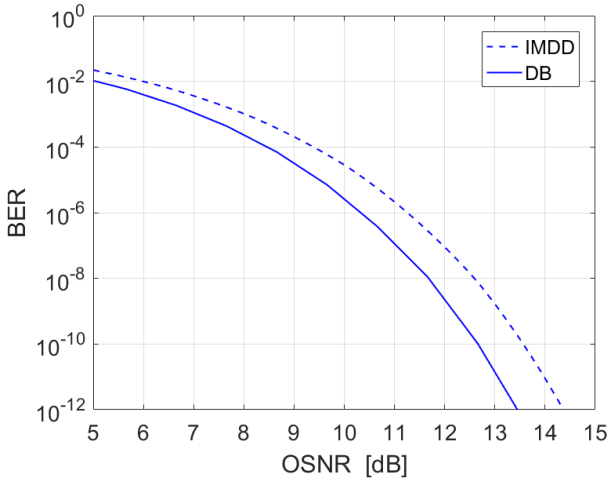

Fig. 4.3.5 Quantum limit of DB and binary signals with quadratic detection in ASE noise limited systems. The quantum limit of binary IMDD is also shown for comparison.

4.3.2 Optical Duobinary (ODB) Transmitter

The first implementations of optical duobinary (ODB) [gu93] were based on the generation of a three-level electrical signal by tight filtering of a standard electrical binary NRZ signal using a half data-rate raised-cosine filter with roll-off equal to 1. The three-level signal was then applied to a standard MZM to generate a three-level intensity-modulated optical signal. A conventional pre-amplified receiver was used, with an appropriately configured logic circuit to perform a dual threshold detection. The sensitivity penalty of this scheme with respect to binary NRZ was very high (~4 dB at BER=10^{-9}). One of the reasons for this penalty was the use of a pure intensity modulation, which allows to transmit and detect only positive values for the signal levels.

In order to reduce the sensitivity penalty, the use of mixed amplitude and phase modulation was proposed [yonenaga95], which allows the use of a symmetric DB constellation, as the one shown in Fig. 4.3.6. The ODB signal is obtained by applying a duobinary-encoded three-level electrical signal to a dual-drive MZM driven between its transmission minima (i.e. in a $2V_\pi$ range), as shown in Fig. 4.3.7. The signal is then decoded using a standard DD receiver. In [price95] a similar approach was proposed, approximating the delay-and-add operation needed to obtain the DB encoding using a narrow electrical filter. In practice, the effect of this modulation scheme is the generation of an optical signal with two intensity levels (corresponding to the "0" or "1" transmitted bits), but the optical phase of the "1" levels may be equal to either 0 or π, depending on the level ("+1" or "-1") of the three level driving signal.

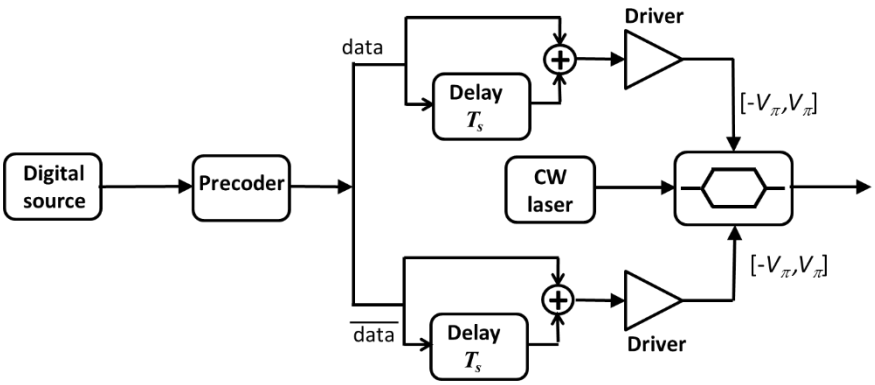

Fig. 4.3.6 Schematic of the AM/PM ODB transmitter.

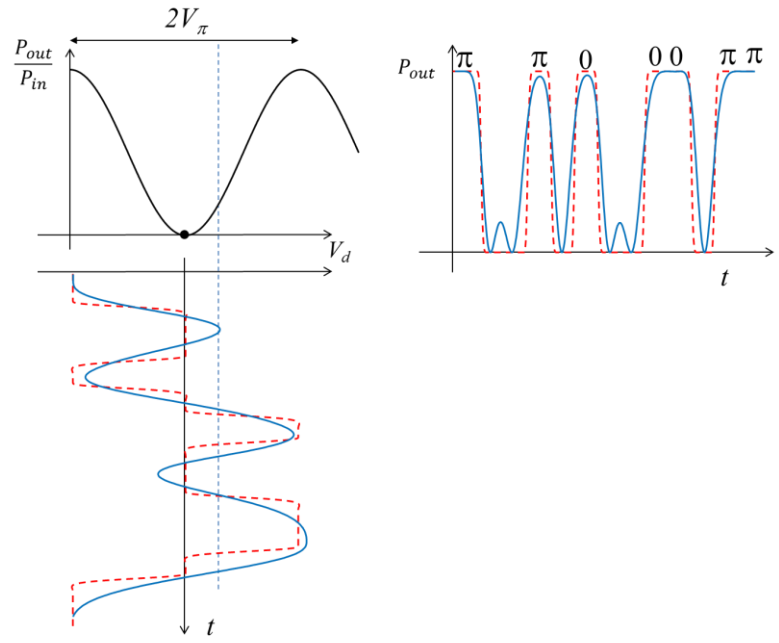

Fig. 4.3.7 MZM driven by a three level signal generated as in [yonenaga95] (dashed lines) or [pennincks97] (solid lines).

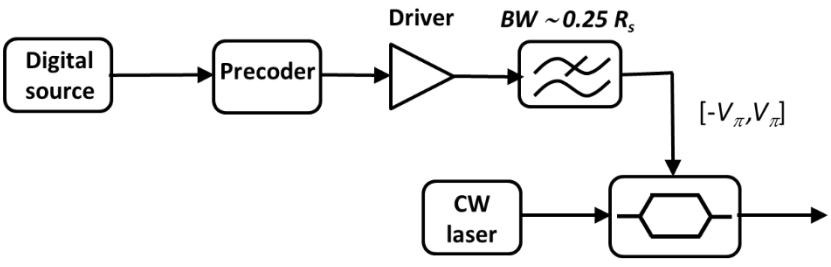

Fig. 4.3.8 Schematic of the PSBT transmitter.

These kinds of modulation techniques (based on a binary intensity signal with phase shifts at the higher levels) have subsequently been named phase-shaped binary transmission (PSBT) by Pennincks et al. in [pennincks96], where a similar but simpler approach was proposed, using a conventional low-pass Bessel filter and a single-drive MZM driven between its transmission maxima (please see Fig. 4.3.7). The schematic of the PSBT transmitter proposed in [pennincks96, pennincks97] is shown in Fig. 4.3.8, where the precoder is followed by a 5-pole Bessel electrical low-pass filter with 3 dB bandwidth $B_{TX,elt} \approx 0.25\ R_b$, which is a good approximation of the first arch of an ideal duobinary filter (a cosine-shaped filter). The modulator can be optionally followed by an optical transmitter filter for further pulse shaping [kim02]. Note that Fig. 4.3.8 shows a transmitter setup with single ended driver configuration and single ODB filter. In practice, an implementation is sometimes preferred in which both arms of the MZM are driven differentially instead. While such set-up requires two ODB filters (one for each MZM arm), each driver only needs to drive a swing of V_π instead of $2V_\pi$ which can lead to lower power dissipation and cost.

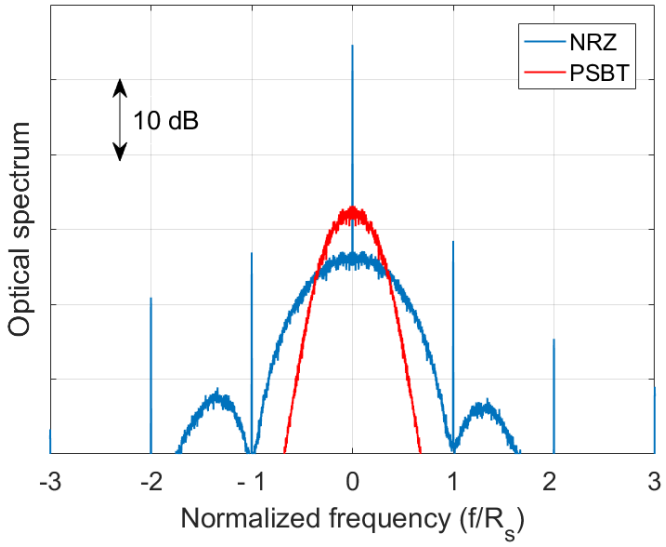

Fig. 4.3.9 A comparison between the power spectrum of NRZ and PSBT modulated signals.

Figure 4.3.9 shows an example of the power spectrum of a PSBT signal, compared with a standard NRZ signal spectrum. Besides its higher resilience to chromatic dispersion [gu96, pennincks96 , yonenaga97], the narrow optical spectrum of PSBT signals reduces the crosstalk between adjacent channels in ultra-dense WDM systems [ono98], allowing a higher spectral efficiency than IMDD systems to be achieved.

Among all ODB generation techniques, the PSBT is the one that has become the most popular in optical transmission research because of its simple implementation and good performance. The next subsection is devoted to a performance analysis of ODB transmission implemented through PSBT.

4.3.4 Back-to-Back Performance and Dispersion Tolerance

Several studies have been published on the optimization of electrical and optical filter bandwidths at the transmitter and/or the receiver side [zheng01, kim02, lyubomirsky04, bosco04b, pavlovic05], in order to improve the back-to-back performance of PSBT transceivers and approach the theoretical curve shown in Fig. 4.3.5. All these studies yielded similar results, which are summarized below:

- The optimum electrical filter bandwidth at the transmitter is in the range 0.25-0.35 R_s.
- The use of an optical filter at the transmitter with optimized bandwidth (around 0.75 R_s) can slightly improve the performance.

- The sensitivity can be significantly improved by using a tight optical filter at the receiver (with bandwidth around 0.75 R_s), and the use of the typical bandwidth of MUX/DEMUX in optical systems can significantly degrade the back-to-back performance.
- The optimum electrical bandwidth of the receiver is typically higher than $2R_s$ and the use of the typical bandwidth values around 0.75 R_s can significantly degrade the performance.

Note however that the above parameters and results are not all independent. In fact, optical and electrical filter bandwidth can be traded-off to some extent. As an example, a narrow optical and wide electrical RX filter can produce similar results than a wider optical filter and a narrower electrical one, as also shown in the following analysis.

Figure 4.3.10 shows an example of back-to-back performance of PSBT, which compares three different system scenarios at the quantum limit in ASE noise limited systems:
- System 1 (an optimized system): 5-pole Bessel electrical low-pass filters with 3 dB bandwidth 0.32 R_s at the TX and 3.5 R_s at the RX; second-order Super-Gaussian RX optical passband filter with 3 dB bandwidth 0.69 R_s.
- System 2 (a realistic PIN RX, with 7.5 GHz bandwidth at 10 Gbaud or 30 GHz bandwidth at 40 Gbaud): 5-pole Bessel electrical low-pass filters with 3 dB bandwidth 0.29 R_s at the TX and 0.75 R_s at the RX; second-order Super-Gaussian RX optical passband filter with 3 dBbandwidth 0.7 R_s.
- System 3 (standard filter bandwidths at the RX for both electrical and optical filters, for example $B_{RX,elt}$ =7.5 GHz and $B_{RX,opt}$ = 35 GHz at 10 Gbaud, with a channel spacing equal to 50 GHz, typical for WDM systems): 5-pole Bessel electrical low-pass filters with 3 dB bandwidth 0.24 R_s at the TX and 0.75 R_s at the RX; second-order Super-Gaussian RX optical passband filter with 3 dB bandwidth 3.5 R_s.

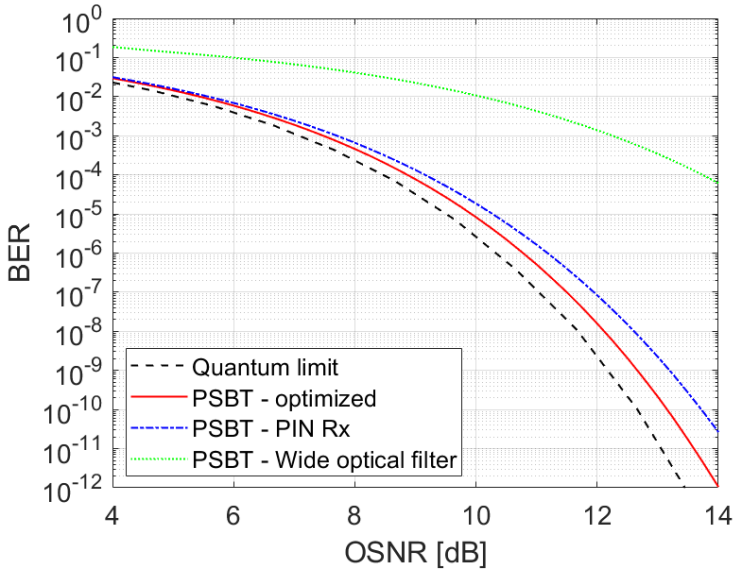

Fig. 4.3.10. BER versus OSNR characteristics for three configurations of PSBT. The theoretical limit curve is also shown for comparison.

The optimized PSBT (system 1) has ~0.4 dB penalty with respect to the quantum limit curve both at a BER=10^{-3} and a BER=10^{-9}. In the more realistic scenario using a standard PIN RX (system 2), the penalty is higher, slightly exceeding 0.6 dB at a BER=10^{-3} and 1 dB at a BER=10^{-9}. Note that the use of a wide optical filter at the RX (system 3) yields a much worse performance, i.e. ~5 dB OSNR penalty at a BER of 10^{-3} with respect to the theoretical limit [lyubomirsky04].

Impact of RX optical filter detuning

One possible drawback of using narrow bandwidth optical filtering to tailor the optimum DB pulse shape is the penalty that may be incurred when the carrier frequency drifts away from the filter center frequency [kim02]. Figure 4.3.11 shows the impact of a frequency detuning Δf between the center frequency of the optical RX filter and the TX laser, in terms of OSNR required to achieve a BER=10^{-3} as a function of the normalized detuning $\Delta f/R_s$. Due to the narrow bandwidth of the optical filter, the performance of the optimized ODB system is extremely sensitive to the frequency offset. The results shown in Fig. 4.3.11 demonstrate that the center of the optical filter should be aligned to the carrier frequency within $\pm 0.15 \cdot R_s$ in order to maintain the sensitivity advantage over the wide filter ODB.

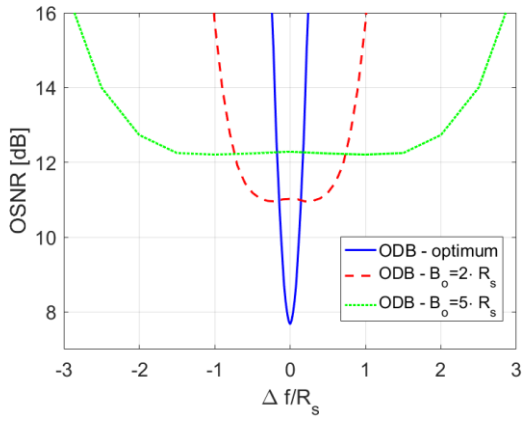

Fig. 4.3.11 Impact of frequency offset between carrier and optical filter for ODB with optimized RX optical filter bandwidth ($0.69 \cdot R_s$) and with larger RX filter bandwidths ($2 \cdot R_s$ and $5 \cdot R_s$), in terms of required OSNR to obtain a BER equal to 10^{-3}. The electrical filter bandwidths have been optimized in each case.

Dispersion tolerance

Due to its narrower spectral width, ODB modulation has a significantly higher tolerance to GVD than binary IMDD. The behavior of ODB in the presence of GVD, though, is strongly dependent on the optical filter bandwidth, as shown in Fig. 4.3.12(a), where the performance of the IMDD-NRZ format is also shown for comparison. The tolerance to PMD is however in general lower for ODB formats [winzer06], as shown in Fig. 4.3.12(b). In all cases, the TX and RX electrical filter bandwidths have been optimized in the back-to-back configuration.

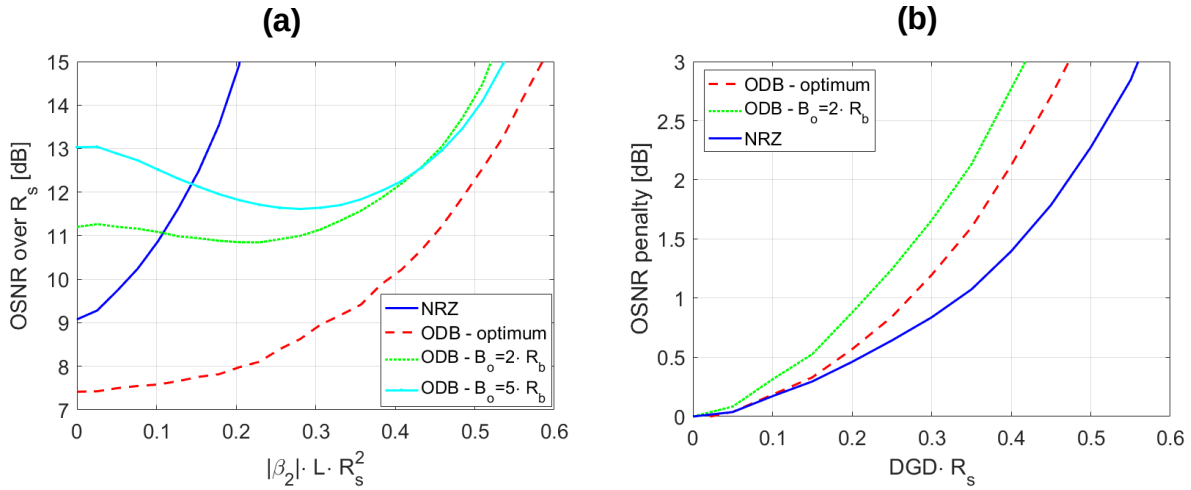

Fig. 4.3.12 (a) GVD tolerance of NRZ and three configurations of ODB in terms of required OSNR (over a bandwidth equal to R_s) to obtain BER=10^{-3} as a function of the normalized accumulated dispersion. (b) First order PMD tolerance of NRZ and three configurations of ODB in terms of OSNR penalty as a function of the normalized DGD in the worst case power splitting ratio between the two PSPs.

4.4 Differential Phase Modulation with Interferometric Detection

This section reviews the transmitter and receiver architectures required to generate and detect different types of optical signals based on differential phase-modulation. In Section 4.4.1 the concept of differential phase modulation is introduced. Section 4.4.2 describes the optical transmitter structure for the generation of binary and quaternary formats with differential phase modulation, named differential phase shift keying (DPSK) and differential quadrature-phase shift keying (DQPSK), respectively. Note that DPSK is also referred to as DBPSK in the literature. In Section 4.4.3, the interferometric receivers used to extract the phase difference between DPSK and DQPSK symbols are described, while section 4.4.4 shows the back-to-back performance of DPSK/DQPSK systems, focusing on the impact of realistic implementation penalties at the transmitter and receiver sides.

4.4.1 Differential Phase-Shift Keying

Phase-shift keying (PSK) is a modulation technique which encodes the information in the phase of the constellation symbols, keeping the amplitude constant. For instance, in the binary version of PSK (known as BPSK or 2PSK), a "1" may correspond to the phase value 0 and a "0" to the phase value π. In general, for an M-level PSK constellation (MPSK), the M information symbols are encoded into M phase values, i.e. $\varphi_n = 2n\pi/M$ with n = 0,1,…,M-1. The complex envelope of PSK modulated signals can be written as equation (4.2.1), with $a_k = e^{j\varphi_k}$ and $\varphi_k \in \{\varphi | \varphi = \frac{2\pi n}{M}$, with $n = 0,1,..,M-1\}$. Figure 4.4.1 shows examples of PSK constellations with M=2, 4 and 8.

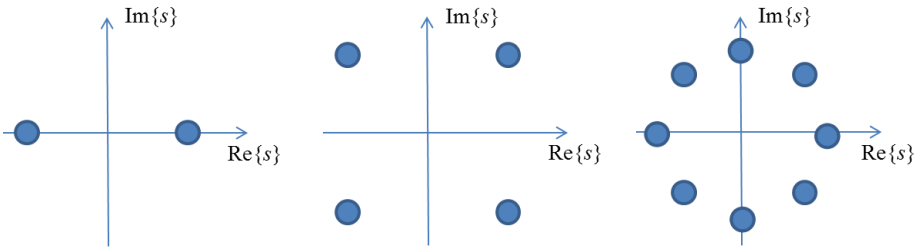

Fig. 4.4.1 Examples of 2PSK, 4PSK and 8PSK constellations

In order to decode a phase modulated signal, the estimate of the absolute carrier phase is required [proakis07]. In practice, however, the carrier phase is extracted from the received signal by performing some nonlinear operation that introduces a phase ambiguity. For instance, the widely used Viterbi&Viterbi phase estimation algorithm [ip07], which raises the signal to the power of M in order to remove the modulation, generates a phase ambiguity equal to $2\pi/M$. Consequently, an absolute estimate of the carrier phase is typically not available for demodulation.

A possible solution to this problem consists in encoding the information in the phase difference between two consecutive symbols. For example, in binary PSK an information bit "1" is transmitted by shifting the phase of the carrier by π with respect to the previous signaling interval, while an information bit "0" is transmitted by applying a zero phase shift relative to the previous signaling interval. In 4PSK the relative phase shifts between successive intervals are 0, $\pi/2$, π, and $3\pi/2$, corresponding to the four possible transmitted bit pairs (00, 01, 11 and 10, respectively). Differentially encoded binary (M=2) and quaternary (M=4) modulation formats are often referred to as differential PSK (DPSK) and differential quadrature phase-shift eying (DQPSK).

Tables 4.4.1 and 4.4.2 show the logical operations of the differential precoder that is used to encode the information bits on the phase difference of the carrier between two consecutive signal intervals for DPSK and DQPSK, respectively [ho05]. For DPSK, the input bit sequence a_k is encoded onto the output sequence p_k, that is used to generate the DSPK waveforms transmitted over the channel. For DQPSK, pairs of input bits (a_k and b_k) are encoded onto two output bit sequences p_k and q_k, corresponding to the in-phase and quadrature components of the DQPSK symbols to be transmitted over the channel.

Input bit a_k	Phase difference	Output bit p_k
0	π	$\overline{p_{k-1}}$
1	0	p_{k-1}

Table 4.4.1 The logical operations of the differential precoder for DPSK.

Input bits a_k b_k	Phase difference	Output bits p_k q_k
0 0	π	$\overline{p_{k-1}}$ $\overline{q_{k-1}}$
0 1	$\pi/2$	q_{k-1} $\overline{p_{k-1}}$
1 0	$3\pi/2$	$\overline{q_{k-1}}$ p_{k-1}
1 1	0	p_{k-1} q_{k-1}

Table 4.4.2 The logical operations of the differential precoder for DQPSK [ho05].

The optimum detector for PSK signals is based on coherent detection, i.e. the received signal is multiplied by a carrier with the same frequency and phase of the transmitted signal and then goes through a low-pass matched filter [proakis07]. Using the optimum demodulator, the bit error probability of both BPSK and QPSK modulations is given by:

$$BER = \frac{1}{2}\text{erfc}\left(\frac{E_b}{N_0}\right) \tag{4.4.1}$$

If differential encoding is applied at the transmitter, the same coherent demodulator can be used, followed by a phase comparator that compares the phases of the demodulated signal over two consecutive intervals in order to extract the information. Coherent demodulation of differentially encoded PSK results in a higher BER than standard PSK modulations. In particular, with differentially encoded PSK an error in the demodulated phase of the signal in any given interval will usually result in decoding errors over two consecutive symbols. Consequently, the symbol error rate (SER) of differentially encoded MPSK is approximately twice the SER of MPSK with absolute phase encoding.

As will be shown in Section 4.4.3, differentially encoded PSK signals can also be demodulated by a direct-detection optical receiver, composed of a pair of conventional photodetectors, through the use of an optical device called the asymmetric MZ interferometer (AMZI) which is able to convert the phase coded signal into an intensity coded signal before quadratic detection. The price to pay to avoid the use of standard coherent detection is a performance penalty with respect to the theoretical results determined by equation (4.4.1).

4.4.2 DPSK and DQPSK Optical Transmitter

Two possible structures of the DPSK optical transmitter are shown in figures 4.4.2 and 4.4.3. The first one is based on the use of a phase modulator, driven in the $[0, V_\pi]$ range. The second and most common one employs an MZM, biased at zero power transmission and driven between its transmission maxima. A pulse carver such as the one shown in Fig. 4.2.8 can be added to generate RZ pulses.

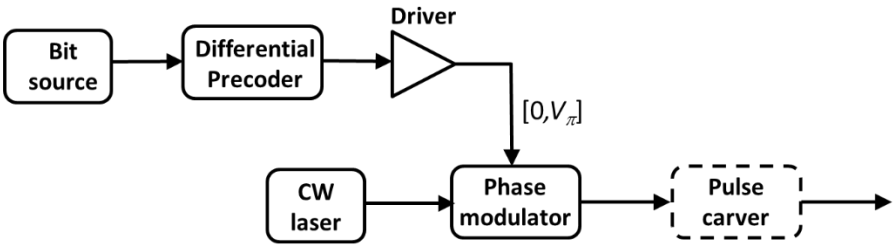

Fig. 4.4.2 A schematic of a DPSK transmitter using a phase modulator.

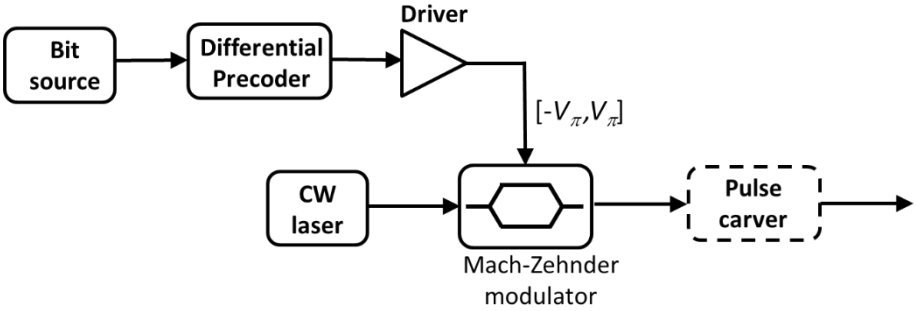

Fig. 4.4.3 A schematic of a DPSK TX using an MZ amplitude modulator.

Figure 4.4.4 shows the schematic of a DQPSK transmitter, which employs an IQ transmitter composed of two MZM's, one for each quadrature of the QPSK modulation. Each MZM is biased at zero power transmission and driven between its transmission maxima. A phase shift of π/2 is introduced between the two arms before recombining the signals. A pulse carver such as the one shown in Fig. 4.2.8 can be added to generate RZ pulses.

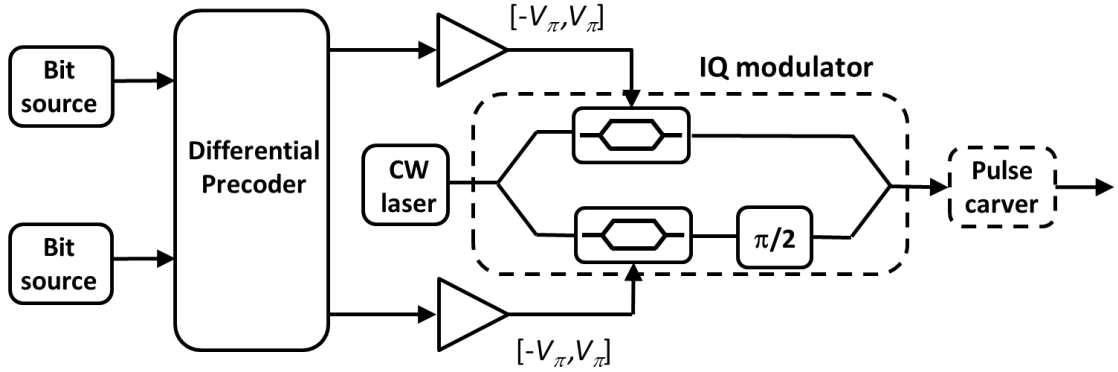

Fig. 4.4.4 A schematic of a DQPSK TX.

4.4.3 Interferometric Receiver

The DPSK RX structure is shown in Fig. 4.4.5. The optical pre-amplifier is followed by an optical filter and an AMZI with differential delay $T_d = 1/R_s$, where R_s is the symbol-rate. Within the AMZI, the input signal is split onto two paths and combined after a path difference corresponding to one bit delay. If $E(t)$ is the optical field at the input of the AMZI, then the signals at the output of the two arms can be written as:

$$E_1(t) = \frac{1}{2}\left[E(t) + E(t - T_d)e^{j\delta\phi}\right] \quad (4.4.2a)$$

$$E_2(t) = \frac{1}{2}\left[E(t) - E(t - T_d)e^{j\delta\phi}\right] \quad (4.4.2b)$$

where $\delta\phi$ is a quantity that should ideally be equal to 0 and that can be controlled, typically by thermal adjustments. A balanced photodetector (BPD) follows, which consists of two photodetectors (one for each output branch of the AMZI), with responsivities R_1 and R_2, connected so as to subtract their currents from each other, and a post-detection electric filter. Ideally, for optimal reception, it should be the case that $R_1 = R_2$ and $\delta\phi = 0$.

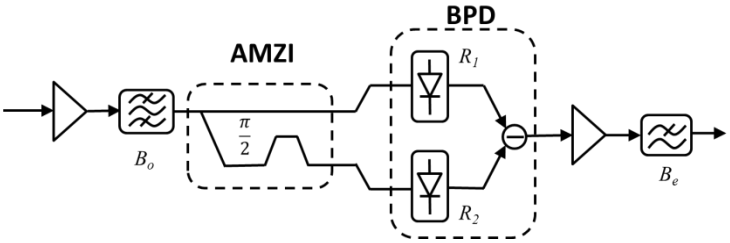

Fig. 4.4.5 A schematic of a DPSK RX.

In practice, the AMZI can be viewed as a filter that converts phase modulation into amplitude modulation. The amplitude modulation is then detected by the photodiodes. When two subsequent bits have the same phase then $E_1(t) = E(t), E_2(t) = 0$, while, if they have opposite phase then $E_1(t) = 0, E_2(t) = E(t)$. In practice, the AMZI performs a *differential demodulation* of the received signal.

The two ports form slightly different IM signals, which give rise to different "eyes", as shown in Fig. 4.4.6, due to the different transfer functions of the two arms of the AMZI (in the absence of phase modulation, the upper and lower branches experience a constructive or destructive interference, respectively). The BPD sums the eyes reinforcing each other. In principle, DPSK can be detected using only one photodiode, on either Out1 or Out2. However, using detection on only one port, the 2.7 dB sensitivity advantage over IMDD is lost [winzer03b].

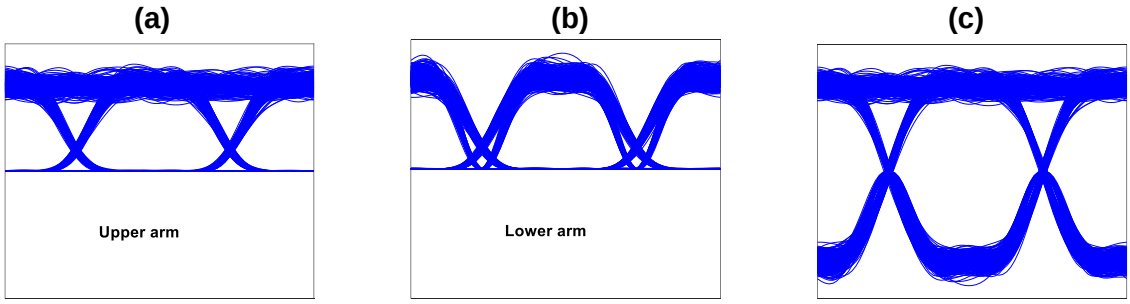

Fig. 4.4.6 Electrical eye diagrams generated at the output of the (a) upper and (b) lower arms of the AMZI and at the (c) output of the balanced photodetector.

The AMZI can also be viewed as a 3 dB splitter followed by a pair of filters whose transfer functions are given by:

$$\left|H_p(f)\right|^2 = \cos^2(\pi(f - f_0)T_d + \delta\phi/2) \quad (4.4.3a)$$

$$|H_m(f)|^2 = \sin^2(\pi(f - f_0)T_d + \delta\phi/2) \quad (4.4.3b)$$

Assuming that DPSK is transmitted at an optical frequency f_0, the optimum demodulation requires that $\left|H_p(f_0)\right| = 1$ and $|H_m(f_0)| = 0$. The phase error $\delta\phi$ can thus be seen as an incorrect tuning of the AMZ filter, by a quantity $\Delta f = R_s\delta\phi/2\pi$. This corresponds to a shift by Δf of the optical frequency of the AMZ filter transfer function. Figure 4.4.7 shows the AMZI transfer functions of equation (4.4.3) when $\delta\phi = 0$.

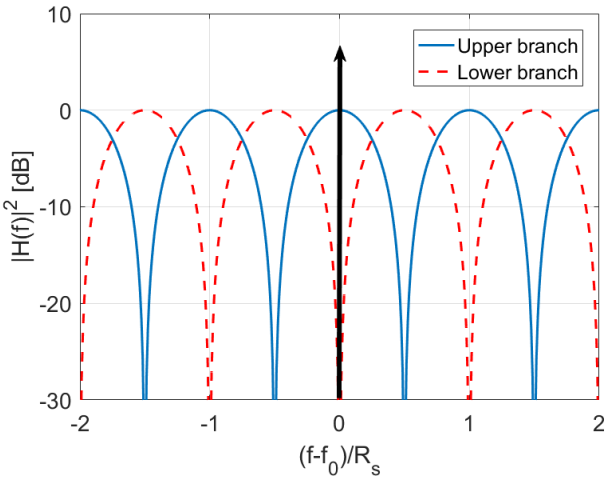

Fig. 4.4.7 Ideal AMZI transfer functions (given by equation (4.4.3), with $\delta\phi = 0$). The thick black line corresponds to the center frequency of the signal at the input of the AMZI.

DQPSK receiver

The DQPSK RX structure is shown in Fig. 4.4.8. It consists of an optical filter, a pair of AMZIs with a differential delay ideally equal to the time duration of a transmitted symbol, each followed by a BPD consisting of two photodetectors (one for each output branch of the AMZIs), connected so as to subtract their currents from each other, and then followed by a post-detection electric filter. The differential optical phase between the interferometer arms should be set to π/4 and −π/4 for the upper and lower branches, respectively.

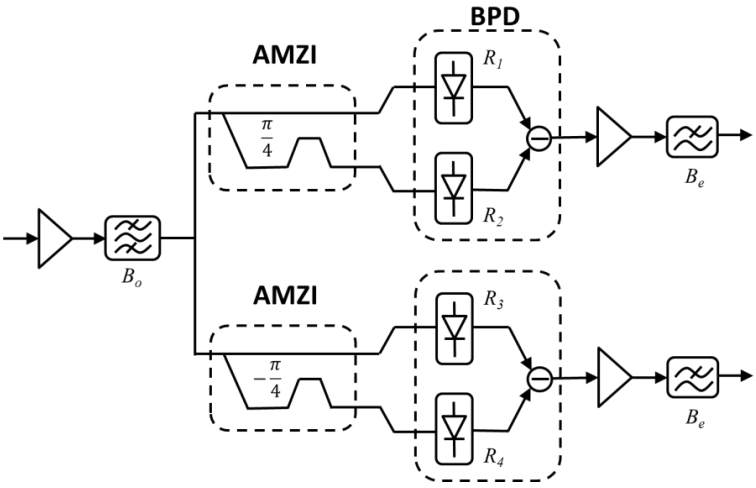

Fig. 4.4.8 A schematic of a DQPSK RX.

If $E(t)$ is the optical field at the output of the RX optical filter, the signals at the output of the upper AMZI can be written as:

$$E_1(t) = \frac{1}{2}\left[E(t) + E(t - T_d)e^{j\frac{\pi}{4}}e^{j\delta\phi}\right] \quad (4.4.4a)$$

$$E_2(t) = \frac{1}{2}\left[E(t) - E(t - T_d)e^{j\frac{\pi}{4}}e^{j\delta\phi}\right] \quad (4.4.4b)$$

where $\delta\varphi$ is a quantity that can be controlled, typically by thermal adjustments of the AMZ. $\delta\varphi$ can be transformed into a frequency detuning parameter Δf of the AMZI transfer function through the relation $\Delta f = R_s\, \delta\varphi/2\pi$. The value $\Delta f = 0$ corresponds to perfect tuning of the AMZI.

4.4.4 Back-to-Back Performance and Dispersion Tolerance

The best performance is achieved when the receiver contains an optical filter matched to the received optical signal, ideal photodetectors and no post-detection electrical filters. In this ideal case, and in the absence of any TX or RX impairment, the BER achievable with the DPSK modulation is equal to [humblet91, poggiolini94]:

$$BER = \frac{1}{2} e^{-2\mathrm{OSNR}} \left(1 + \frac{1}{2}\mathrm{OSNR}\right) \tag{4.4.6}$$

where OSNR is defined by equation (4.2.15) over a bandwidth equal to the symbol-rate R_s. The BER versus OSNR curve for DPSK is shown in Fig 4.4.9 as a solid red line. Comparing it to the optimum matched filter performance of OOK-IMDD (dash-dotted blue line), an OSNR gain of approximately 3 dB is achieved by DPSK. The performance curve of DQPSK is shown in Fig. 4.4.9 as a dashed green line. It has been estimated using the semi-analytical technique described in [bosco06], since a closed-form formula for performance evaluation is not available for DQPSK. The reference bandwidth for the OSNR is equal to R_s, thus the reported curves give a direct comparison of systems operating at the same symbol rate. DQPSK allows transmitting information at a double rate with respect to the binary formats, at the expenses of an OSNR penalty of ~1 dB with respect to IMDD and ~3.5 dB with respect to DPSK, at a reference BER of 10^{-3}.

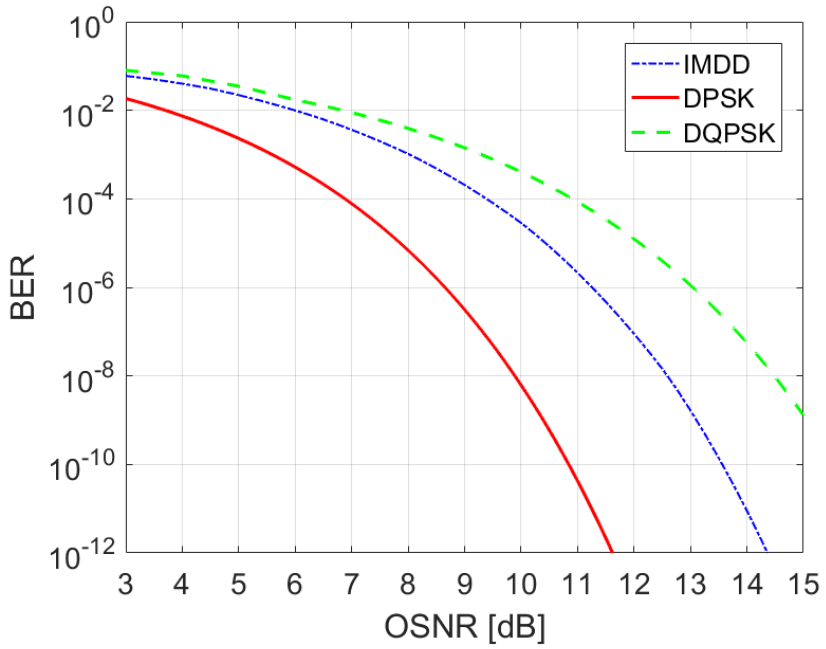

Fig. 4.4.9 Ideal performance of DPSK and DQPSK systems with interferometric detection. The performance of IMDD is also shown for comparison.

The sensitivity gain of DPSK and DQPSK with respect to IMDD depends on the practical implementation of the transceiver (for example on the electrical and optical filter bandwidths). In [winzer03b,gnauck05,bosco06] it was shown that, like for OOK formats, a careful optimization of the filter bandwidths can yield a performance very close to the theoretical matched filter limits, provided that a narrowband optical filter is available at the receiver. If the optical filter bandwidth is wide, the performance penalty with respect to the ideal performance can be kept below 1 dB by optimizing the TX and RX electrical bandwidths [bosco06].

Table 4.4.3 shows an example of optimized 3 dB filter bandwidths when a second-order super-Gaussian optical passband filter and a 5-pole Bessel electrical low-pass filter are used at the RX. Six different cases have been considered, i.e. IMDD, DPSK and DQPSK all with either NRZ or RZ modulation. In the case of NRZ modulations, the transmitted pulses are shaped by a 5-pole Bessel low-pass filter with 3 dB bandwidths equal to $0.75 \cdot R_s$ for IMDD, $0.9 \cdot R_s$ for DPSK and $0.45 \cdot R_s$ for DQPSK. The OSNR (over a bandwidth equal to R_s) required to achieve BER=10^{-3} is also shown, together with the penalty with respect to the matched filter case.

	B_o/R_s	$B_{e,RX}/R_s$	OSNR@BER=10^{-3}	OSNR penalty
IMDD-NRZ	1.2	0.8	9.0 dB	1.0 dB
IMDD-RZ	2.0	1.0	8.5 dB	0.5 dB
DPSK-NRZ	1.2	1.6	5.9 dB	0.3 dB
DPSK-RZ	2.0	1.2	5.7 dB	0.1 dB
DQPSK-NRZ	1.2	1.6	9.7 dB	0.4 dB
DQPSK-RZ	2.0	1.2	9.5 dB	0.2 dB

Table 4.4.3 Optimized RX filter bandwidths in different configurations and corresponding system performance and OSNR penalty with respect to the ideal matched filter receiver.

Interferometric receiver implementation impairments

The receiver architecture used for both DPSK and DQPSK is more complex than a standard DD receiver, requiring the additional use of an AMZI and a pair of BPD or each quadrature. The performance of the system can thus be affected by imperfections in the AMZI or in the BPD, such as:

- **AMZI frequency detuning Δf** with respect to the transmit laser, due to a non-zero phase mismatch $\delta\phi$ between the two branches of the AMZI (please see equations (4.4.3) and (4.4.4)): $\Delta f / R_s = \delta\phi / 2\pi$.
- **AMZI delay error $\Delta\tau_{AMZI}$**, due to a mismatch between the delay T_d between the two arms of the AMZI and the symbol time T_s: $\Delta\tau_{AMZI} = T_d - T_s$.
- **BPD delay imbalance $\Delta\tau_{BPD}$**, due to a time mismatch in the propagation paths in the two arms of the BPD.
- **BPD gain imbalance K**, due to a mismatch between the responsivities R_1 and R_2 of the photodiodes in the two arms of the BPD defined as $K=R_1/R_2$.

In the following, the impact of such impairments on the performance is estimated for both DPSK and DQPSK, in terms of OSNR penalty with respect to the ideal case with no imperfections at a reference BER equal to 10^{-3} (which assumes the use of a hard decision FEC scheme). The filter parameters used in simulations are those shown in Table 4.4.3. The results, shown in Fig. 4.4.10 for DPSK and 4.4.11 for DQPSK, indicate that the tolerance to AMZI and BPD imperfections is in general higher for DPSK than for DQPSK, when operating at the same symbol rate (note that all time and frequency errors in the x-axes of figures 4.4.10 and 4.4.11 are normalized with respect to symbol time/symbol rate). RZ-DPSK is less tolerant that NRZ-DPSK to delay errors (both in the AMZI and in the BPD), whilst the impact is almost the same for RZ-DQPSK and NRZ-DQPSK. The most critical parameter is the frequency detuning between the AMZI and the transmit laser: an offset of only 6% of the symbol rate induces a 1 dB penalty on DPSK and more than 3 dB penalty on DQPSK. Note that this frequency offset could fully be compensated for by proper tuning of the path length difference within the AMZI on an optical wavelength scale, by inserting a phase shifter in one of the AMZI paths [winzer03]. However, the results shown in figures 4.4.10a and 4.4.11a may set stringent requirements to the wavelength stability of the transmit laser. Similar analyses can be found in [winzer03, kim03, ho04, bosco05, bosco06], where much lower values of reference BER (10^{-9} or 10^{-10}) were used, which imply a slightly lower tolerance to the imperfections than the one observed at BER=10^{-3}.

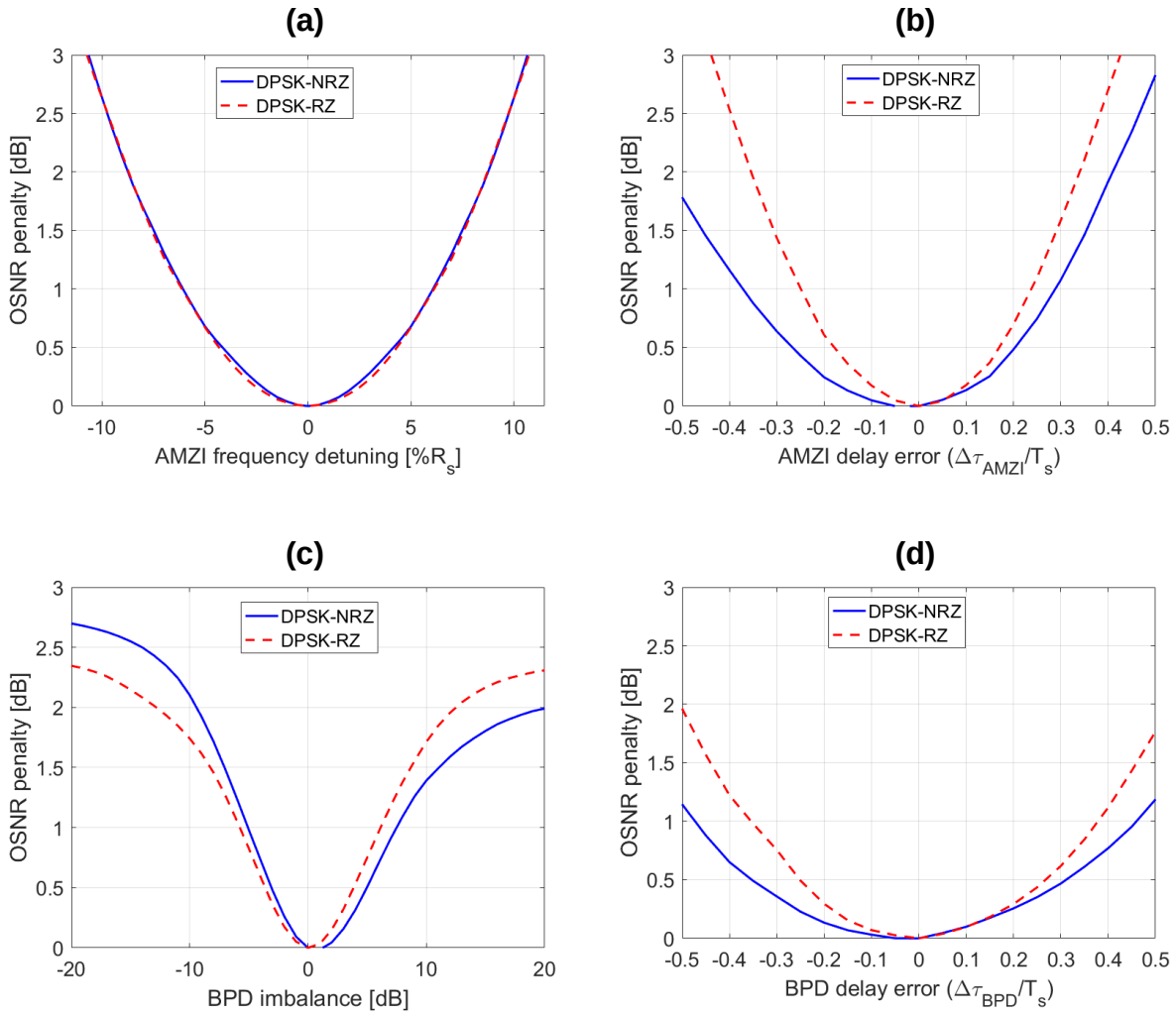

Fig. 4.4.10 Impact of interferometric RX implementation impairments on DPSK-NRZ and DPSK-RZ in terms of OSNR penalty. The target BER is 10^{-3}, and the values of reference OSNR (over a bandwidth equal to R_s) in the absence of impairments are shown in Table 4.4.3.

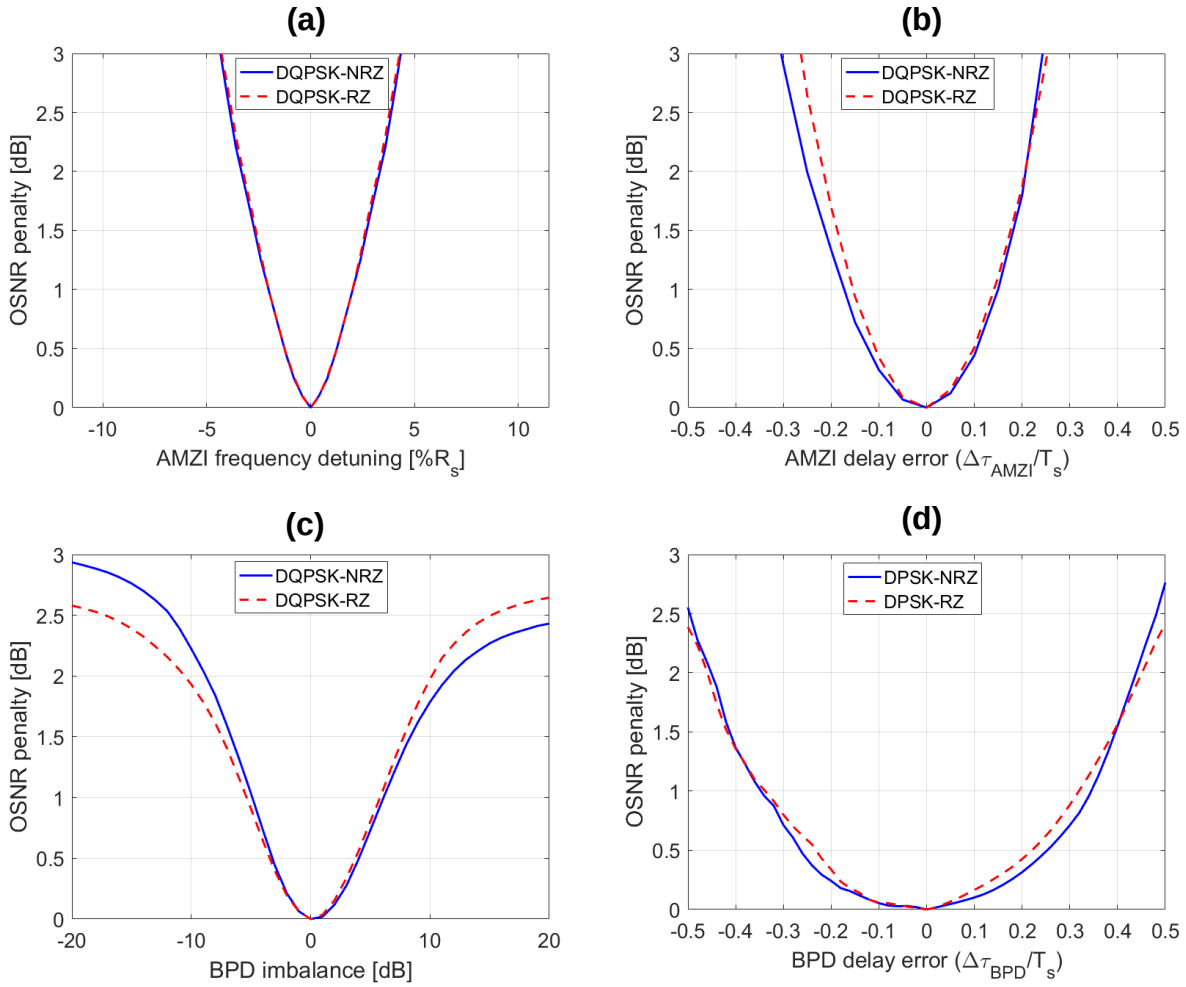

Fig. 4.4.11 Impact of interferometric RX implementation impairments on DQPSK-NRZ and DQPSK-RZ in terms of OSNR penalty. The target BER is 10^{-3}, and the values of reference OSNR (over a bandwidth equal to R_s) in the absence of impairments are shown in Table 4.4.3.

Dispersion tolerance

Fig. 4.4.12 shows the performance of DPSK and DQPSK modulation formats (with either RZ or NRZ line coding) in the presence of either GVD or a first-order PMD. The simulation setup is the same as described in section 4.2.4, with optimized RX filters bandwidth (as shown in Table 4.4.3). Linear fiber propagation was assumed, while first-order PMD was emulated by inserting a deterministic DGD value $\Delta\tau_{DGD}$ between the two principal sates of polarization (PSPs). The worst-case of equal power splitting ratio between the two PSPs was considered. The curve for IMDD-NRZ is also shown for comparison.

For the system configurations considered in Fig. 4.4.12, at the highest GVD tolerance is achieved by DPSK-NRZ, while the other formats have a much lower GVD tolerance. However, it must be noted that the comparison is performed at the same symbol rate, i.e. DQPSK has double bit-rate with respect to DPSK and IMDD. The tolerance to GVD for DQPSK operating at the same bit rate would thus be increased by a factor of 4, achieving a higher tolerance than the binary formats, thanks to its narrower spectral width. The DGD tolerance is instead similar for all formats (at the same symbol rate).

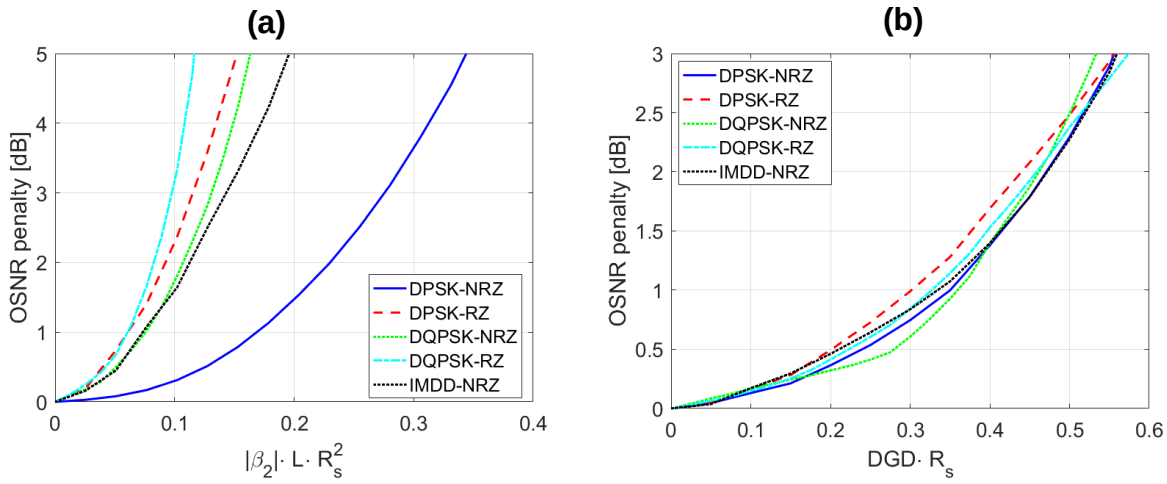

Fig. 4.4.12 GVD and first-order PMD tolerance of DPSK and DQPSK in terms of OSNR penalty with respect to back-to-back performance as a function of either (a) the normalized accumulated dispersion or (b) the normalized DGD in the worst case power splitting ratio between the two PSPs. The performance of IMDD-NRZ is also shown for comparison. The target BER is 10^{-3} and the values of reference back-to-back OSNR (over a bandwidth equal to R_s) are shown in Table 4.4.3.

4.5 IQ modulation with Coherent Detection

This section reviews the transmitter and receiver architectures required to generate and detect different types of high-order modulation formats employing coherent detection. Section 4.5.1 reviews the architecture of an IQ transmitter, which can be used to generate arbitrary two dimensional (2D) constellations or four-dimensional (4D) constellations if polarization multiplexing is employed. The architecture of a coherent-detection optical receiver is described in Section 4.5.2, while Section 4.5.3 introduces the Nyquist WDM multiplexing technique, highlighting the compromise between spectral efficiency and performance. Finally, Section 4.5.4 focuses on flexible transponders, designed to dynamically adapt the transmission speed and modulation format to the channel conditions.

4.5.1 IQ Transmitter

Combining amplitude modulation and phase modulation, the class of modulation formats known as QAM (quadrature amplitude modulation) is obtained. The complex envelope of QAM modulated signals can be written as [proakis07]:

$$s_T(t) = \sum_k (p_k + jq_k)\, g_T(t - kT_s) \tag{4.5.1}$$

where p_k and q_k are the coordinates of the constellation points on the in-phase and quadrature axes, respectively. T_s is the symbol time, and $g_T(t)$ is the optical pulse shape in the time domain. For each symbol slot, M alternative waveforms can be transmitted, depending on the value of the information bits. M is called the cardinality of the constellation. The maximum number of bits n_b that can be carried by each constellation symbol is equal to $\log_2(M)$. The transmission speed, i.e. the *bit rate*, is given by $R_b = n_b/T_s$. Fig. 4.5.1 shows a few examples of QAM constellations (for M=4, 16, 32, 64).

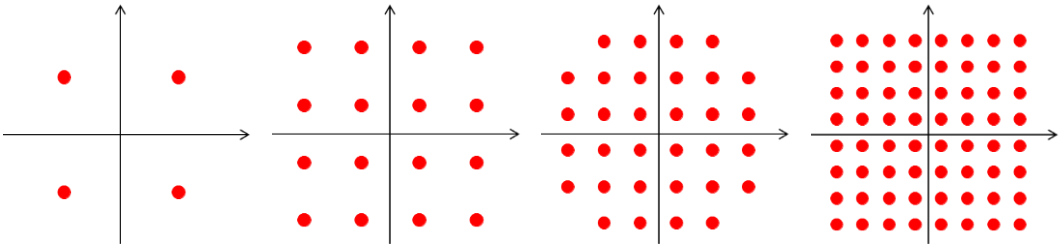

Fig. 4.5.1 High order square QAM modulation formats constellations (for M = 4, 16, 32, 64).

Any optical QAM signal could be in principle generated by using a single dual-drive MZM [ho05b]. However, the required number of levels of the electrical driving signals would be quite high (for example for a 16-ary driving signals are needed for 16QAM), trading the simplicity of the optical part for a big electrical effort. Another method to generate arbitrary QAM constellations is based on the use of two consecutive optical modulators: an MZM for amplitude modulation and a phase modulator to set the phase. Also in this case, the simplicity of the optical TX part implies the use of a complex electrical level generator which cannot be easily implemented for high data rates [seimetz09].
The most commonly used TX configuration to generate QAM signals is based on an IQ modulator, like the one used in the generation of DQPSK signals (please see Fig. 4.4.4). This configuration exploits the fact that each constellation point can be projected on the in-phase and quadrature axes, in order to reduce the number of required levels for the driving signal (which is equal to $\log_2(M)$ for M-QAM). The scheme of the conventional IQ transmitter is shown in Fig. 4.5.2. Two multi-level electrical driving signals are generated (one for the in-phase and the other for the quadrature component of the QAM signal), each of them driving one of the two MZMs in the IQ modulator. In general, an adaptive and precise bias control algorithm for the IQ modulator is essential to minimize transmitter impairments and to maintain long-term stable operation [cho06, yoshida10, kawakami10, sotoodeh11, yanfu11].

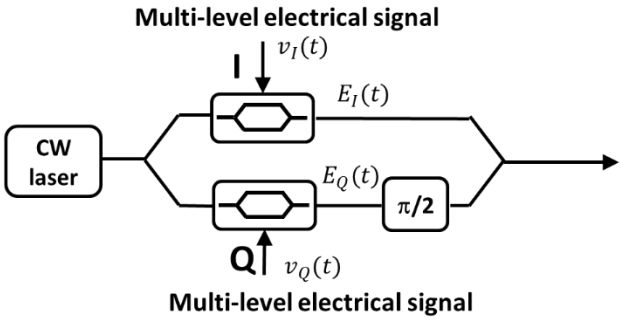

Fig. 4.5.2 A single polarization IQ transmitter.

Combining two IQ transmitters using a polarization beam splitter/combiner, polarization multiplexed QAM (PM-QAM) signals can be generated, as shown in Fig. 4.5.3. The light from a single laser signal is split and sent into four separate Mach-Zehnder modulators. The upper and lower portions of this super-MZM structure each generate an M-QAM signal. The signals are then sent into a polarization beam combiner (PBC), after applying a polarization rotation to the lower branch, so that the signal from the upper half of the circuit becomes X-polarized, while the signal from the lower half of the circuit becomes Y-polarized.

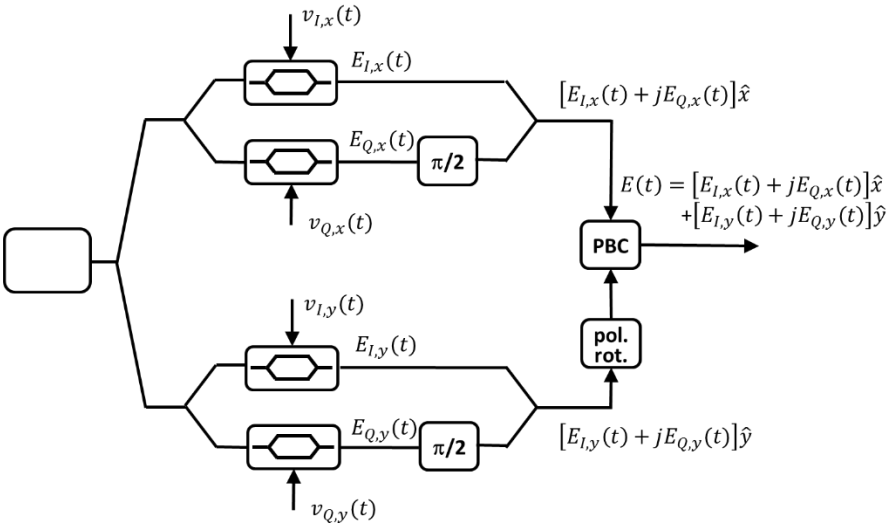

Fig. 4.5.3 A dual polarization IQ transmitter. PBC: polarization beam combiner.

Generation of the multi-level driving signals

Multi-level driving signals with a desired pulse shape can be efficiently generated using a digital signal processing (DSP) block, followed by a digital to analog converter (DAC) which generates the driving electrical signal. Any DAC device is characterized by two main parameters, which set a limit to its performance, these are:

- The sampling speed f_{DAC}, which limits the achievable symbol rate $R_s = f_{DAC}/N_{SpS}$, where N_{SpS} is the number of samples per symbol (SpS), also indicated as the "oversampling factor".
- The number of resolution bits N_{DAC}, which limits the cardinality of the modulation format. In fact, the higher the order of the modulation format, the higher is the required value of N_{DAC}.

Typically, if f_{DAC} increases, N_{DAC} decreases. The achievable symbol rate can clearly be increased by decreasing the oversampling factor. In doing so, penalties could be incurred due to interference produced by spectral replica of the useful spectrum in the DAC process. In [cigliutti12], a 1.5 SpS DAC-supported Nyquist-WDM PM-16QAM experiment was reported, using a DAC with f_{DAC} = 23.4 GHz and thus achieving a symbol rate R_s = 15.6 Gbaud. In

[schmogrow13], 1.33 SpS were employed in a 100-km PM-64QAM single channel transmission at 252 Gbit/s. In [nespola14], an oversampling factor as low as 1.15 was used, limiting the penalty due to spectrum replica thanks to the use of antialiasing electrical filters. The distortions on the useful signal introduced by the bandwidth limitations of the TX can be compensated for in the digital domain using a properly designed pre-equalizer in the DSP block before the DAC [khanna16].

4.5.2 Coherent Optical Receiver

The basic structure of the most commonly used coherent optical receiver is shown in Fig. 4.5.4. It is a phase diversity RX [davis87, derr92] which is able to retrieve the in-phase and quadrature components of the complex amplitude of an optical signal without locking the frequency and phase of the local oscillator (LO). The only requirement is that the frequency offset between the TX laser and the LO is limited to a fraction of the symbol rate. This type of coherent detection without active optical phase lock loop is also known as *intradyne* coherent detection.

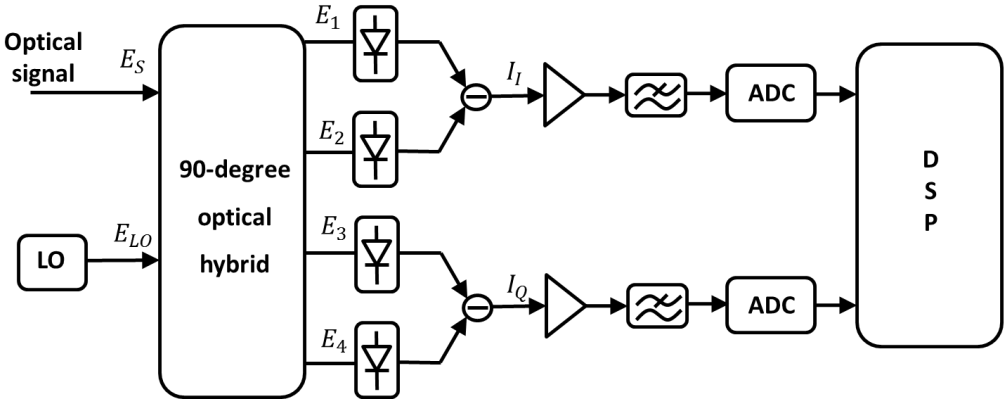

Fig. 4.5.4 A coherent intradyne receiver based on phase diversity detection. ADC: analog-to-digital converter, LO: local oscillator; DSP: digital signal processing.

In the schematic shown in Fig. 4.5.4, the optical data signal is mixed with a signal generated by an LO through a six-port optical device called "90° hybrid" [kikuchi88], which consists of a two-by-two optical coupler with a 90-degree phase delay function implemented in one arm of the coupler. The input/output characteristic of a 90° hybrid is given by:

$$\begin{bmatrix} E_1(t) \\ E_2(t) \\ E_3(t) \\ E_4(t) \end{bmatrix} = \begin{bmatrix} +1 & +1 \\ +1 & -1 \\ +1 & -j \\ +1 & +j \end{bmatrix} \begin{bmatrix} E_S(t) \\ E_{LO}(t) \end{bmatrix} \tag{4.5.2}$$

with:

$$E_S(t) = \sqrt{P_S(t)}e^{j(2\pi f_S t + \phi_D(t))} \tag{4.5.3a}$$

$$E_{LO}(t) = \sqrt{P_{LO}}e^{j(2\pi f_{LO} t + \phi_{LO}(t))} \tag{4.5.3b}$$

The output signals are then converted from the optical domain into the electronic domain with a pair of balanced photodetectors, whose output currents are given by:

$$I_I(t) = R(|E_1(t)|^2 - |E_2(t)|^2) \tag{4.5.4a}$$

$$I_Q(t) = R(|E_3(t)|^2 - |E_4(t)|^2) \tag{4.5.4b}$$

where R is the responsivity of the photodiode (which is ideally the same for all four photodetectors). Substituting equations (4.5.2) and (4.5.3) into equation (4.5.4), gives:

$$I_I(t) = 4R \cdot \text{Real}\{E_S(t)E_{LO}^*(t)\} = 4R\sqrt{P_S(t)P_{LO}^*}\cos\left(2\pi\delta f t + \phi_D(t) - \phi_{LO}(t)\right) \quad (4.5.5a)$$

$$I_Q(t) = 4R \cdot \text{Imag}\{E_S(t)E_{LO}^*(t)\} = 4R\sqrt{P_S(t)P_{LO}^*}\sin\left(2\pi\delta f t + \phi_D(t) - \phi_{LO}(t)\right) \quad (4.5.5b)$$

where $\delta f = f_S - f_{LO}$ is the frequency offset between the TX laser and the LO. Combining the two photo-currents into a complex signal format gives:

$$I_{IQ}(t) = I_I(t) + jI_Q(t) = 4R\sqrt{P_S(t)P_{LO}^*}e^{j\left(2\pi\delta f t + \phi_D(t) - \phi_{LO}(t)\right)} \quad (4.5.6)$$

which has the same phase as the data signal $E_s(t)$ except for the frequency offset and the additional phase noise introduced by the LO. Both, phase noise and frequency offset, can be compensated for using properly designed DSP algorithms that can be applied to the received samples after the analog to digital conversion process, together with the compensation of the propagation effects. Note that, if a single photodetector was used instead of a balanced one, it would be necessary to employ a local oscillator laser with 20 to 25 dB more power than the incoming signal in order for the resulting coherent signal term to dominate [kikuchi88]. By using a balanced photodetector it is possible to employ a much less powerful local oscillator.

The electrical low-pass filters (LPFs) shown in Fig. 4.5.4 represents the cascade of all band limiting components in the RX. An additional antialiasing electrical filter may be needed before the ADCs in order to reduce the bandwidth of the input signal, thus relaxing the requirements for the ADC sampling frequency f_{ADC}, which, in order to avoid a performance degradation due to *aliasing* [proakis07], has to be higher than twice the bandwidth of the input signal. The distortions introduced on the useful signal by the bandwidth limitations of the RX can be compensated for in the digital domain by the adaptive or static equalizers present in the DSP chain (please see Chapter 6 for further details).

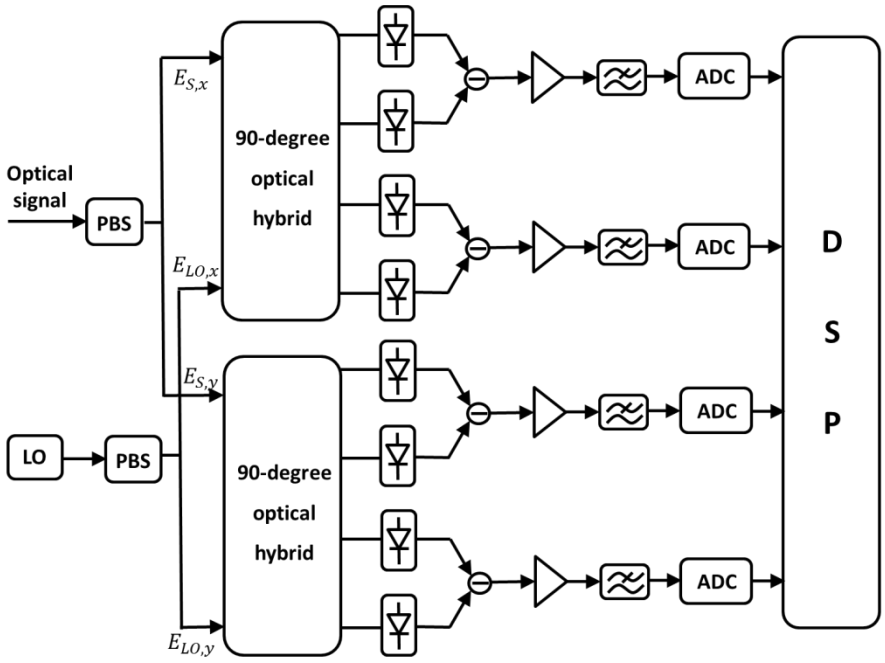

Fig. 4.5.5 A dual polarization coherent intradyne receiver based on phase and polarization diversity detection. ADC: analog-to-digital converter, LO: local oscillator; DSP: digital signal processing: PBS: polarization beam splitter.

A polarization controller is needed at the input of the receiver in Fig. 4.5.4 in order to align the polarization states of the LO and the data signal. However, in practical systems, the polarization of the incoming signal is unlikely to remain aligned to the SOP of the LO because of random changes in the birefringence of transmission fibers [kikuchi15]. To deal with this problem, polarization diversity detection has been introduced into the coherent receiver. The schematic of the dual-polarization coherent receiver, based on polarization-diversity, is shown in Fig. 4.5.5. The incoming optical signal passes through a polarization beam splitter (PBS), which divides the signal into two orthogonal polarization signal components. Each component is combined with a LO through an independent 90-degree optical hybrid circuit.

The eight signals are then converted from the optical domain into the electronic domain using four balanced photodetectors. In the case of the polarization-multiplexed system, the polarization tributaries can be de-multiplexed from the four outputs of the receiver using DSP algorithms [savory08].

Customarily, the performance of optical coherent systems is estimated by means of the OSNR, defined by equation (4.2.15). To find the BER, the OSNR is inserted into a suitable formula, which depends on the transmission format. For instance, the ideal BER performance of square PM-QAM formats with M constellation points is given by [proakis07]:

$$BER_{PM-MQAM} = \frac{2\left(1-1/\sqrt{M}\right)}{\log_2 M} e\mathrm{rfc}\left(\sqrt{\frac{3}{2(M-1)}\mathrm{OSNR}}\right) \quad (4.5.7)$$

where OSNR is measured over a bandwidth equal to the symbol rate. Equation (4.5.7), as well as textbook formulas addressing other formats, assume that the RX operates by filtering the incoming signal through a baseband transfer function $H_{RX}(f)$ that is matched to the transmitted signal baseband pulse. It is also assumed that the ISI be absent. Otherwise, they are no longer valid, in the sense that there is a penalty with respect to what they predict. Note that in modern coherent systems, the DSP adaptive equalizer tends to make $H_{RX}(f)$ converge to a matched shape, so that this condition is typically well satisfied

Under the mentioned assumptions of a matched $H_{RX}(f)$ and no ISI, the OSNR in equation (4.2.15) also corresponds exactly to the signal-to-noise ratio SNR that can be directly measured on the RX electrical signal constellation, at the input of the decision stage. In addition, such SNR also coincides with the communications theory widely used parameter 'energy-per-symbol versus noise spectral density' [proakis07], that is SNR=E_s/N_0.

4.5.3 Nyquist-WDM

Today, transmission at 100 Gbit/s, enabled by the use of quadrature phase shift keying (QPSK) at 32 Gbaud with polarization multiplexing (PM), has reached maturity and widespread deployment, and 200 Gbit/s PM-16QAM coherent transceivers are already commercially available. Industry efforts are currently devoted to the ASIC development for transceivers for 400 Gbit/s and soon they will move to 1 Tbit/s. Since the transmission speed R_b is given by the product of the symbol rate R_s and the number of bits per symbol n_{bps} ($R_b = R_s \cdot n_{bps}$), higher values of R_b can be obtained by increasing either R_s or n_{bps} (i.e. the order of the modulation format). Note that the first solution would have a strong impact on the hardware complexity, whilst the second one would mainly impact the DSP complexity. As an example, a raw transmission rate of 480 Gbit/s can be achieved either with 120-Gbaud PM-QPSK (n_{bps} =4) or 30-Gbaud PM-256QAM (n_{bps} =16). Figure 4.5.6 shows the theoretical back-to-back performance of high-order modulation formats, which highlights the fact that an increase in the n_{bps} introduces a higher requirement in terms of SNR, which in turns results in a significantly reduced achievable transmission distance [bosco11].

Figure 4.5.7 shows the values of symbol rate and number of bits per symbol needed to achieve a target net transmission speed of 100 Gbit/s, 200 Gbit/s, 400 Gbit/s or 1 Tbit/s, assuming that an FEC with 20% overhead is used. The curves in Fig. 4.5.7 highlight the fact that serial interface rates well beyond those provided by state-of-the art components (such as electro-optic (E/O) converters, O/E converters, DACs, and ADCs) are needed to achieve transmission speeds beyond 200 Gbit/s. This electronic bottleneck can be efficiently circumvented through the use of super-channels, which exploit optical parallelism to provide high per channel data rates and better spectral utilization [liu14]. A super-channel is a collection of optical signals that are modulated and multiplexed together with high spectral efficiency (SE) at a common originating site, transmitted and routed over a common optical link as a single entity and received at a common destination site. Typically, the super-channels use spectrally efficient advanced modulation formats in combination with advanced multiplexing schemes such as orthogonal frequency division multiplexing (OFDM) [chadra09] or Nyquist-WDM [bosco11]. In [bosco10] it was shown that both techniques have potentially the same performance, but Nyquist-WDM is much more robust to practical implementation RX constraints, such as limited analog bandwidth and limited ADC speed. In the following, we focus on the use of the Nyquist-WDM technique, briefly describing its generation and detection processes.

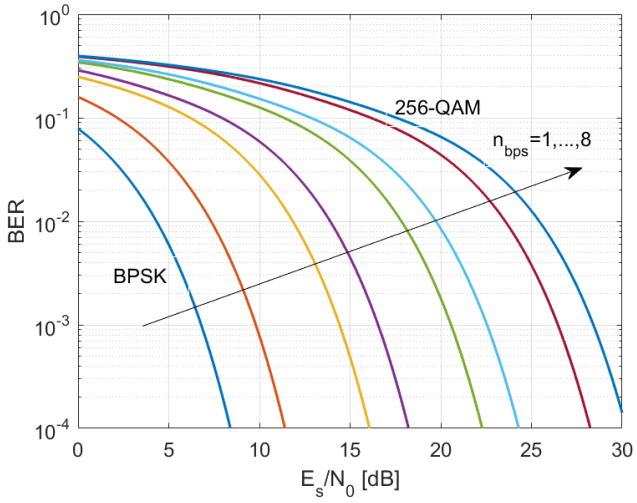

Fig. 4.5.6 Ideal back-to-back performance of high-order QAM formats with coherent detection.

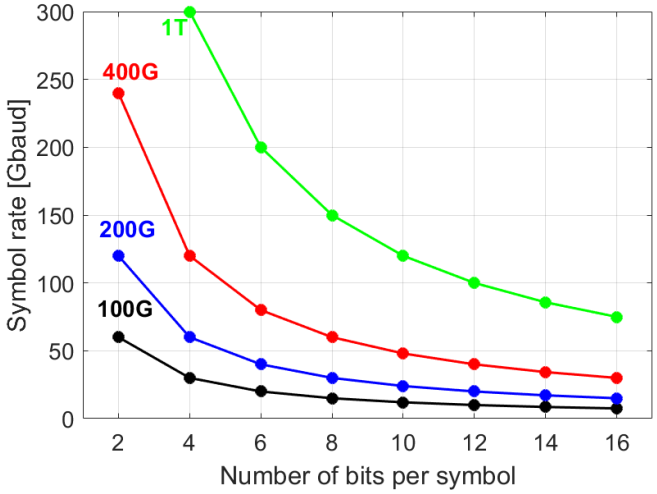

Fig. 4.5.7 Symbol rate versus number of bits per symbol needed to achieve a target net transmission speed of 100 Gbit/s, 200 Gbit/s, 400 Gbit/s or 1 Tbit/s (assuming that an FEC with 20% overhead is used) [bosco17].

Generation of a Nyquist-WDM signal

Nyquist-WDM signal generation and transmission have been demonstrated using either optical filters or DSP-based electrical filters [cigliutti11, cai12, foursa13]. Compared to the optical filter solution, the DSP-based approach is more flexible as the same hardware can be used to generate different filter shapes and modulation formats [bosco12, hillerkus12]. In practice, the system cost is limited by the complexity, speed, and power consumption. Therefore, it is necessary to optimize the digital Nyquist design for the required signal in order to minimize complexity and speed [zhou12, zhou13b, cai14].

In order to satisfy the Nyquist criterion for the absence of ISI among adjacent pulses [proakis07], a raised-cosine (RC) spectral shape is typically used. The RC transfer function is defined as follows:

$$H_{RC}(f) = \begin{cases} T_s, & |f| \le \frac{1-\rho}{2T_s} \\ \frac{T_s}{2}\left\{1 - \cos\left[\frac{\pi T_s}{\rho}\left(f - \frac{1+\rho}{2T_s}\right)\right]\right\}, & \frac{1-\rho}{2T_s} \le |f| \le \frac{1+\rho}{2T_s} \\ 0, & |f| \ge \frac{1+\rho}{2T_s} \end{cases} \quad (4.5.8)$$

where T_s is the symbol time (reciprocal of the symbol rate) and ρ is the "roll-off" factor, that can take values in the range [0,1]. The impulse response corresponding to a RC spectrum is:

$$h_{RC}(t) = \frac{\sin(\pi t/T_s)}{\pi t/T_s}\frac{\cos(\rho\pi t/T_s)}{1-(2\pi t/T_s)^2} \quad (4.5.9)$$

In the case in which the channel has a flat frequency response, the optimum receiver filter is matched to the transmit one and both assume a square-root raised cosine (SRRC) shape: $H(f) = \sqrt{H_{RC}(f)}$. Fig. 4.5.8 shows examples of RC pulses in time and frequency domain, for different values of ρ.

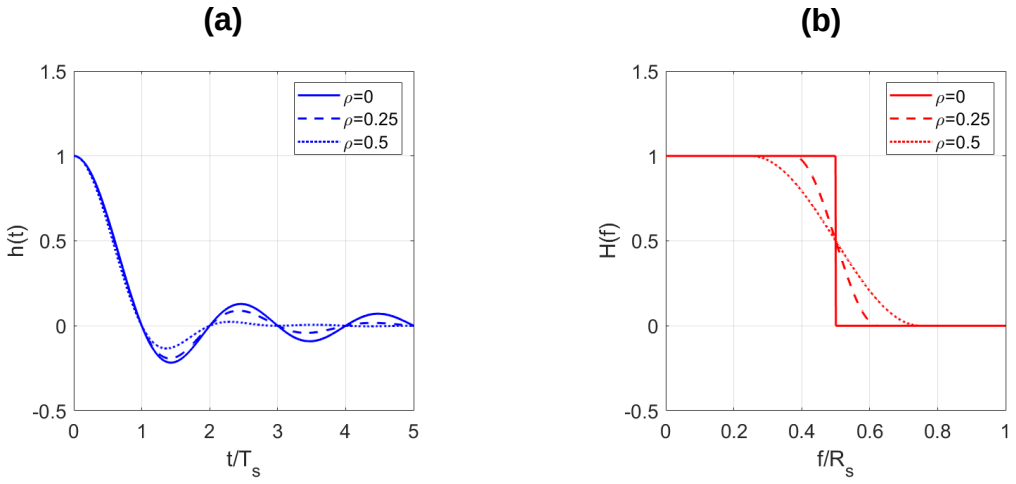

Fig. 4.5.8 RC pulses in time domain (a) and frequency domain (b).

In Nyquist-WDM transmission with RC or SRRC spectra and frequency spacing equal to Δf, ideally no cross-talk is present between adjacent WDM channels if $\Delta f > (1 + \rho)\, R_s$. As an example, if ρ=0.1, the penalty due to linear cross-talk is negligible if the channel spacing is larger than 1.1 R_s, i.e., if the normalized spacing $\Delta f/R_s$ exceeds 1.1. For lower values of channel spacing, a cross-talk penalty is present, as shown in Fig. 4.5.9 for three different modulation formats (QPSK, 16QAM, and 64QAM). If $\Delta f/R_s > 1.1$, the performance of all three formats converges to the theoretical value, whilst for lower spacing values an SNR penalty is present, which is higher for higher cardinality modulation formats.

Typically, Nyquist pulse shaping is performed in the digital domain using FIR filters. The required length of the digital filters that generate SRRC or RC pulses depends on the roll-off factor: for low values of ρ, the length of the pulse in time domain increases (as shown in Fig. 4.5.8(a)), thus a larger number of FIR filter taps is needed to properly approximate it. Complexity and performance of digital pulse shaping was investigated in [sano12], showing that the use of FIR filters with 17 taps allows for a reduction in channel spacing to 1.1 times the symbol rate with a 1 dB penalty. If the channel spacing is tighter, a higher number of FIR filter taps are needed, as shown in [schmogrow11], where a 32 tap FIR filter was used to shape 14 Gbaud PM-16QAM Nyquist-like pulses with frequency spacing equal to $1.06 \cdot R_s$ without substantial cross-talk penalty.

The achievable symbol rate and cardinality of the modulation format are limited by the DAC characteristics, as discussed in Section 4.5.1.

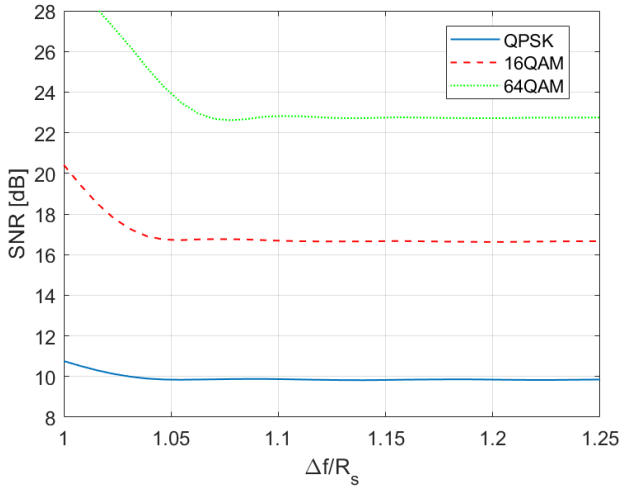

Fig. 4.5.9 The SNR needed to achieve a target bit error rate of 10^{-3} as a function of the normalized frequency spacing $\Delta f/R_s$. SRRC filters with roll-off equal to 0.1 when used both at the TX and RX sides. [bosco16b].

Detection of a Nyquist-WDM signal

Nyquist-WDM signals can be efficiently detected using the standard coherent optical receiver described in Section 4.5.2. The single WDM channel is selected by tuning the local oscillator (LO) to its center frequency and the sharp filter shapes needed to cut out the adjacent channels are efficiently implemented in the digital domain. This enables the detection of single WDM channels without the need of any tight optical filtering at the RX. However, the use of anti-aliasing electrical filters before the ADCs might be beneficial, since they would reduce the signal bandwidth and thus relax the requirements for the ADC sampling frequency f_{ADC} (which, in order to satisfy the Nyquist sampling theorem, needs to be larger than twice the absolute bandwidth of the input signal [proakis07]). The ratio between the ADC sampling frequency f_{ADC} and the symbol rate R_s determines the number of samples per symbol N_{SpS} at the output of the ADC. Typically, $f_{ADC} = 2 \cdot R_s$, which corresponds to $N_{SpS} = 2$, but lower values can be used without incurring any substantial penalties [mazurczyk14, bosco10, bosco16b].

Fig. 4.5.10(a) shows an example of back-to-back SNR penalty as a function of the number of samples per symbol N_{SpS} at the output of the ADC. The reference BER was 10^{-3} and the penalty was evaluated with respect to the two samples per symbol case. The results were obtained through numerical simulations [bosco16b], where Nyquist-WDM signals were generated with an SRRC shape and $\rho = 0.1$. A fifth-order electrical Bessel low-pass filter with 3 dB bandwidth B_{RX} was used at the RX. The value of B_{RX} was optimized for each value of N_{SpS}, obtaining the optimum values as shown in Fig. 4.5.10(b) (normalized with respect to the symbol rate). Since a low value of N_{SpS} corresponds to a low value of f_{ADC}/R_s, the RX bandwidth has to be decreased accordingly in order to avoid aliasing. This, however, causes a distortion on the useful signal, which in turn induces an SNR penalty, which is greater for higher-order modulation formats, as shown in Fig. 4.5.10(a).

In [zhou12] it was shown that the complexity of the blind equalizer can be significantly reduced by incorporating the matched SRRC filter in the bulk CD equalizer. It was also pointed out that Nyquist-WDM systems with matched filtering can be extremely sensitive to the frequency offset between the transmitter laser and the local oscillator, and that the induced penalty is higher for low values of the SRRC roll-off factor.

Another critical point of Nyquist-WDM signals that has to be taken into account is related to the difficulty in performing clock recovery. i.e. in extracting the timing information from the incoming signal so that the frequency and phase of the local clock is adjusted, and the transmitted symbols may be correctly recovered. In fact, modern

optical transceivers have demanding jitter tolerance and generation requirements [G.8251], and must operate under high noise loading conditions with signals that are distorted by GVD, PMD, optical filtering and non-linear phase noise. Whilst Nyquist pulse-shaping does not result in ISI in the center of the eye, significant horizontal eye closure is introduced, presenting further difficulties for clock recovery and requiring the use of advanced DSP algorithms to minimize the penalty, as discussed in [fludger13].

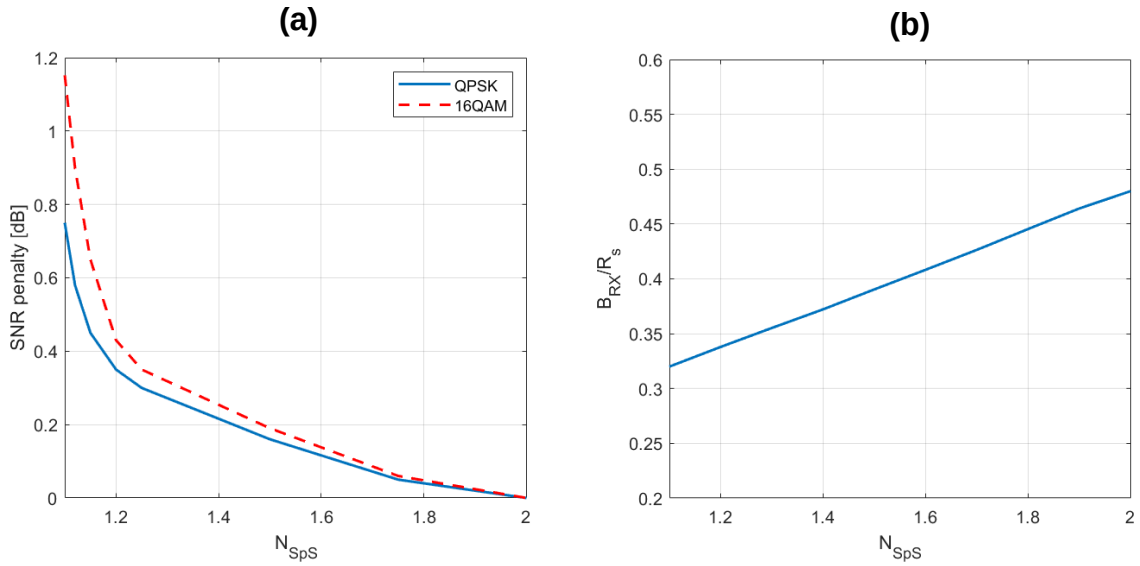

Fig. 4.5.10 The (a) SNR penalty and (b) optimum RX bandwidth as a function of the number of samples per symbol at the output of the ADC. The reference BER is 10^{-3}.

4.5.4 Flexible Transceivers

The key design parameters to optimally exploit all available resources in long-haul and high-capacity optical transmission systems with coherent detection are the spectral efficiency (SE) and the maximum transmission reach. Nonbinary modulation with coherent detection maximizes SE and improves tolerance to transmission impairments, while enabling effective, low-complexity electrical compensation of these impairments [winzer12]. SE can be increased by minimizing the frequency spacing between WDM channels (e.g. using the "Nyquist-WDM" technique), using FEC codes with low overhead or increasing the modulation cardinality. In turn, the maximum transmission reach can be increased by using energy-efficient modulation formats (e.g. low-cardinality QAM) which reduce the SNR requirements at the receiver, using FEC codes with high overhead to ensure reliable transmission or applying proper techniques to mitigate the non-linear propagation effects in the optical fiber. In practice, a compromise has to be made between SE and achievable reach. For example, a transceiver that operates on a short network segment with high SNR can achieve a high SE to maximize the net data rate. Similarly, a transceiver operating on a long network segment with low SNR should use either a lower order modulation format or a FEC code with high overhead to ensure reliable transmission, at the expenses of a loss in SE.

Since the huge amount of traffic foreseen for the near future cannot be efficiently supported by static increases in network capacity, optical transport networks are currently migrating from a static configuration with little flexibility to the concept of software-defined optical networks [gerstel12]. In the scenario of next generation optical networks, a key role will be played by flexible and scalable optical transceivers, able to dynamically adapt the modulation format and the transmission rate to the network conditions [jinno09].

For flexibility, today's coherent optical transceivers typically use a set of different modulation formats based on standard QAM constellations, generated through the combination of two PAM formats in the in-phase and quadrature components. For these standard QAM formats, a gap to Shannon capacity remains, which can be expressed in terms

of a penalty in SNR. Also, the standard QAM formats only offer a coarse granularity in spectral efficiency and hence also a coarse granularity in the achievable transmission reach.

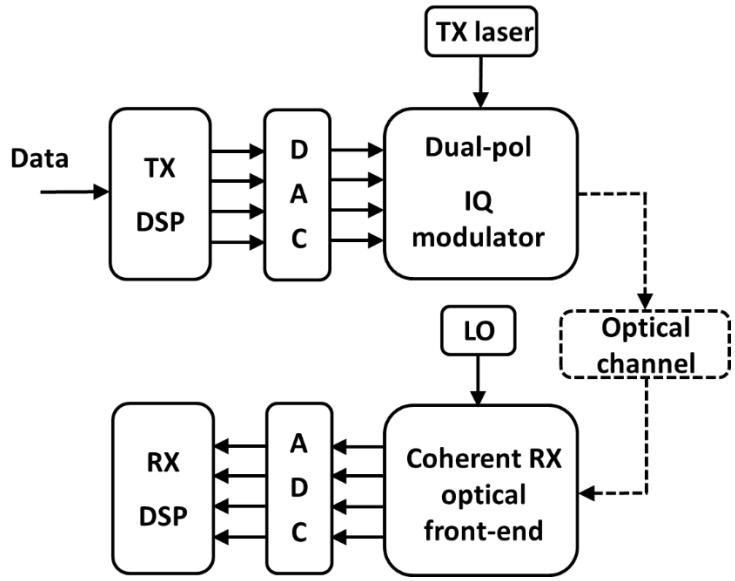

Fig. 4.5.11 Block diagram of a DSP-based optical TX/RX pair that can be used to generate/detect signals employing SCM, TDHF or PS techniques, as well as standard single-carrier QAM modulation formats. DAC: digital-to-analog converter; ADC: analog-to-digital converter; DSP: digital signal processing; LO: local oscillator.

To overcome the lack in granularity, several techniques are currently under study, which take advantage of the high flexibility provided by commercially available high-speed digital-to-analog converters (DACs), allowing to fully design the transmitted signal in the digital/electrical domain. This means that, using the same hardware, different modulation formats can be generated and different transmission rates can be achieved. Examples of techniques used to increase the flexibility of optical transceivers are: subcarrier multiplexing (SCM), implemented as either Nyquist frequency-domain multiplexing (Nyquist-FDM) [qiu14] or orthogonal frequency-domain multiplexing (OFDM) [shieh08], time-domain hybrid formats (TDHF) [zhuge13] and probabilistic shaping (PS) [buchali16]. The great advantage of all these methods is that the flexibility is achieved without requiring any additional hardware, thus allowing to reuse currently available single-carrier transceivers by simply reprogramming the transmitted signal. The general schematics of the TX/RX pair that can be used to generate SCM, TDHF or PS signals, as well as standard QAM signals, is shown in Fig. 4.5.11: the same hardware is used in all cases, the difference is in the DSP algorithms implemented at the TX and RX side. In the following, the above mentioned techniques are briefly reviewed.

Orthogonal frequency-domain multiplexing (OFDM)

Orthogonal frequency-division multiplexing (OFDM) has been widely researched in optical communications due to its high spectral efficiency, resistance to chromatic dispersion, simplicity of one-tap equalization, and flexibility in modulation format [lowery07,shieh08,armstrong09]. This technique is based on the use of electrical subcarriers, each carrying symbols of a QAM constellation, with a sinc-function spectrum to achieve subchannel orthogonality.

Recently, the real-valued OFDM signal (i.e. discrete multi-tone, DMT) has been the object of intense investigations for intensity-modulation and direct-detection (IM/DD) optical systems, as an alternative to multi-level PAM formats for the optical interconnects such as passive optical networks, data centers and system-on-chip interconnects [nadal14, takahara14,dong16]. However, OFDM signals show relatively high peak-to-average power ratio (PAPR) and high computational complexity, which hinder its practical application in the cost-sensitive and power-sensitive optical interconnects [zhong09].

Nyquist-FDM

Like OFDM, this technique consists in electrically decomposing a high symbol-rate signal into a given number of electrical subcarriers, each of which operating at a lower symbol-rate [schmogrow12,dou16,baeuerle17]. In Nyquist-FDM signals the cross-talk between adjacent subcarriers is avoided by using a Nyquist shaping on the electrical subcarriers. Depending on the optical system under test, several degrees of freedom can be optimized, such as the number of subcarrier components, the inter-subcarrier spacing and the associated modulation format and pulse shaping. The granularity of the subcarriers allows to control the subcarrier symbol duration by keeping a constant overall bandwidth. This ability of optimizing the symbol duration allows to adapt the signal for non-linearity tolerance and can therefore be used to extend the reach of optical transport systems [qiu14, poggiolini14]. Furthermore, Nyquist-FDM allows the flexible adaption of the bandwidth [schindler14] and modulation format [krause17] of each individual subcarrier. This allows for a flexible design of the spectral efficiency and therefore a finer granularity in transmission reach. A disadvantage of Nyquist-FDM scheme is its larger sensitivity concerning transmitter impairments, like the IQ-skew which needs a more precise calibration or additional calibration algorithms [bosco16b, baeuerle16].

Time-domain hybrid formats (TDHF)

The TDHF technique consists in transmitting different modulation formats interleaved in the time domain. By changing the ratio of symbols carrying the different modulation formats, the spectral efficiency can be adjusted in fine steps [zhou13]. In this way, a high degree of flexibility is achieved, since the transmission rate and, consequently, the SNR performance can be tuned by simply modifying the pattern of the QAM formats. However, even if the composition of hybrid formats is optimized, the SNR performance is still far from that of the optimum Gaussian constellation [buchali14,curri14,idler15].

Constellation shaping (PS)

To overcome the gap to Shannon capacity of QAM constellations, modulation formats that have a Gaussian-like shape can be used [dar12,yankov14,smith12]. Two main approaches have been proposed to achieve a Gaussian distribution, i.e. the “geometrical shaping” (GS) and the “probabilistic shaping” (PS). The first approach (GS) consists in designing non-square constellations with a Gaussian-like distribution of points and equal transmission probability for all symbols. The second approach (PS) is based on the use of a standard QAM modulation with a non-uniform distribution of the occurrence probability of the symbols of a given constellation. PS can be implemented either using modified FEC codes [smith12, fehenberger15] or using a distribution matcher [buchali16]. The main advantages of PS over GS in terms of flexibility are that the net data rate can be adjusted with arbitrary granularity and that the same DSP unit can be used to equalize the signal at different spectral efficiencies. In addition, a sensitivity gain on the order of 1 dB can be achieved with respect to standard QAM constellations [buchali16, pilori17, guiomar17], whilst a more limited gain can be obtained with GS [steiner17].

4.6 Transponder Architectures

In the previous subchapters, the concept of a transponder has been introduced and different line interface variants have been presented. In what follows, the transponder concept will be generalized in section 4.6.1. An explanation of which transponder types exist and what their hardware architectures look like will be given in section 4.6.2. In section 4.6.3, the relevant interface standards will be listed and the pluggable optical transceiver modules used in modern transponder implementations will be discussed.

Transponders are realized on printed circuit boards (PCBs) and are therefore often called “transponder cards”. They fit into monolithic or modular WDM transport platforms and may comprise multiple ports to improve equipment density and to provide additional functionality. Monolithic WDM equipment commonly uses a 1 HU (height unit) chassis which is sometimes referred to as a “pizza box” due to its apparent similarity (1 HU equals 1 ¾ inches or 44.45 mm). Multiples of these shelves can be combined in a rack and stack fashion if more capacity is needed at a particular location. A modular chassis provides multiple slots (4 to 64 being typical amounts) into which transponders and other cards (for instance amplifier, filter and ROADM cards) can be accommodated. Placed into a 19 (or 21) inch rack with 300 or 600 mm depth, the height of a particular node can vary between 1 and 45 HU depending on the slot configuration and the amount of optical cards required. Modular shelves are typically used for large node configurations. Common equipment functions such as power supplies, fans, management and control, alarm contacts, and system timing can be shared between all cards in the same shelf. An optional high speed backplane may provide data plane interconnections between cards. This allows the pairing of card slots and to split transponder functions across multiple cards, for example into cards containing only network ports (“line cards”) and cards containing only client ports (“tributary cards”). An electronic switch fabric, typically distributed across two or more cards for redundancy reasons, can turn a transponder shelf into an electronic cross-connect, which can switch at the wavelength, OTN and/or SDH/SONET traffic levels. Adding packet processing functions converts such equipment into a packet optical transport platform (POTP). Traffic processing at layer 2 or 3 only effectively turns the platform into a packet switch or router with integrated colored interfaces.

Fig. 4.6.1 WDM transport equipment comprising different shelf variants and different transponder cards (courtesy of ADVA Optical Networking).

4.6.1 Transponder Types

Generalizing the transponder definition from section 4.1, then four basic card types can be distinguished: a transponder, a muxponder, an add-drop-multiplexer and a cross-connect. Line cards can be made configurable to support more than one of these functionalities. Figure 4.6.2 illustrates the basic card types.

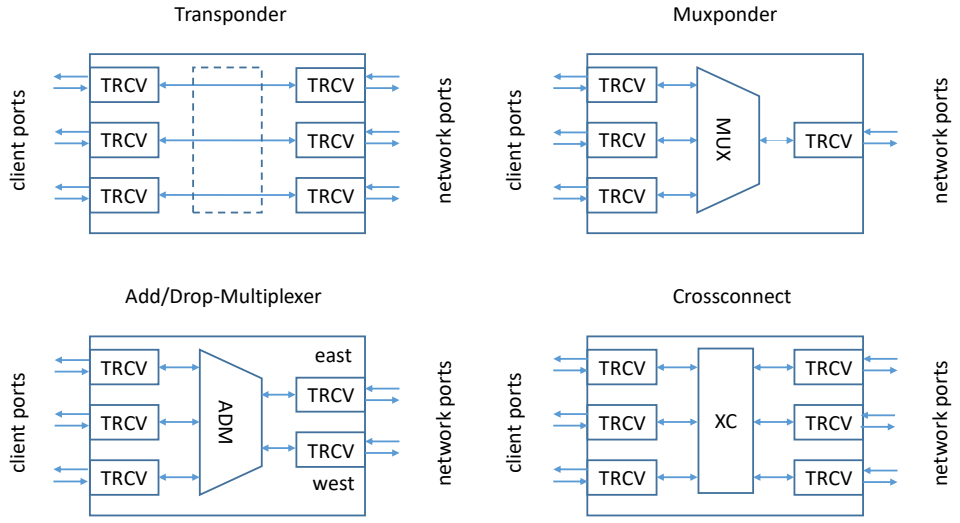

Fig. 4.6.2 Basic card types and operational modes. TRCV: transceiver, MUX: multiplexer, ADM: add/drop multiplexer, XC: cross-connect.

A *transponder* is characterized by a 1-to-1 relationship between client and network ports. There are two basic modes of operation: transparent and mapped, both will be described below.

In *transparent* mode, the transponder performs a 2R (reamplifying and reshaping) or 3R (with additional retiming) regeneration between client and network ports without any intermediate protocol processing. Such a configuration can be attractive because of its low complexity and latency, but only allows limited signal monitoring and conditioning. If the same optical interface types are employed on the network and client side, the transponder acts as a simple regenerator. If different optical interface types are used on both sides, the transponder performs a media conversion and can serve as a demarcation point between different network or equipment domains. A switching function between client and network ports - if available - can be used for signal restoration: in the case of failures on the network side, client ports can be switched to an alternative network port. Depending on the switching capabilities and the number of supported ports then 1+1, 1:1 or 1: N protection schemes can be supported. If client and line interfaces are realized with pluggable transceivers, only those transceivers need to be equipped which are required for the desired functionality.

In *mapped* mode, then the transponder also performs a protocol conversion between the client and line signals. Multiple services such as local area network (LAN), storage area network (SAN), high-performance computing (HPC), video distribution, passive optical networking, synchronous digital hierarchy (SDH)/synchronous optical network (SONET), optical transport network (OTN) and generic constant bit rate (CBR) or packetized signals on the client side can be mapped into a transport signal on the line side. Please see chapter 12.2.8 for a summary of the most popularly used client signals. While SDH and SONET have been used since the late 1980's, OTN was introduced in 2001 and has since then established itself as the common transport protocol on the network side. Adding a protocol mapper to a transponder allows the monitoring of client and line signals which eases operations, administration and maintenance (OAM) of the signal and offers increased performance by optional forward error correction (FEC). It can also provide fault and performance management capabilities as well.

A *muxponder* is a combination of a multiplexer and a transponder. It is characterized by an N-to-1 relationship between client and network ports. Several client signals are multiplexed together to obtain a higher speed line signal. 10G and

100G muxponders are the most commonly used today (note that the letters “M” and “G” are used to denote the data rate units “Mb/s” and “Gb/s” respectively). The client ports can support different service types and data rates and may require specific mapping processes depending on the selected service. OAM functions allow the integrity of the service to be monitored and to take the necessary actions in case of faults or performance issues. As client ports generally run on independent clocks, an adaptation to the common clock of the line signal is required (for example by bit or byte stuffing). Multiplexing can be done in one or more stages and based on SDH/SONET, OTN or other technologies. Aggregation of services at a packet level is also possible if the muxponder is equipped with packet processing functions.

An *add/drop multiplexer* is an extension of the muxponder where a second network port is available to enable the support of ring or protected point-to-point applications. The two network ports are often named “east” and “west” ports indicating that they are connected to two diverse fiber routes or ring directions. An add/drop multiplexer can pass traffic between the network ports (called pass-through traffic) and can terminate a portion of the traffic locally (called add/drop traffic) at each network port. A predefined mapping and multiplexing structure as well as a time slot approach is required to be able to isolate the client signals contained within the aggregate line signals. Client signals can be protected against link failures by switching the respective traffic from one to the other network port. In many cases, an add/drop multiplexer can also be operated as two independent muxponders, provided enough client ports are available to match the capacity of the line signal. While add/drop-multiplexers commonly operate on layer 1, adding and dropping of client signals can also be performed at layer 2 or 3, thereby providing oversubscription and statistical multiplexing capabilities.

A *cross-connect* allows a flexible switching between network and client ports, including hair-pinning for client-to-client connections. Multiple colored network ports allows multi-degree network nodes to be supported, switching signals between more than two fiber directions. Client ports provide local add/drop access. Depending on the card architecture, the distinction between network and client port can be removed, and any port can serve as network or client port. Switching can be performed on multiple levels and are not restricted to simple port-to-port connectivity only. Higher-order SDH and SONET cross-connects operating on a VC-4 (155M) and STS-1 (51M) granularity, respectively. OTN cross-connects can switch on ODUk (where if k=0 then the data rate is 1.25G, if k=1 2.5G, if k=2/2e 10G, if k=3 40G, and if k=4 100G) and ODUflex (supporting multiples of 1.25G) levels. They can operate with tributary slot granularities of 1.25G, 2.5G or 5G. If a cross-connect supports switching at the packet level, packet flows at Mb/s or lower granularities can also be supported. In principle, SDH/SONET, OTN and packet traffic require dedicated switching matrices. As the size of these matrices needs to be determined upfront, this either limits the flexibility leading to blocking of signals or requires an over-provisioning of switch capacity. A universal switch matrix can alleviate these disadvantages and is of particular interest if cross-connect functions are split across multiple cards [gringeri07]. In a packet based universal switch, signals are segmented into packets at ingress, passed over the fabric, and then reassembled at egress. The functional unit performing the packetization is often called a segmentation and reassembly (SAR) block. Typical packet lengths are 128, 256 or 512 bytes. Although, care needs to be exercised so that client timing (phase and frequency) is maintained and latency as well as latency variations across the fabric are minimized. This can be achieved by variable length packets in which the packet size is slightly varied over time, for instance by lengthening or shortening the packet size by one byte [oif-otn]. Small cross-connects can be realized on a single line card, whereas large cross-connects can occupy a modular equipment shelf or even require multi-shelf configurations scaling up to tens of Tb/s of switching capacity.

4.6.2 The Anatomy of a Line Card

WDM platforms often use a generic line card approach. A common base design provides the functions necessary for the operation of any card. Customization is then performed to accommodate specific optical and electronic components for realization, for instance a transponder, an amplifier or a wavelength-selective switch card. In multi-slot systems, a backplane is used to connect the line cards with the host platform. It provides power and control to the line cards and may include high-speed data plane connections between line cards or to a central switch fabric.

Common card functions include DC/DC converters, control logic and the card processor. WDM platforms run off a -48V or +12V DC (often redundant) power supply which feeds the line cards via the backplane. DC/DC converters on

the card then derive all the necessary supply voltages from the base voltage. An onboard microprocessor connects the card to the shelf or network element controller, it is responsible for controlling and managing all card functions as well as collecting associated fault and performance data. The microprocessor system may contain Electronically Erasable Programmable Read-Only Memory (EEPROM) and flash memory for storing the card calibration data and the card firmware, respectively. Often, the microprocessor is accompanied by additional control logic such as field-programmable gate arrays (FPGAs) which are used for more elaborate control tasks while complex programmable logic devices (CPLDs) are often employed whenever simple logic operations need to be performed in a hard wired manner (for example laser safety actions).

Figure 4.6.2 shows the block diagram of a simple OTN transponder line card. In the text, the signal flow only in one direction will be described for clarity, while the other direction passes through the same functional blocks in the reverse order.

A grey transceiver on the client port receives the incoming optical signal, performs an optical to electrical conversion, and passes the signal on to an OTN mapper device. At lower speeds, the electrical interface between the transceiver and the mapper comprises only a single digital lane per direction. At higher speeds, the interface can be implemented over multiple parallel lanes. It then requires a multi-lane distribution (MLD) algorithm to distribute the transceiver signal over the lanes at one side and to reassemble it at the other side, taking into account the fact that delay differences between the lanes need to be compensated for by appropriate skew management. If enabled, client side FEC is applied before the signal is passed onto the next step. Often, a non-intrusive monitoring of the client signal is provided to ensure that the incoming signal is of good quality and that the client side network connection is working properly. If the client signal is not already an OTN signal, the client mapper then maps the received signal into an optical payload unit (OPU). The mapping is client specific and can be performed employing a bit-synchronous (BMP), asynchronous (AMP), generic (GMP) or idle (IMP) mapping procedure [G.709]. With BMP, the line clock is phase-locked to the client signal. AMP, GMP and IMP typically operate with a line clock that is independent from the client clock and therefore require stuffing of bits, bytes or control characters to compensate for clock rate differences between the line and client clocks. Since its introduction in 2009, GMP has become the preferred mode for all new mappings due to its flexibility and capability to compensate large clock tolerances. Constant bit rate (CBR) signals can directly be mapped into OPU, while packetized signals must first undergo an adaptation step using the Generic Framing Procedure (GFP) [G.7041] or IMP. Timing transparent transcoding (TTT) [G.709] may be used as an intermediate step for CBR signals to reduce the data rate of client signals by compressing the employed line coding overhead. In the OxU (OTU/ODU/OPU) framer, the OPU signal is mapped into an Optical Data Unit (ODU) and the ODU is mapped into an Optical Transport Unit (OTU). After adding FEC information, the signal is then sent to the colored transceiver on the line side (using MLD in case of multiple electrical lanes) where the electrical signal is converted into an optical DWDM signal.

The client and line side transceivers may be realized as pluggable modules or discrete implementations on the transponder line card. They may contain clock-and-data recovery as well as basic equalization capabilities to compensate for the PCB trace losses between the transceivers and the mapper device. If the number of optical lanes and electrical lanes is different, they may also incorporate a multiplexer or gearbox IC. For higher data rates and longer reach applications, an enhanced FEC function may also be included. Coherent transceivers typically use a dedicated digital signal processor (DSP). In this case, some OTN mapping and multiplexing functions may be incorporated into the DSP, eliminating the need for a separate OTN mapper device in certain applications.

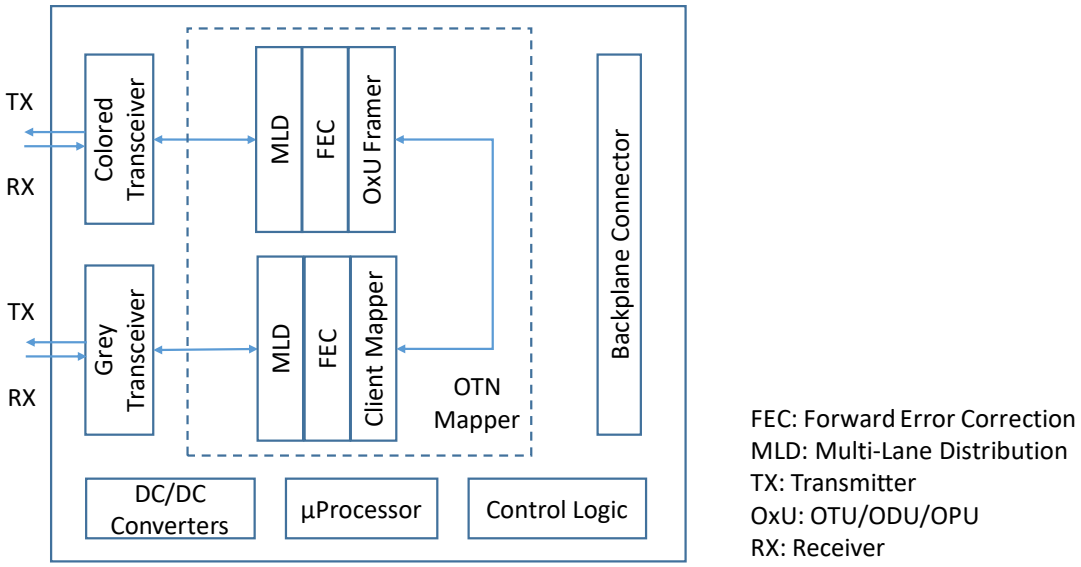

Fig. 4.6.3 Block diagram of a simple OTN transponder line card

Extending the functions available to the transponder card described above, Fig. 4.6.4 shows a universal OTN line card which facilitates access to CBR, packet (for example Ethernet or IP/MPLS flows), TDM traffic (SDH/SONET) and OTN traffic from each of the optical interfaces. The interfaces may be implemented using pluggable transceivers. At data rates up to 10G, colored (line side) and grey (client side) transceivers may use the same pluggable module standard. If the protocol processing capabilities are then the same for each port, a flexible allocation of ports to network and client side traffic is possible. The OTN mapper device offers configurable protocol processing blocks which can either pass the frames through sequentially or make them accessible via device internal switches which allow individual signal paths for each port to be programmed. Assuming that each of the blocks can be bypassed if it is not required, Fig. 4.6.4 depicts a sequential arrangement of processing blocks. Incoming OTN signals from the transceivers are passed through the MLD and FEC blocks and then enter the OxU framer, where they are demapped and forwarded to the ODU multiplexer. If the OTN signSal comprises a multiplex of lower order ODUk signals, then a demultiplexing is performed to access these lower order signals. While an OTN signal in principle may be multiplexed over multiple stages (for example ODU0 to ODU1 to ODU2 to ODU3 to ODU4), practical considerations and hardware constraints often limit the MUX block inside the mapper device to two multiplexing and several mapping stages which can be arbitrarily selected. At this point, multiple processing paths are possible: ODUk signals can directly be cross-connected (XC) to other ports of the same mapper device or passed on to a centralized switch matrix. A SAR device packetizes the OTN signals which are delivered to a universal packet based switch fabric via a fabric interface chip (FIC). Typically, an Interlaken interface is used between the OTN mapper and the FIC. For smaller switch configurations, a direct interconnection of OTN mapper devices between paired cards is also sometimes possible, alleviating the need for a FIC in between. FEC and time stamping may be provided to improve the transmission and timing performance over the fabric. If CBR, packet or TDM client signals inside an ODUk are to be accessed, the signals are passed on to a client mapper which extracts the traffic and cross-connects it either to another transceiver port or to the universal switch matrix via a SAR and an FIC. For advanced processing of packet traffic, an external packet processor (PM) and traffic manager (TM) is often used before the traffic is passed on to the switch matrix via the FIC. Packet traffic does not need to pass through the SAR block, as it is supported natively by the packet fabric. CBR, TDM or packet traffic entering from a grey transceiver may pass the MLD and FEC blocks and is then

directly processed in the client mapper, bypassing the OxU framer and ODU MUX stages. It can then be switched to another transponder port as in the case of the simple transponder of Fig. 4.6.3, directly fed to the switch fabric, or wrapped into an ODU structure first and then passed through the ODU MUX block.

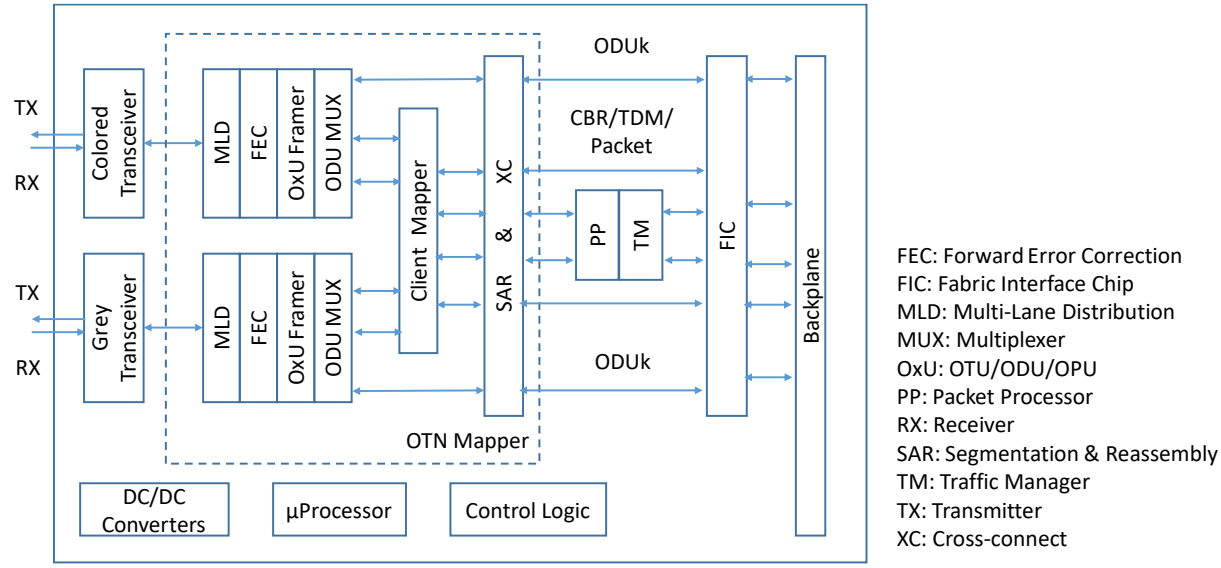

Fig. 4.6.4 Block diagram of a universal OTN line card

4.6.3 Interface Standards

Standards are necessary to facilitate a line card design based on interoperable building blocks which can be procured from multiple sources. The most important areas of standardization include transceiver modules as well as their respective optical, electrical and control interfaces. While transceivers historically were implemented using discrete optics and electronics, multi-source agreements (MSA) for transceivers emerged in the late 1990's and allowed the use of integrated transceiver modules instead.

Hot pluggable, front plate accessible transceiver modules were introduced starting with the Gigabit Interface Converter (GBIC) in 1995, followed by the 10 Gigabit Ethernet Transceiver Package (XENPAK) and the Small Form Factor Pluggable (SFP) Transceiver in 2001, the 10 Gigabit Small Form Factor Pluggable (XFP) module in 2002, the Quad Small Form Factor Pluggable (QSFP) transceiver and the 1 x 10 Gb/s Small Form Factor Pluggable (SFP+) transceiver in 2006, as well as the 10 Gb/s 4x Pluggable Transceiver (QSFP+) in 2009. SFP+ and QSFP+ modules are available in different speed classes. To distinguish them, the nominal electrical lane speed is often appended instead of the "+" symbol (for example SFP10 and QSFP10). The MSA's define the mechanics, the electrical connector, the power supply as well as the high and low speed signaling along with implementation and measurement descriptions. The specifications are maintained by the Storage Networking Industry Association (SNIA) small form factor (SFF) Technology Affiliate Technical Work Group [snia]. New developments include the QSFP Double Density (QSFP-DD) [qsfp-dd] and the Octal SFP (OSFP) [osfp] targeting 400G and the SFP Double Density (SFP-DD) [sfp-dd] targeting 100G applications.

Also the 40G/100G Form Factor (CFP) MSA group [cfp] has developed specifications for 100G+ transceivers offering more space for component integration and a higher power dissipation than their SFP and QSFP counterparts. Since

formation of the group in 2009, three generations of 100G Small Form Factor Pluggable (CFP) modules (CFP, CFP2 and CFP4) were brought to market, while the CFP8 specification has just been released in 2017.
The most common front pluggable optical modules are illustrated in Fig. 4.6.5 with a twisted pair RJ45 copper cable connector for comparison, along with new module standards in development for 400G and beyond. QSFP-DD is by many the favored 400G interface standard, although it is the most challenging from an integration and thermal management point of view, as it possesses a smaller module surface area compared to the OSFP and CFP8.

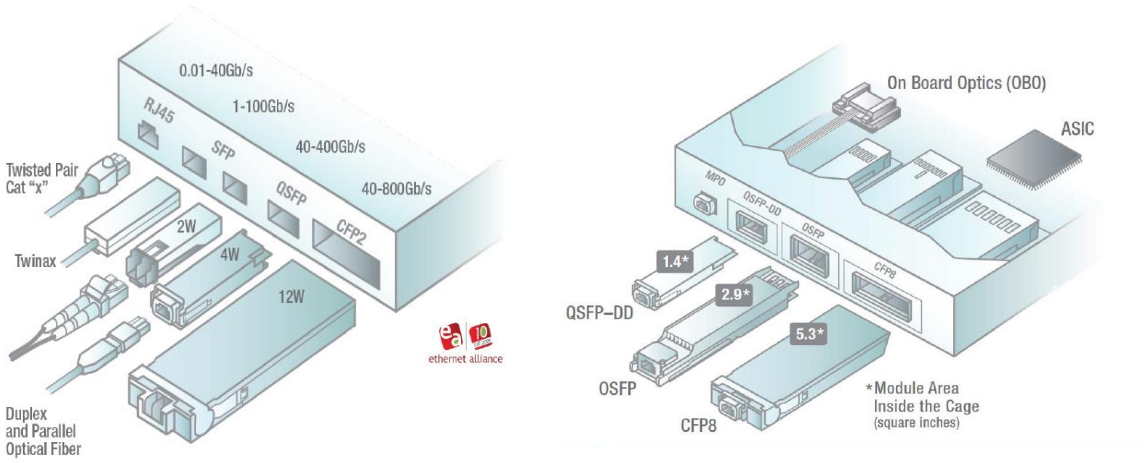

Fig. 4.6.5 Pluggable module form factors (left: current modules, right: modules in development for 400G), adapted from [EA].

In addition to front pluggable modules, MSAs have been drawn up for PCB mountable optical transceivers (on-board optics - OBO). This development started with 300 pin transceivers for 10G applications in a 5 x 7 inch footprint which were first released in 2001. Subsequently a smaller form factor variant (2.2 x 3 inches) and 40G support were added and the first 40G MSA modules became available in 2006. While the primary design target was colored WDM applications, MSA modules for grey interface applications were also offered. For 100G coherent long haul applications, the OIF published an implementation agreement for a 5 x 7 inch 168 pin transmission module in 2011 [oif-168] which was augmented in 2015 by a second release targeting a smaller module footprint (4 x 5 inches). Advances in CMOS technology and photonic integration since then have allowed integrating digital coherent 100G/200G transceivers also into CFP and CFP2 front pluggable modules (digital coherent optics or DCO modules). As an intermediate step to the CFP2-DCO module, a CFP2-ACO analog coherent optics transceiver was released which integrates all optics and RF electronics but not the coherent DSP. Further development directions include the definition of 400G and 800G on-board optical modules as currently being pursued by the Consortium on On-Board Optics (COBO) [cobo] as well as an integration of 400G coherent transceiver technology into next generation optical modules (QSFP-DD, OSFP, CFP8 or coherent OBO).
Client side optical interface standards are defined by the industry bodies responsible for the respective protocol specifications. These are Telcordia for SONET, the ITU-T Study Group 15 for SDH, OTN and PON, the IEEE 802.3 group for Ethernet and Ethernet-PON, the International Committee for Information Technology Standards (Incits) Task Group 11 (T11) for Fiber Channel, the Infiniband Trade Association (IBTA) for Infiniband, the CPRI group for the Common Public Radio Interface, and the Society of Motion Picture and Television Engineers (SMPTE) for video distribution.
An overview of Ethernet interfaces over single mode (SMF) and multi-mode (MMF) fiber along with their electrical host side interfaces is shown in Tab. 4.6.1. Note that the numbers stated after the interface classifier indicate the number of parallel signaling lanes (with exception of the 4WDM interfaces where the numbers indicate the reach in

km). NRZ signaling is commonly used up to 25G, and PAM4 signaling above this rate on optical and electrical interfaces.

	Electrical Interface	MMF	Parallel SMF	2km SMF	10km SMF	40km SMF
100BASE-		FX			LX	
1000BASE-		SX			LX	
10GBASE-	SFI, XFI, XSBI, XAUI	SR			LR	ER
25GBASE-	25GAUI	SR			LR	ER
40GBASE-	XLAUI	SR4	PSM4	FR	LR4	ER4
50GBASE-	LAUI-2/ 50GAUI-2 50GAUI-1	SR		FR	LR	ER
100GBASE-	CAUI-10 CAUI-4/ 100GAUI-4 100GAUI-2 100GAUI-1	SR10 SR4 SR2	PSM4 DR	10x10 CWDM4 CLR4 100G-FR	10x10 LR4 4WDM-10 100G-LR	ER4 4WDM-40
200GBASE-	200GAUI-4 200GAUI-2	SR4	DR4	FR4	LR4	ER2
400GBASE-	400GAUI-16 400GAUI-8 400GAUI-4	SR16	DR4	FR8 FR4	LR8	ER8 ER4

Table 4.6.1 Ethernet interface standards and related nomenclature, adapted from [EA]. Color code: black = IEEE standard, blue = non-IEEE standard but complies to IEEE electrical interfaces, red: under discussion in standardization.

Optical client side interfaces for SDH/SONET and OTN signals are defined in the Telcordia GR-253 standard as well as the ITU-T G.957, G.691-693, G.695 and G.959.1 recommendations. Colored line side interfaces are described in the ITU-T G.698 series of recommendations. Published ITU-T recommendations can be accessed online here [itu-t]. The OIF Common Electrical I/O Implementation Agreement (CEI IA) defines electrical and jitter requirements for electrical chip-to-module, chip-to-chip and backplane interfaces. Currently included are interfaces with 3G, 6G, 11G and 28G signaling rates [oif-cei], new revisions including 56G and 112G are already in development. The CEI forms the basis of the 10 to 400G attachment unit interfaces (AUI) as well as the SFP (SFI) and XFP (XFI) interfaces connecting Ethernet transceivers to the attached host board chip. For the AUI, a change of the speed classes is occurring translating from Arabic to Roman numerals (e.g. from CAUI where “C” denotes 100 to 100GAUI). Protocol specific aspects such as MLD are defined in the IEEE 802.3 standard. The CEI IA also defines the electrical parameters for SDH/SONET and OTN module-to mapper/framer-interfaces. At 10G, these interfaces typically need only a single serial electrical lane (SFI/XFI) and therefore do not require any MLD. At 40G, a group of four synchronous (STL256.4) and optical transport lanes (OTL3.4) as defined in ITU-T G.707 and G.709 are used for SDH/SONET and OTN signals, respectively. 100G OTN signals are transported over a 10x10G (OTL4.10) or a 4x25G (OTL4.4)

interface. Beyond 100G module-to-framer interfaces can use multiple 100G optical transport lane (OTLC) groups or a FlexO Interface (FOIC) as described in ITU-T G.Sup58 [G.Sup58]. Future interface standards are expected to increase the signaling rate and reduce the number of lanes further.

Digital control of transceiver modules relies on either a two wire serial (TWS) or a management data input/output (MDIO) interface as defined in IEEE 802.3. Currently, the management interface specification (MIS) forms part of module MSA documentation and is specifically developed for it. In the future, a common MIS (CMIS) may be created from which a module MIS can be derived.

References

[agrawal11] G.P. Agrawal: *Fiber-Optic Communication System* (John Wiley & Sons, Inc., Hoboken, New Jersey, 2011)

[armstrong09] J. Armstrong: OFDM for Optical Communications, J. Lightwave Technol. **27**(3), 189–204 (2009).

[atia99] W. A. Atia, R. S. Bondurant: Demonstration of return-to-zero signaling in both OOK and DPSK formats to improve receiver sensitivity in an optically preamplified receiver, Proc. of IEEE Lasers and Electro-Optics Society Annual Meeting (LEOS '99), Orlando, 1999,vol. 1, pp. 226–227.

[baeuerle16] B. Baeuerle, A. Josten, R. Bonjour, D. Hillerkuss, and J. Leuthold: Effect of Transmitter Impairments on Nyquist-FDM Signals with Increasing Sub-band Granularity," Proc. of Advanced Photonics 2016, Vancouver, 2016, paper SpW3F.4

[baeuerle17] B. Baeuerle, A. Josten, M. Eppenberger, D. Hillerkuss, J. Leuthold: FPGA-based Realtime Receivers for Nyquist-FDM, Proc. of Advanced Photonics 2017, New Orleans, 2017, paper SpM3F.3.

[bakhshi01] B. Bakhshi, M. Vaa, E. A. Golovchenko, W. W. Patterson, R. L. Maybach, and N. S. Bergano: Comparison of CRZ, RZ and NRZ modulation formats in a 64x12.3 Gb/s WDM transmission experiment over 9000 km, Proc. Optical Fiber Communication Conference (OFC), Anaheim, 2001, paper WF4.

[bergano98] N.S. Bergano, C.R. Davidson, M. Ma, A. Pilipetskii, S. G. Evangelides, H. D. Kidorf, M. Darcie, E. Golovchenko, K. Rottwitt, P.C. Corbett, R. Meges, M.A. Mills, B. Pedersen, D. Peckham, A. A. Abramov, A.M. Vengsarkar: 320 Gb/s WDM Transmission (64x5 Gb/s) over 7,200 km using Large Mode Fiber Spans and Chirped Retum-to-Zero Signals, Proc. of Optical Fiber Communication Conference (OFC), San Jose, 1998, paper PDI2.

[bergano02] N. S. Bergano: Undersea communication systems, in *Optical Fiber Telecommunication IV* (I. Kaminow and T. Li, Eds. New York: Academic, 2002)

[bigo01] S. Bigo, Y. Frignac, G. Charlet, W. Idler, S. Borne, H. Gross, R. Dischler, W. Poehlmann, P. Tran, C. Simonneau, D. Bayart, G. Veith, A. Jourdan, and J. Hamaide: 10.2Tbit/s (256x42.7Gbit/s PDM/WDM) transmission over 100km TeraLight fiber with 1.28bit/s/Hz spectral efficiency, Proc. Optical Fiber Communication Conference (OFC), Anaheim (2001), paper PD25.

[birk05] M. Birk, C. Skolnick, R. Curto, R. Marlieb, T. J. Schmidt, R. Saunders, H. Zech, H. Schucht, J. Heinrich, and C. Weiske: Field Trial of a 40 Gbit/s PSBT Channel Upgrade to an Installed 1700 km 10 Gbit/s System, Proc. of Optical Fiber Communication Conference and Exposition (OFC), Anaheim, 2005, paper OTuH3.

[bissesur01] H. Bissessur, G. Charlet, C. Simonneau, S. Borne, L. Pierre, C. De Barros, P. Tran, W. Idler, R. Dischler: 3.2 Tb/s (80x40 Gb/s) C-band transmission over 3x100 km with 0.8 bit/s/Hz efficiency," Proc. of 27th European Conference on Optical Communication, Amsterdam, 2001, Paper PD.M.1.11

[bosco01] G. Bosco, R. Gaudino, P. Poggiolini: An exact analysis of RZ versus NRZ sensitivity in ASE noise limited optical systems, Proc. of 27th European Conference on Optical Communication, Amsterdam, 2001, vol. 4, pp. 526–527.

[bosco02] G. Bosco, A. Carena, V. Curri, R. Gaudino, P. Poggiolini: On the Use of NRZ, RZ, and CSRZ Modulation at 40 Gb/s With Narrow DWDM Channel Spacing, J. Lightwave Technol. **20**(9), 1694–1704 (2002)

[bosco03] G. Bosco, A. Carena, V. Curri, R. Gaudino and P. Poggiolini: Quantum limit of direct detection optically preamplified receivers using duobinary transmission, IEEE Photonic Technology Letters **15**(1), 102–104 (2003)

[bosco04] G. Bosco, A. Carena, V. Curri, R. Gaudino and P. Poggiolini: Modulation formats suitable for ultrahigh spectral efficient WDM systems, IEEE Journal of Selected Topics in Quantum Electronics **10**(2), 321–328 (2004)

[bosco04b] G. Bosco, A. Carena, V. Curri, P. Poggiolini: Best optical filtering for duobinary transmission", in *Optical Communication Theory and Techniques* (Springer, Boston, 2005), pp. 21-28.

[bosco05] G. Bosco, P. Poggiolini: The impact of receiver imperfections on the performance of optical direct-detection DPSK, J. Lightwave Technol. **23**(2), 842–848 (2005)

[bosco06] G. Bosco, P. Poggiolini: On the joint effect of receiver impairments on direct-detection DQPSK systems, J. Lightwave Technol. **24**(3), 1323–1333 (2006)

[bosco10] G. Bosco, A. Carena, V. Curri, P. Poggiolini, F. Forghieri: Performance limits of Nyquist-WDM and CO-OFDM in high-speed PM-QPSK systems, IEEE Photonics Technol Lett. **22**(15), 1129–1131 (2010)

[bosco11] G. Bosco, V. Curri, A. Carena, P. Poggiolini, F. Forghieri: On the Performance of Nyquist-WDM Terabit Superchannels Based on PM-BPSK, PM-QPSK, PM-8QAM or PM-16QAM Subcarriers, J. Lightw. Technol. **29**(1), 53–61 (2011)

[bosco12] G. Bosco: Spectral shaping in ultra-dense WDM systems: Optical vs. electrical approaches, Proc. of Optical Fiber Communication Conference, Los Angeles, 2012, paper OM3H.1.

[bosco16] G. Bosco: Spectrally Efficient Multiplexing: Nyquist-WDM, book chapter in *Enabling Technologies for High Spectral-efficiency Coherent Optical Communication Networks* (John Wiley & Sons, Inc., New Jersey, 2016), pp. 123–156.

[bosco16b] G. Bosco, S.M. Bilal, A. Nespola, P. Poggiolini, F. Forghieri: Impact of the Transmitter IQ-Skew in Multi-Subcarrier Coherent Optical Systems, Proc. of Optical Fiber Communication Conf. and Exposition (OFC), Anaheim, 2016, paper W4A.5.

[bosco17] G. Bosco, D. Pilori, P. Poggiolini, A. Carena, F. Guiomar: Scalable modulation technology and the tradeoff of reach, spectral efficiency, and complexity, SPIE Proceedings 10130: *Next-Generation Optical Communication: Components, Sub-Systems, and Systems VI* (Guifang Li; Xiang Zhou, Editors, 2017)

[buchali14] F. Buchali, L. Schmalen, K. Schuh, and W. Idler: Optimization of time-division hybrid-modulation and its application to rate adaptive 200 Gb transmission, Proc. of European Conference on Optical Communication (ECOC), Cannes, 2014, paper Tu.4.3.1.

[buchali16] F. Buchali, F. Steiner, G. Böcherer, L. Schmalen, P. Schulte, W. Idler: Rate adaptation and reach increase by probabilistically shaped 64-QAM: An experimental demonstration, J. Lightw. Technol. **34**(7), 1599–1609 (2016)

[cai12] J-X. Cai: 100G transmission over transoceanic distance with high spectral efficiency and large capacity, J. Lightwave Technol. **30**(24), 3845–3856(2012)

[cai14] J.-X. Cai, H. Zhang, H.G. Batshon, M. Mazurczyk, O.V. Sinkin, D.G. Foursa, A.N. Pilipetskii, G. Mohs, N.S. Bergano: 200 Gb/s and dual wavelength 400 Gb/s transmission over transpacific distance at 6.0 bit/s/Hz spectral efficiency, J. Lightwave Technol. **32**(4), 832–939 (2014)

[cfp] 100 G Formfaktor Pluggable (CFP) Multi Source Agreement Group, online at http://www.cfp-msa.org/

[chandra09] S. Chandrasekhar, X. Liu, B. Zhu, and D. W. Peckham: Transmission of a 1.2-Tb/s 24-carrier no-guard-interval coherent OFDM superchannel over 7200-km of ultra-large-area fiber, in Proc. Eur. Conf. Opt. Commun., Vienna, 2009, paper PD2.6.

[chinn96] S. R. Chinn, D. M. Boroson, and J. C. Livas: Sensitivity of optically preamplified DPSK receivers with Fabry-Perot filters, J. Lightw. Technol. **14**(9), 370–376 (1996)

[cho06] P. S. Cho, J. B. Khurgin, I. Shpantzer: Closed-loop bias control of optical quadrature modulator, IEEE Photon. Technol. Lett. **18**(21), 2209–2211 (2006)

[cigliutti11] R. Cigliutti, E. Torrengo, G. Bosco, N.P. Caponio, A. Carena, V. Curri, P. Poggiolini, Y. Yamamoto, T. Sasaki, F. Forghieri: Transmission of 9x138 Gb/s prefiltered PM-8QAM signals Over 4000 km of pure silica-core fiber, J. Lightwave Technol. **29**(15), 2310–2318 (2011)

[cigliutti12] R.Cigliutti, A. Nespola, D. Zeolla, G. Bosco, A. Carena, V. Curri, F. Forghieri, Y. Yamamoto, T. Sasaki, P. Poggiolini: 16×125 Gb/s Quasi-Nyquist DAC-generated PM-16QAM transmission over 3590 km of PSCF, IEEE Photonics Technol Lett. **24**(23), 2143–2146 (2012).

[cobo] Consortium on On-Board Optics (COBO), online at http://onboardoptics.org/

[curri14] V. Curri, A. Carena, P.Poggiolini, R. Cigliutti, F.Forghieri, C. R. Fludger, T. Kupfer: Time-division hybrid modulation formats: Tx operation strategies and countermeasures to nonlinear propagation, Proc. of Optical Fiber Communication Conf. and Exposition (OFC), San Francisco, 2014, paper Tu3A.2.

[czotscher99] K. Czotscher, S. Weisser, A. Leven, and J. Rosenzweig: Intensity modulation and chirp of 1.55-μm multiple-quantum-well laser diodes: Modeling and experimental verification, IEEE J. Sel. Topics Quantum Electron. **5**(3), 606–612 (1999)

[dar14] R. Dar, M. Feder, A. Mecozzi, and M. Shtaif: On shaping gain in the nonlinear fiber-optic channel," in Proc. IEEE Int. Symp. Inf. Theory (ISIT), Honolulu, 2014, pp. 2794–2798.

[davis87] A. W. Davis, M. J. Pettitt, P. J. King, S. Wright: Phase diversity techniques for coherent optical receivers, J. Lightw. Technol. **5**(4), 561–572(1987)

[derr92] F. Derr: Coherent optical QPSK intradyne system: Concept and digital receiver realization, J. Lightw. Technol. **10**(9), 1290–1296 (1992)

[dong16] P. Dong, J. Lee, K. Kim, Y. Chen, and C. Gui: Ten-channel discrete multi-tone modulation using silicon microring modulator array, Proc. of Optical Fiber Communication Conference (OFC), Anaheim, 2016, paper W4J.4.

[dou16] L. Dou, X. Su, Y. Fan, H. Chen, Y. Zhao, Z. Tao, T. Tanimura, T. Hoshida, J. Rasmussen: 420Gbit/s DP-64QAM Nyquist-FDM Single-Carrier System, Proc. of Optical Fiber Communication Conference (OFC), Anaheim, 2016, paper Tu3A.5.

[EA] Ethernet Alliance, online at https://ethernetalliance.org/

[eiselt16] N. Eiselt, H. Griesser, J. Wei, A. Dochhan, R. Hohenleitner, M. Ortsiefer, M. Eiselt, C. Neumeyr, J. J. V. Olmos, and I. T. Monroy: Experimental Demonstration of 56 Gbit/s PAM-4 over 15 km and 84 Gbit/s PAM-4 over 1 km SSMF at 1525 nm using a 25G VCSEL, Proc. of European Conference on Optical Communication (ECOC), Amsterdam, 2016, paper Th.1.C.1.

[essiambre10] R.-J. Essiambre, G. Kramer, P. J. Winzer, G. J. Foschini, B. Goebel: Capacity Limits of Optical Fiber Networks, J. Lightwave Technol. **8**(7), 662–698 (2010)

[fehenberger15] T. Fehenberger, G. Böcherer, A. Alvarado, N. Hanik, LDPC coded modulation with probabilistic shaping for optical fiber systems, Proc. of Optical Fiber Communication Conference (OFC), Los Angeles, 2015, paper Th2A.23.

[filer16] M. Filer, J. Gaudette, M. Ghobadi, R. Mahajan, T. Issenhuth, B. Klinkers, J. Cox: Elastic Optical Networking in the Microsoft Cloud, J. Optical Commun. and Networking **8**(7), A45–A54 (2016)

[fishman06] D. A. Fishman, W.A.Thompson, L. Vallone: LambdaXtreme transport system: R&D of a high capacity system for low cost, ultra-long haul DWDM transport, Bell Labs Tech. J. **11**(2), 27–53 (2006)

[fludger08] C.R.S. Fludger, T. Duthel, D. van den Borne, C. Schulien, E.-D. Schmidt, T. Wuth, J. Geyer, E. De Man, G.-D. Khoe, H. de Waardt: Coherent equalization and POLMUX-RZDQPSK for robust 100-GE transmission, J. Lightw. Technol. **26**(1), 64–72 (2008)

[fludger13] C.R.S. Fludger, T. Duthel, P. Hermann, T. Kupfer: Jitter tolerant clock recovery for coherent optical receivers, Proc. of Optical Fiber Communication Conference (OFC), Anaheim, 2013, paper OTh1F.3

[foschini99] G.J. Foschini, R.M. Jopson, L.E. Nelson, H. Kogelnik: The Statistics of PMD-Induced Chromatic Fiber Dispersion, J. Lightwave Technol. **17**(9), 1560–1565 (1999)

[foursa13] D.G. Foursa, H.G. Batshon, H. Zhang, M. Mazurczyk, J.-X. Cai, O. Sinkin, A. Pilipetskii, G. Mohs, N.S. Bergano: 44.1 Tb/s transmission over 9,100 km using coded modulation based on 16QAM signals at 4.9 bits/s/Hz spectral efficiency, Proc. European Conference on Optical Communication, London, 2013, Paper PD3.E.1.

[fyath89] R.S. Fyath, J.J. O'Reilly: Performance of optically preamplified direct-detection receivers in the presence of laser chirp. Part I. Ideal travelling-wave amplifier, IEE Proceedings J. Optoelectronics **136**(5), 249–255 (1989)

[G.691] ITU-T Recommendation G.691: Optical interfaces for single channel STM-64 and other SDH systems with optical amplifiers, online at https://www.itu.int/rec/T-REC-G/en

[G.694.1] ITU-T Recommendation G.694.1: Spectral grids for WDM applications: DWDM frequency grid, online at https://www.itu.int/rec/T-REC-G/en

[G.694.2] ITU-T Recommendation G.694.2: Spectral grids for WDM applications: CWDM wavelength grid, online at https://www.itu.int/rec/T-REC-G/en

[G.698.2] ITU-T Recommendation G.698.2: Amplified multichannel dense wavelength division multiplexing applications with single channel optical interfaces, online at https://www.itu.int/rec/T-REC-G/en

[G.709] ITU-T Recommendation G.709: Interfaces for the optical transport network, online at https://www.itu.int/rec/T-REC-G/en

[G.7041] ITU-T Recommendation G.7041: Generic framing procedure, online at https://www.itu.int/rec/T-REC-G/en

[G.8251] ITU-T Recommendation G.8251: The control of jitter and wander within the optical transport network (OTN), online at https://www.itu.int/rec/T-REC-G/en

[G.975.1] ITU-T Recommendation G.975.1: Forward error correction for high bit-rate DWDM submarine systems, online at https://www.itu.int/rec/T-REC-G/en

[G.Sup39] ITU-T Recommendation G.Sup39: Optical system design and engineering considerations, online at https://www.itu.int/rec/T-REC-G/en

[G.Sup58] ITU-T Recommendation G.Sup58: Optical transport network (OTN) module framer interfaces, online at https://www.itu.int/rec/T-REC-G/en

[ghazisaeidi13] A. Ghazisaeidi, P. Tran, P. Brindel, O. Bertran-Pardo, J. Renaudier, G. Charlet, S. Bigo: Impact of Tight Optical Filtering on the Performance of 28 Gbaud Nyquist-WDM PDM-8QAM over 37.5 GHz Grid, Proc. Optical Fiber Communication Conf. (OFC), Anaheim, 2013, OTu3B.6

[gene10] J.M. Gene, Peter J. Winzer: First-Order PMD Outage Prediction Based on Outage Maps, J. Lightwave Technol. **28**(13), 1873–1881 (2010)

[gerstel12] O. Gerstel, M. Jinno, A. Lord, S.J. Ben Yoo: Elastic optical networking: A new dawn for the optical layer?, IEEE Signal Process. Mag. **50**(2), s12–s20 (2012)

[gnauck02] G. Rayhnn, S. Chandrasekhar, J. Leuthold, C. Dnerr, L. Stulz, A. Agarwal, S. Banerjee, D. Grnsz, S. Hunsche, A. Kung, A. Marhelyuk, D. Maywar, M. Mnvassaghi, X. Liu, C. Xu, X. Wei and D. M. Gill: 2.5 Tb/s (64x42.7 Gb/s) transmission over 40x100 km NZDSF using RZ-DPSK format and all-Raman-amplified spans, Proc. Optical Fiber Communication Conf. (OFC), Anaheim, 2002, Paper FC2

[gnauck05] A. H. Gnauck and P. J. Winzer: Optical phase-shift-keyed transmission, J. Lightw. Technol. **23**(1), 115–130 (2005)

[gnauck08] A.H. Gnauck, R. W. Tkach, A. R. Chraplyvy: High-Capacity Optical Transmission Systems, J. Lightwave Technol. **26**(9), 1032–1045 (2008)

[gnauck10] A.H. Gnauck, P.J. Winzer, S. Chandrasekhar, X. Liu, B. Zhu, and D.W. Peckham: 10 x 224-gb/s WDM transmission of 28-Gbaud PDM 16-QAM on a 50-Ghz grid over 1,200 km of fiber, Proc. of Optical Fiber Communication (OFC), San Diego, 2010, paper PDPB8.

[griffin02] R. A. Griffin and A. C. Carter: Optical differential quadrature phase-shift key (oDQPSK) for high capacity optical transmission," Proc. Optical Fiber Communication Conf. (OFC), Anaheim, 2002, Paper WX6
[gu93] X. Gu, L.C. Blank: 10 Gbit/s unrepeated optical transmission over 100 km of standard fibre, Electron. Lett. **29**(25), 2209–2211 (1993)

[gringeri07] S. Gringeri, N. Bitar, R. Egorov, B. Basch, C. Suitor, H. Peng: Optimizing Transport Systems to Integrate TDM and Packet Services", Proc. National Fiber Optic Engineers Conference (NFOEC), Anaheim, 2007, paper NTuA4

[gu96] X. Gu, S. J. Dodds, L. C. Blank, D. M. Spirit, S. J. Pycock, A. D. Ellis: Duobinary technique for dispersion reduction in high capacity optical systems-modelling, experiment and field trial, IEE Proceedings – Optoelectronics **143**(4), 228–236 (1996)

[guoimar17] F.P. Guiomar, L. Bertignono, D. Pilori, A. Nespola, G. Bosco, A. Carena, F. Forghieri,: Comparing Different Options for Flexible Networking: Probabilistic Shaping vs. Hybrid Subcarrier Modulation, Proc. of European Conference on Optical Communication (ECOC), Goteborg, 2017, paper Th1.E.3.

[haxell00b] I. Haxell, M. Ding, A. Akhtar, H. Wang, P. Farrugia: 52 x 12.3 Gb/s DWDM transmission over 3600km of True Wave fiber with 100km amplifier spans“, Proc. of Optical Amplifiers and their Applications, OSA Technical Digest Series (Optical Society of America, Washington, D.C., 2000), postdeadline paper PD5

[hillerkus12] D. Hillerkuss, R. Schmogrow, M. Meyer, S. Wolf, M. Jordan, P. Kleinow, N. Lindenmann, P.C. Schindler, A. Melikyan, X. Yang, S. Ben-Ezra, B. Nebendahl, M. Dreschmann, J. Meyer, F. Parmigiani, P. Petropoulos, B. Resan, A. Oehler, K. Weingarten, L. Altenhain, T. Ellermeyer, M. Moeller, M. Huebner, J. Becker, C. Koos, W. Freude, J. Leuthold: Single-laser 32.5 Tbit/s Nyquist WDM transmission," J. Opt. Commun. Netw. **4**(10), 715–723 (2012).

[ho04] K.-P. Ho: The effect of interferometer phase error on direct-detection DPSK and DQPSK signals," IEEE Photon. Technol. Lett. **16**(1), 308–310 (2004)

[ho05] K.-Po Ho: *Phase-modulated optical communication systems* (Springer, New York, 2005)

[ho05b] Keang-Po Ho, Han-Wei Cuei: Generation of Arbitrary Quadrature Signals Using One Dual-Drive Modulator, J. Lightwave Technol. **23**(2), 764–770 (2005)

[humblet91] P. A. Humblet, M. Azizoglu: On the bit error rate of lightwave systems with optical amplifiers, J. Lightwave Technol. **9**(11), 1576–1582 (1991)

[idler15] W. Idler, F. Buchali, L. Schmalen, K. Schuh, H. Buelow: Hybrid modulation formats outperforming 16QAM and 8QAM in transmission distance and filtering with cascaded WSS," Proc. of Optical Fiber Communication Conference (OFC), Los Angeles, 2015, paper M3G.4.

[ip07] E. Ip and J. M. Kahn: Feedforward carrier recovery for coherent optical communications, J. Lightw. Technol. **25**(9), 2675–2692 (2007)

[itu-t] International Telecommunication Union - Standardization Sector, G series recommendations, online at https://www.itu.int/rec/T-REC-G/en

[jinno09] M. Jinno, H. Takara, B. Kozicki, Y. Tsukishima, Y. Sone, S. Matsuoka: Spectrum-efficient and scalable elastic optical path network: Architecture, benefits, and enabling technologies, IEEE Signal Process. Mag. **47**(11), 66–72(2009)

[joindot08] M. Joindot, G. Bosco, A. Carena, V. Curri, P. Poggiolini: Fundamental performance limits of optical duobinary, Optics Express **16**(24), 19600–19614 (2008)

[jopson99] R. M. Jopson, L. E. Nelson, G. J. Pendock, and A. H. Gnauck: Polarization-mode dispersion impairment in return-to-zero and non return-to-zero systems, Proc. Optical Fiber Communication Conf. (OFC), San Diego, 1999, paper WE3.

[kahn04] J.M. Kahn, K.-Po Ho: Spectral Efficiency Limits and Modulation/Detection Techniques for DWDM Systems, J. Selec. Topicis in Quantum Elec. **10**(2), 259–272 (2004)

[kahn07] E. Ip and J.M Kahn: Digital Equalization of Chromatic Dispersion and Polarization Mode Dispersion" J. Lightwave Technol. **25**(8), 2033–2043 (2007).

[kawakami10] H. Kawakami, E. Yoshida, Y. Miyamoto: Asymmetric dithering technique for bias condition monitoring in optical QPSK modulator, Electronics Letters **46**(6), 430–431 (2010)

[kazovsky96] L. Kazovsky, S. Benedetto, A. Willner: *Optical Fiber Communication Systems* (Artech House Inc., Norwood, USA, 1996)

[khanna16] G. Khanna, B. Spinnler, S. Calabrò, E. De Man, and N. Hanik: A Robust Adaptive Pre-Distortion Method for Optical Communication Transmitters, IEEE Photon. Tehcnol. Lett. **28**(7), 752–755 (2016).

[kikuchi15] Kazuro Kikuchi: Fundamentals of Coherent Optical Fiber Communications, J. Lightwave Technol. **34**(1), 157–179 (2016)

[kikuchi88] T. Okoshi and K. Kikuchi: *Coherent Optical Fiber Communications* (Kluwer, Boston, 1988)

[kim02] Hoon Kim, C. X. Yu: Optical duobinary transmission system featuring improved receiver sensitivity and reduced optical bandwidth, IEEE Photon. Technol. Lett. **14**(8), 1205–1207 (2002)

[kim03] H. Kim and P. J. Winzer: Robustness to laser frequency offset in direct detection DPSK and DQPSK systems, J. Lightw. Technol. **21**(9), 1887–1891 (2003)

[kingsley95] F.A. Kingsley: *The Development of Radar Equipments for the Royal Navy, 1935–45* (Palgrave Macmillan, London, 1995)

[krause17] D. Krause, A.Awadalla, A. Karar1, H. Sun, K.-T. Wu: Design Considerations for a Digital Subcarrier Coherent Optical Modem, Proc. of Optical Fiber Communication Conference (OFC), Los Angeles, 2017, paper Th1D.1

[laperle07] C. Laperle, B. Villeneuve, Z. Zhang, D. McGhan, H. Sun, and M. O'Sullivan: Wavelength Division Multiplexing (WDM) and Polarization Mode Dispersion (PMD) Performance of a Coherent 40Gbit/s Dual-Polarization Quadrature Phase Shift Keying (DP-QPSK) Transceiver, Proc. of Optical Fiber Communication Conference and Exposition (OFC), Anaheim, 2007, paper PDP16.

[laperle08] C. Laperle, B. Villeneuve, Z. Zhang, D. McGhan, Han Sun, M. O'Sullivan: WDM Performance and PMD Tolerance of a Coherent 40-Gbit/s Dual-Polarization QPSK Transceiver, J. Lightw. Technol. **26**(1), 168–175 (2008)

[lavigne16] B. Lavigne, M. Lefrançois, O. Bertran-Pardo, M. Le Monnier, L. Raddatz, S. Weisser, R. Peruta, G.A. Azzini, L. Suberini: Real-time 200 Gb/s 8-QAM transmission over a 1800-km long SSMF-based system using add/drop 50 GHz-wide filters, Proc. of Optical Fiber Communication (OFC), Anaheim, 2016, paper W3G.2

[lender63] A. Lender: The Duobinary technique for high-speed data transmission, IEEE Trans. on Commun. Technol. **82**(2), 214–218 (1963)

[li16] C. Li, Z. Zhang, J. Chen, T. Ding, Z. Xiao, F. Shah, J. Mitra, H. Xiang, X. Cui: Advanced DSP for Single-Carrier 400-Gb/s PDM-16QAM, Proc. of Optical Fiber Communication Conference (OFC), Anaheim, 2016, paper W4A.4

[liu14] X. Liu, S. Chandrasekhar, P. Winzer: Digital signal processing techniques enabling multi-Tb/s superchannel transmission," IEEE Signal Process. Mag. **31**(2), 16–24 (2014)

[lowery07] A. J. Lowery, L. B. Du, J. Armstrong: Performance of Optical OFDM in Ultralong-Haul WDM Lightwave Systems, J. Lightwave Technol. **25**(1), 131–138 (2007).

[lyubomirsky02] I. Lyubomirsky, S. Shetty, J. Roman, M. Y. Frankel: Optimum 10-Gb/s NRZ receiver bandwidths for ultradense WDM transmission systems, IEEE Photon. Technol. Lett. **14**(6), 870–872 (2002)

[lyubomirsky04] I. Lyubomirsky and B. Pitchumani: Impact of Optical Filtering on Duobinary Transmission, IEEE Photon. Technol. Lett. **16**(8), 1969-1971 (2004)

[lyubomirsky16] Lyubomirsky and W. A. Ling: Advanced Modulation for Datacenter Interconnect, Proc. of Optical Fiber Communication Conf. and Exposition (OFC), Anaheim, 2016, paper W4J.3.

[mazurczyk14] M. Mazurczyk: Spectral shaping in long haul optical coherent systems with high spectral efficiency, J. Lightwave Technol. **32**(16), 2915–2924 (2014)

[mikkelsen06] B. Mikkelsen, C. Rasmussen, P. Mamyshev, F. Liu: Partial DPSK with excellent filter tolerance and OSNR sensitivity Tolerance, Electron. Lett. **42**(23), 1363–1364 (2006)

[miyamoto99] Y. Miyamoto, A. Hirano, K. Yonenaga, A. Sano, H. Toba, K. Murata and O.Mitomi: 320 Gbit/s (8 x 40 Gbit/s) WDM transmission over 367 km with 120-km repeater spacing using carrier-suppressed return-to-zero format, Electron. Lett. **35**(23), 2041–2042 (1999)

[nadal14] L. Nadal, M. S. Moreolo, J. M. Fabrega, A. Dochhan, H. Grießer, M. Eiselt, J.-P. Elbers: DMT modulation with adaptive loading for high bit rate transmission over directly detected optical channels, J. Lightw. Technol. **32**(21), 3541–3551 (2014)

[nagarajan11] R. Nagarajan, D. Lambert, M. Kato, V. Lal, G. Goldfarb, J. Rahn, J. Mcnicol, K.-T. Wu, M. Kuntz, J. Pleumeekers, A. Dentai, H.-S. Tsai, R. Malendevich, M. Missey, J. Tang, J. Zhang, O. Khayam, T. Butrie, H. Sun, A. Nilsson, V. Dangui, M. Mitchell, M. Reffle, F. Kish, D. Welch: Five-channel, 114 Gbit/s per channel, dual carrier, dual polarisation, coherent QPSK, monolithic InP receiver photonic integrated circuit, Electron. Lett. **47**(9), 555–556 (2011)

[nespola14] A. Nespola, S. Straullu, G. Bosco, A. Carena, J. Yanchao, P. Poggiolini, F. Forghieri, Y. Yamamoto, M. Hirano, T. Sasaki, J. Bauwelinck, K. Verheyen: 1306-km 20x124.8-Gb/s PM-64QAM transmission over PSCF with Net SEDP 11,300 (b·km)/s/Hz using 1.15 samp/symb DAC, Opt Express **22**(1), 1796–1805 (2014).

[noe05] R. Noe: PLL-free synchronous QPSK polarizationmultiplex/diversity receiver concept with digital I&Q baseband processing, IEEE Photon. Technol. Lett. **17**(4), 887–889 (2005)

[ohta08] A. Ohta, D. Tanimura, T. Kyakuno, S. Iio: 43-Gbps RZ-DQPSK transponder for long-haul optical transmission system, Yokogawa Tech. Report English Edition **46**, 3–6 (2008)

[oif-168] Optical Internetworking Forum (OIF): OIF-MSA-100GLH-EM-02.1 – Multisource Agreement for Generation 2.0 100G Long-Haul DWDM Transmission Module – Electromechanical (March 2015), online at http://www.oiforum.com/

[oif-cei] Optical Internetworking Forum (OIF): OIF-CEI-03.1 – Common Electrical I/O (CEI) – Electrical and Jitter Interoperability agreements for 6G+ bps, 11G+ bps, 25G+ bps I/O (February 2014), online at http://www.oiforum.com/

[oif-otn] Optical Internetworking Forum (OIF): OTN Over Packet Fabric Protocol (OFP). Implementation Agreement, online at http://www.oiforum.com/

[oif] Optical Internetworking Forum (OIF), 400G –ZR coherent interface, http://www.oiforum.com/

[ono98] T. Ono, Y. Yano, K. Fukuchi, T. Ito, H. Yamazaki, M. Yamaguchi, K. Emura: Characteristics of optical Duobinary signals in terabit/s capacity, high spectral efficiency WDM systems, IEEE/OSA J. of Lightwave Technol. **16**(5), 788–797 (1998)

[osfp] Octal Small Form Factor Pluggable (OSFP) Multi Source Agreement (MSA) Group, online at http://osfpmsa.org/index.html

[pauer01] M. Pauer, P. J. Winzer, W. R. Leeb: Bit error probability reduction in direct detection optical receivers using RZ coding, J. Lightwave Technol. **19**(9), 1255–1262 (2001)

[pavlovic05] N. B. Pavlovic, A. V. T. Cartaxo: Optimized Bandwidth Limited Duobinary Coding Format for Ultra Dense WDM Systems, Proc. of International Conference on Transparent Optical Networks (ICTON 2005), Barcelona, Spain, 2005 paper We P.3.

[penninckx96] D. Penninckx, M. Chbat, L. Pierre, J.-P. Thiery: The Phase-shaped Binary Transmission (PSBT): A new technique to transmit far beyond the chromatic dispersion limit, in Proc. European Conference on Optical Communication (ECOC'96), Oslo, 1996, vol. 2, pp. 173–176.

[penninckx97] D. Penninckx, M. Chbat, L. Pierre, and J.-P. Thiery: The Phase-Shaped Binary Transmission (PSBT): A New Technique to Transmit Far Beyond the Chromatic Dispersion Limit, IEEE Photon. Technol. Lett. **9**(2), 259–261 (1997)

[pfennigbauer02] M. Pfennigbauer, M. M. Strasser, M. Pauer, P. J. Winzer: Dependence of optically preamplified receiver sensitivity on optical and electrical filter bandwidths-measurement and simulation, IEEE Photon. Technol. Lett. **14**(6), 831–833 (2002)

[pilori17] D. Pilori, L. Bertignono, A. Nespola, F. Forghieri, G. Bosco: Comparison of Probabilistically Shaped 64QAM with Lower-Cardinality Uniform Constellations in Long-Haul Optical Systems, to be published in J. Lightwave Technol.

[poggiolini07] P. Poggiolini, G. Bosco: Impact of Chromatic Dispersion on DPSK and DQPSK Direct-Detection Optical Systems, Annals of Telecommunications **62**(5-6), 531–549 (2007)

[poggiolini14] P. Poggiolini, A. Nespola, Y. Jiang, G. Bosco, A. Carena, L. Bertignono, S.M. Bilal, S: Abrate, F. Forghieri: Analytical and experimental results on system maximum reach increase through symbol rate optimization, J. Lightw. Technol., **34**(8), 1872–1885 (2016)

[poggiolini94] P. Poggiolini and S. Benedetto: Theory of polarization spreading techniques—Part I, IEEE Trans. Commun. **42**(5), 2105–2118 (1994)

[pratt03] A. R. Pratt, P. Harper, S. B. Alleston, P. Bontemps, B. Charbonnier, W. Forysiak, L. Gleeson, D. S. Govan, G. L. Jones, D. Nesset, J. H. B. Nijhof, I. D. Phillips, M. F. C. Stephens, A. P. Walsh, T. Widdowson, N. J. Doran: 5,745 km DWDM transcontinental field trial using 10 Gbit/s dispersion managed solitons and dynamic gain equalization, Proc. of Optical Fiber Communication Conference, Atlanta, 2003, Paper PD26

[price95] A. J. Price, L. Pierre, R. Uhel, and V. Havard: 210 km Repeaterless 10 Gb/s Transmission Experiment Through Nondispersion-Shifted Fiber Using Partial Response Scheme, IEEE Photon. Technol. Lett. **7**(10), 1219–1221 (1995)

[proakis07] J. Proakis: *Digital Communications* (McGraw Hill, New York, USA, 2007)

[qiu14] M. Qiu, Q. Zhuge, M. Chagnon, Y. Gao, X. Xu, M. Morsy-Osman, D. V. Plant: Digital subcarrier multiplexing for fiber nonlinearity mitigation in coherent optical communication systems, Opt. Express **22**(15), 18770–18777 (2014)

[qsfp-dd] Quad Small Form Factor Pluggable Double Density (QSFP-DD) Multi Source Agreement (MSA) Group, online at http://www.qsfp-dd.com/

[rebola00] J. Rebola and A. Cartaxo: Optimization of level spacing in quaternary optical communication systems, Proc. SPIE, Quebec, Canada, 2000, vol. 4087, pp. 49–59

[rebola02] J. L. Rebola, A. V. T. Cartaxo: Power penalty assessment in optically preamplified receivers with arbitrary optical filtering and signal-dependent noise dominance, J. Lightwave Technol. **20**(3), 401–408 (2002)

[roberts09] K. Roberts, M. O'Sullivan, K.-T. Wu, H. Sun, A. Awadalla, D.J. Krause, C. Laperle: Performance of Dual-Polarization QPSK for Optical Transport Systems, J. Lightwave Technol. **27**(16), 3546–3559 (2009)

[roberts17] K. Roberts, Q. Zhuge, I. Monga, S. Gareau, C. Laperle: Beyond 100 Gb/s: Capacity, Flexibility, and Network Optimization [Invited], J. Opt. Comm. and Netw. **9**(4), C12–C24 (2017)

[saito91] T. Saito, N. Henmi, S. Fujita, M. Yamaguchi, and M. Shikada: Prechirp technique for dispersion compensation for a high-speed long span transmission, IEEE Photon. Technol. Lett. 3(1), 74–76 (1991).

[sano12] A. Sano, T. Kobayashi, S. Yamanaka, A. Matsuura, H. Kawakami, Y. Miyamoto, K. Ishihara, H. Masuda: 102.3-Tb/s (224 x 548-Gb/s) C- and extended L-band all-Raman transmission over 240 km using PDM-64QAM single carrier FDM with digital pilot tone, Proc. of Optical Fiber Communication Conference, Los Angeles, 2012, Paper PDP5C.3.

[sato05] K. Sato, S. Kuwahara, Y. Miyamoto: Chirp Characteristics of 40-Gb/s Directly Modulated Distributed-Feedback Laser Diodes, J. Lightwave Technol. **23**(11), 3799–3797 (2005).

[savory06] S.J. Savory, A.D. Stewart, S. Wood, G. Gavioli, M.G. Taylor, R.I. Killey, P. Bayvel: Digital equalization of 40 Gbit/s per wavelength transmission over 2480 km of standard fibre without optical dispersion compensation, Proc. of European Conference on Optical Communication (ECOC), Cannes, 2006, Paper Th2.5.5.

[savory08] S. J. Savory: Digital filters for coherent optical receivers, Opt. Exp. **16**(2), 804–817 (2008)

[schindler14] P. C. Schindler, R. Schmogrow, S. Wolf, B. Baeuerle, B. Nebendahl, C. Koos, W. Freude, and J. Leuthold, "Full flex-grid asynchronous multiplexing demonstrated with Nyquist pulse-shaping," Opt. Express 22, 10923–10937 (2014)

[schmogrow11] R. Schmogrow, M. Winter, M. Meyer, D. Hillerkuss, B. Nebendahl, J. Meyer, M. Dreschmann, M. Huebner, J. Becker, C. Koos, W. Freude, J. Leuthold, “Real-Time Nyquist Pulse Modulation Transmitter Generating Rectangular Shaped Spectra of 112 Gbit/s 16QAM Signals,” in Proc. of 2011 OSA Summer Topical Meeting on Signal Processing in Photonics Communications (SPPCom), Toronto, Canada, 2011, Paper SPMA5.

[schmogrow12] R. Schmogrow, S. Wolf, B. Baeuerle, D. Hillerkuss, B. Nebendahl, C. Koos, W. Freude, J. Leuthold: Nyquist Frequency Division Multiplexing for Optical Communications, Proc. of Conference on Lasers and Electro-Optics, San Jose, 2012, paper CTh1H.2.

[schmogrow13] R. Schmogrow, M. Meyer, P.C. Schindler, A. Josten, S. Ben-Ezra C. Koos, W. Freude, J. Leuthold: 252 Gbit/s real-time Nyquist pulse generation by reducing the oversampling factor to 1.33, Proc. of Optical Fiber Communication Conference, Anaheim , 2013, Paper OTu2I.1.

[seimetz09] M. Seimetz: *High Order Modulation for Optical Fiber Transmission* (Springer, Berlin, 2009)

[sfp-dd] Small Form Factor Pluggable Double Density (SFP-DD), online at http://sfp-dd.com/

[shieh08] W. Shieh, H. Bao, Y. Tang: Coherent optical OFDM: theory and design," Opt. Express **16**(2), 841–859 (2008)

[smith12] B. Smith, F. Kschischang: A pragmatic coded modulation scheme for high-spectral-efficiency fiber-optic communications, J. Lightw. Technol. **30**(13), 2047–2053 (2012)

[snia] Storage Networking Industry Association (SNIA) Small Form Factor (SFF) Technology Affiliate Technical Work Group, online at https://ta.snia.org/higherlogic/ws/public

[sotoodeh11] M. Sotoodeh, Y. Beaulieu, J. Harley, D.L. McGhan: Modulator Bias and Optical Power Control of Optical Complex E-Field Modulators, J. Lightwave Technol. **29**(15), 2235–2248 (2011)

[steiner17] F. Steiner, G. Boecherer: Comparison of Geometric and Probabilistic Shaping with Application to ATSC 3.0, Proc. of 11th International ITG Conference on Systems, Communications and Coding (SCC 2017), Hamburg, 2017.

[sterling07] C.H. Sterling, *Military Communications: From Ancient Times to the 21st Century* (ABC-CLIO, Santa Barbara, 2007)

[sun97] Y. Sun, J.B. Judkins, A.K. Srivastava, L. Garrett, J.L. Zyskind, J.W. Sulhoff, C. Wolf, R.M. Derosier, A.P. Gnauck, R.W. Tkach, J. Zhou, R.P. Espindola, A.M. Vengsarkar, A.R. Chraplyvy: Transmission of 32-WDM 10-Gb/s channels over 640 km using broad-band, gain-flattened erbium-doped silica fiber amplifiers, IEEE Photon. Technol. Lett. **9**(12), 1652–1654(1997)

[takahara14] T. Takahara, T. Tanaka, M. Nishihara, Y. Kai, L. Li, Z. Tao, J. Rasmussen: Discrete multi-tone for 100 Gb/s optical access networks, Proc. of Optical Fiber Communication Conference (OFC), San Francisco, 2014, paper M2I.1.

[tanaka99] K. Tanaka, T. Tsuritani, N. Edagawa, M. Suzuki: 320 Gbit/s (32×10.7 Gbit/s) error-free transmission over 7280 km using dispersion flattened fibre link with standard SMF and slope compensating DCF, Electronics Lett. **35**(21), 1860–1862 (1999)

[taylor04] M. G. Taylor: Coherent detection method using DSP for demodulation of signal and subsequent equalization of propagation impairments, IEEE Photon. Technol. Lett. **16**(2), 674–676 (2004)

[tibuleac15] M. Alfiad, S. Tibuleac: 100G Superchannel Transmission Using 4 × 28 Gb/s Subcarriers on a 25-GHz Grid", IEEE Photon. Tech. Lett. **27**(2), 157–160 (2015)

[tucker85] R. S. Tucker: High-speed modulation of semiconductor lasers, IEEE Trans. Electron Devices, **ED-32**(12), 2572–2584 (1985).

[walklin99] S. Walklin, J. Conradi: Multilevel signaling for increasing the reach of 10 Gb/s lightwave systems, J. Lightwave Technol. **17**(11), 2235–2248 (1999)

[wang04] J. Wang and J. M. Kahn: Impact of chromatic and polarization-mode dispersions on DPSK systems using interferometric demodulation and direct detection, J. Lightw. Technol. **22**(2), 362–371 (2004)

[winzer01] P. J. Winzer, M. Pfennigbauer, M. M. Strasser, W. R. Leeb: Optimum filter bandwidths for optically preamplified RZ and NRZ receivers, J. Lightwave Technol. **19**(9) 1263–1273 (2001)

[winzer03] P. J. Winzer, Hoon Kim: Degradations in balanced DPSK receivers, IEEE Photonics Technology Letters **15**(9), 1282–1284 (2003)

[winzer03b] P. J. Winzer, S. Chandrasekhar, Hoon Kim: Impact of filtering on RZ-DPSK reception, IEEE Photonics Technology Letters **15**(6), 840–842 (2003)

[winzer03c] P. J. Winzer, H. Kogelnik, C. H. Kim, H. Kim, R. M. Jopson, L. E. Nelson, and K. Ramanan: Receiver impact on first-order PMD outage, IEEE Photon. Technol.Lett. **15**(10), 1482–1484 (2003)

[winzer04] P. J. Winzer, C. Dorrer, R.-J. Essiambre, and I. Kang: Chirped Return-to-Zero Modulation by imbalanced Pulse Carver Driving Signals, IEEE Photon. Technol. Lett. **16**(5), 1379–1381 (2004).

[winzer04b] P. J. Winzer, H. Kogelnik K. Ramanan: Precise outage specifications for first-order PMD, IEEE Photon. Technol. Lett. **16**(2), 449–451 (2004)

[winzer06] P. J. Winzer, R. -J. Essiambre: Advanced Optical Modulation Formats, Proceedings of the IEEE **94**(5), 952–985 (2006)

[winzer06b] P. J. Winzer, R. -J. Essiambre: Advanced Modulation Formats for High-Capacity Optical Transport Networks, J. Lightwave Technol. **24**(12), 4711–4728 (2006)

[winzer10] P. J. Winzer: Beyond 100G Ethernet, IEEE Commun. Mag. **48**(7), 26–30 (2010)

[winzer12] P. Winzer: High-Spectral-Efficiency Optical Modulation Formats, J. Lightwave Technol. **30**(24), 3824–3835 (2012)

[winzer99] P. J. Winzer, A. Kalmar: Sensitivity enhancement of optical receivers by impulsive coding, J. Lightwave Technol. **17**(2), 171–177 (1999)

[xie03] C. Xie, S. Shen, and L. Moller: Effects of transmitter imperfection on polarization mode dispersion impairments, IEEE Photon. Technol. Lett. **15**(4), 614–616 (2003)

[yanfu11] Yanfu Yang, Chao Lu, Alan Pak Tao Lau, Yong Yao, Yunxu Sun, Jun Jun Xiao, H. Y. Tam, P. K. A. Wai: A robust and dither-free technique for controlling driver signal amplitude for stable and arbitrary optical phase modulation, Optics Express **19**(27), 26353– 26358 (2011)

[yankov14] M.P. Yankov, D. Zibar, K.J. Larsen, L.P.B. Christensen, S. Forchhammer: Constellation shaping for fiber-optic channels with QAM and high spectral efficiency, IEEE Photon. Technol. Lett. **26**(23), 2407–2410 (2014)

[yonenaga95] K. Yonenaga, S. Kuwano, S. Norimatsu and N. Shibata: Optical Duobinary transmission system with no receiver sensitivity degradation, Electron. Lett. **3**(4), 302–304 (1995)

[yonenaga97] K. Yonenaga, and S. Kuwano: Dispersion tolerant optical transmission system using duobinary transmitter and binary receiver, J. Lightwave Technol. **15**(8), 1530–1537 (1997).

[yonenaga98] K. Yonenaga, A. Hirano, M. Yoneyama, Y. Miyamoto, K. Hagimoto, K. Noguchi: "Expansion of tolerable dispersion range in a 40 Gbit/s optical transmission system using an optical duobinary signal, Electronics Letters **34**(4), 385–386 (1998)

[yoshida10] T. Yoshida, T. Sugihara, K. Uto, H. Bessho, K. Sawada, K. Ishida, K. Shimizu, T. Mizuochi: A study on automatic bias control for arbitrary optical signal generation by dual-parallel Mach-Zehnder modulator, Proc. of European Conference on Optical Communication (ECOC), Torino, 2010, paper Tu.3.A.6

[zheng01] X. Zheng, F. Liu, and P. Jeppesen: Receiver optimization for 40-Gb/s optical duobinary signal, IEEE Photon. Technol. Lett. **13**(7), 744–746 (2001)

[zhong09] K. Zhong, X. Zhou, T. Gui, L. Tao, Y. Gao, W. Chen, J. Man, L. Zeng, A. P. T. Lau, C. Lu: Experimental study of PAM-4, CAP-16, and DMT for 100 Gb/s short reach optical transmission systems, Opt. Express **23**(2), 1176–1189 (2015).

[zhou12] X. Zhou, L.E. Nelson, P. Magill, R. Isaac, B. Zhu, D.W. Peckham, P.I. Borel, K. Carlson: PDM-Nyquist-32QAM for 450-Gb/s per-channel WDM transmission on the 50 GHz ITU-T grid, J Lightwave Technol. **30**(4), 553–559 (2012)

[zhou13]] X. Zhou, L.E. Nelson, P. Magill, R. Isaac, B. Zhu, D.W. Peckham, P.I. Borel, K. Carlson: High spectral efficiency 400 Gb/s transmission using PDM time-domain hybrid 32-64 QAM and training-assisted carrier recovery, J Lightwave Technol. **31**(7), 999–1005 (2013)

[zhou13b] X. Zhou, L. Nelson, P. Magill: Rate-adaptable optics for next generation long-haul transport networks, IEEE Commun. Mag., **51**(3), 41–49 (2013)

[zhuge13] Q. Zhuge, M. Morsy-Osman, X. Xu, M. Chagnon, M. Qiu, D. Plant: Spectral efficiency-adaptive optical transmission using time domain hybrid QAM for agile optical networks, J. Lightw. Technol. **31**(15), 2621–2628 (2013)